

# Dynamic Momentum Recalibration in Online Gradient Learning

Zhipeng Yao<sup>1,2\*</sup> Rui Yu<sup>2†</sup> Guisong Chang<sup>3</sup> Ying Li<sup>1</sup> Yu Zhang<sup>1</sup> Dazhou Li<sup>1†</sup>  
<sup>1</sup>Shenyang University of Chemical Technology <sup>2</sup>University of Louisville <sup>3</sup>Northeastern University  
 yiucp@outlook.com, rui.yu@louisville.edu, gschang@mail.neu.edu.cn  
 Gooddayli12358@outlook.com, zhangy@syuct.edu.cn, lidazhou@syuct.edu.cn  
 <https://github.com/LiYau350/SGDF-Optimizer>

## Abstract

*Stochastic Gradient Descent (SGD) and its momentum variants form the backbone of deep learning optimization, yet the underlying dynamics of their gradient behavior remain insufficiently understood. In this work, we reinterpret gradient updates through the lens of signal processing and reveal that fixed momentum coefficients inherently distort the balance between bias and variance, leading to skewed or suboptimal parameter updates. To address this, we propose SGDF (SGD with Filter), an optimizer inspired by the principles of Optimal Linear Filtering. SGDF computes an online, time-varying gain to dynamically refine gradient estimation by minimizing the mean-squared error; thereby achieving an optimal trade-off between noise suppression and signal preservation. Furthermore, our approach could extend to other optimizers, showcasing its broad applicability to optimization frameworks. Extensive experiments across diverse architectures and benchmarks demonstrate SGDF surpasses conventional momentum methods and achieves performance on par with or surpassing state-of-the-art optimizers.*

## 1. Introduction

In deep learning optimization, the optimizer plays a pivotal role in refining model parameters to capture underlying data patterns, while strategically navigating complex loss landscapes [18] to identify regions that promote strong generalization [39]. Its choice profoundly affects training efficiency, convergence speed, generalization, and robustness to data shifts [2], with suboptimal selections potentially causing slow or failed convergence, whereas effective ones accelerate learning and bolster model resilience [66]. Thus, the design and refinement of optimizers remain essential challenges in enhancing the capabilities of models.

Stochastic Gradient Descent (SGD) [57] and its variants, including momentum-based methods [63, 71] and adap-

tive techniques like Adam [40] and RMSprop [32], which have advanced training efficiency [7]. However, these approaches face challenges in high-dimensional, non-convex settings [27], where adaptive methods often yield rapid convergence but suffer from poor generalization [38]. Efforts to mitigate this have led to Adam variants [8, 49, 52, 88] that refine adaptive learning rates, yet they fall short of fully closing the generalization gap, highlighting the ongoing need for innovative optimization strategies that better balance estimation accuracy and practical performance.

Actually, the issues that arise from the optimizer during training, particularly in terms of optimization and generalization, are inherently tied to the trade-off between bias and variance [24, 58]. High bias leads to underfitting, while high variance results in overfitting. Similarly, the gradients used by the optimizer to update weights also face this challenge. Intuitively, high bias in the gradients may lead to convergence at a suboptimal plateau [77, 84], while high variance can lead to instability in the optimization path, causing oscillations that hinder convergence [6, 20]. Therefore, a good optimizer should strike a balance between the bias and variance in its gradient estimates.

From a statistical signal processing perspective, we analyze the mechanism behind optimizer updates. Specifically, we decompose the optimizer’s gradients used for updating model weight into bias and variance components. Then, We identify a key limitation in momentum-based optimization techniques supplemented with examining the statistical distribution of gradients within the model: they struggle to balance bias and variance components in gradients, often introducing a gradient shift phenomenon, which we term *bias gradient estimate*. This bias estimate, arising from fixed momentum coefficients, accumulates over time, leading to bias. As a result, the model may struggle to adapt to variations in curvature across different layers, resulting in suboptimal or directionally skewed updates [17, 85].

To address this issue, we introduce SGDF, a novel method that uses principles from Optimal Linear Filter to adjust gradient estimation dynamically. SGDF derives an optimal,

\* Work initiated at <sup>1</sup> and further developed at <sup>2</sup>, † Equal advising.

time-varying gain to minimize mean-squared error in gradient estimation, balancing noise reduction with signal preservation. This filter mechanism provides a more accurate first-order gradient estimate and avoids the limitations of fixed momentum parameters, allowing SGDF to adjust dynamically throughout training. Additionally, SGDF’s flexibility extends to other optimization frameworks, which enhance performance across a range of tasks. Through extensive empirical validation across diverse model architectures and visual tasks, we demonstrate that SGDF consistently outperforms traditional momentum-based and variance reduction methods, achieving competitive or superior results relative to state-of-the-art optimizers.

The main contributions can be summarized as follows:

- We quantify the bias-variance trade-off in momentum-based gradient estimation (EMA and CM) using a unified SDE framework, revealing their static limitations.
- We introduce SGDF, an optimizer that combines historical and current gradient data to estimate the gradient, addressing the trade-off between bias and variance in the momentum method.
- We theoretically analyze the convergence property of SGDF in both convex optimization and non-convex stochastic optimization (Sec. 3.3), and empirically verify the effectiveness of SGDF (Sec. 4).
- We preliminarily explore the extension of SGDF’s first-moment filter estimation to adaptive optimization algorithms (e.g., Adam), which shows a promising enhancement in their generalization capability (Sec. 4.2), surpassing traditional momentum-based methods.

## 2. The Gradient Estimation Dilemma

### 2.1. Bias and Variance

Stochastic gradient-based optimization lies at the core of modern machine learning. We revisit this and found that it grapples with a fundamental challenge: the trade-off between gradient bias and variance. To dissect this dilemma, we begin by unifying two prominent momentum strategies under a single framework. The proof of this section can be found in Appendix A.

**Definition 2.1.** The unified momentum update rule is defined as:

$$m_t = \beta m_{t-1} + u g_t, \quad \theta_t = \theta_{t-1} - \alpha m_t, \quad (1)$$

where  $\alpha$  is the learning rate,  $\beta \in [0, 1)$  is the momentum coefficient, and  $u \geq 1 - \beta$  scales the current gradient. For all  $\theta \in \mathbb{R}^d$ ,  $f_t(\theta) = f(\theta; \xi_t)$  denotes the stochastic objective at iteration  $t$  with data sample  $\xi_t \sim \mathcal{D}$ . The expected objective is  $f(\theta) = \mathbb{E}_\xi[f(\theta; \xi)]$ , and  $g_t = \nabla f_t(\theta_t) + \epsilon_t$  (where  $\epsilon_t \sim \mathcal{N}(0, \sigma^2 I)$ ) is the stochastic gradient. Specific cases include:

- $u = 1 - \beta$ : Exponential Moving Average (EMA),
- $u = 1$ : Classical Momentum (CM) [63, 71].

This formulation encapsulates EMA and CM, two cornerstones of gradient estimation, differing in how they weight the current gradient against historical trends. EMA through a balanced mean update, while CM aggressively incorporates the gradient direction. We dissect the nature of the two methods, quantified by the mean square error.

**Lemma 2.2.** For any gradient estimator  $\hat{g}_t = \mathcal{A}(g_1, \dots, g_t)$ , the estimation of the mean square error decomposes as:

$$\mathbb{E}[(\hat{g}_t - \nabla f(\theta_t))^2] = \underbrace{(\mathbb{E}[\hat{g}_t] - \nabla f(\theta_t))^2}_{\text{Bias}^2} + \underbrace{(\hat{g}_t - \mathbb{E}[\hat{g}_t])^2}_{\text{Variance}} \quad (2)$$

Lemma 2.2 establishes that the error in gradient estimation arises from two sources: bias, reflecting systematic deviation from the true gradient, and variance, capturing sensitivity to stochastic fluctuations. To explore how EMA and CM navigate this trade-off, we extend prior work on stochastic differential equations (SDEs) for vanilla SGD [70], reformulating momentum in continuous time.

**Theorem 2.3.** Consider the unified momentum estimator  $m(t)$  defined by the stochastic differential equation (SDE) from Lemma A.4, with solution given in Lemma A.6. Let the bias be defined relative to the expected true gradient:  $\text{Bias}(m(t)) = \mathbb{E}[m(t)] - \mathbb{E}[\nabla f(\theta(t))]$ . Assuming that the gradient  $\nabla f(\theta(t))$  is bounded and Lipschitz continuous, the asymptotic bounds (as  $t \rightarrow \infty$ ) for the bias and variance of  $m(t)$  as an estimator are given by:

$$\|\text{Bias}(m(t))\|^2 \leq \left( \frac{u^2 \alpha L G}{(1 - \beta)^3} + \frac{u^2 \alpha \sigma L}{\sqrt{2}(1 - \beta)^{2.5}} + \left( \frac{u}{1 - \beta} - 1 \right) G \right)^2, \quad (3)$$

where  $L$  is the Lipschitz constant,  $G$  bounds the gradient norm  $\|\nabla f(\theta(t))\|$ , and the second term inside the parenthesis explicitly captures the parameter-shift bias induced by the stochastic noise  $\sigma$ .

$$\text{Var}(m(t)) \leq \frac{u^2 \sigma^2}{1 - \beta} + \frac{2u^2 V^2}{(1 - \beta)^2}, \quad (4)$$

where  $\sigma^2$  is the total variance of the stochastic gradient noise, and  $V^2$  conservatively bounds the variance of the true gradient sequence, i.e.,  $\text{Var}(\nabla f(\theta(t))) \leq V^2$ .

Prior analyses typically regarded momentum-based gradient estimators as unbiased under the assumption that the parameter  $\theta_t$  remains stationary [11, 40, 71]. However, as  $\theta_t$  evolves over training, an additional *parameter-shift bias* arises. Theorem 2.3 explicitly quantifies this effect to fill a critical gap left by prior analyses, revealing that the stochastic noise  $\sigma$  itself exacerbates this shift.

Table 1. Bias and variance bounds for different momentum estimators. As  $\beta \rightarrow 1$ , static estimators suffer from either diverging bias or diverging variance, highlighting the fundamental trade-off.

Method	Bias Bound	Variance Bound	Limit as $\beta \rightarrow 1$
SGD ( $\beta = 0$ )	0 (Assuming $\alpha \rightarrow 0$ )	$\sigma^2 + 2V^2$	N/A
EMA ( $u = 1 - \beta$ )	$\left(\frac{\alpha LG}{1-\beta} + \frac{\alpha \sigma L}{\sqrt{2(1-\beta)}}\right)^2$	$(1-\beta)\sigma^2 + 2V^2$	Bias $\rightarrow \infty$ , Var $\rightarrow 2V^2$
CM ( $u = 1$ )	$\left(\frac{\alpha LG}{(1-\beta)^2} + \frac{\alpha L \sigma}{\sqrt{2(1-\beta)^2}} + \frac{\beta G}{1-\beta}\right)^2$	$\frac{\sigma^2}{1-\beta} + \frac{2V^2}{(1-\beta)^2}$	Bias $\rightarrow \infty$ , Var $\rightarrow \infty$

To illustrate the implications of this theorem, Tab. 1 summarizes the bias and variance bounds for standard momentum formulations and their asymptotic behaviors. For EMA ( $u = 1 - \beta$ ), the initialization bias strictly vanishes. EMA effectively acts as a low-pass filter: as  $\beta \rightarrow 1$ , it successfully damps high-frequency stochastic noise (variance drops), but at the severe expense of unbounded bias driven by outdated gradients and accumulated noise-drift. Consequently, EMA is unbiased only under strict, often unrealistic conditions in deep learning, such as the learning rate or curvature approaching zero ( $\alpha, L \rightarrow 0$ ). Conversely, CM ( $u = 1$ ) exhibits an aggressive momentum nature. As shown in Tab. 1, both its bias and variance diverge sharply as  $\beta \rightarrow 1$ , amplifying systematic lag and noise susceptibility (the complex mechanics of CM are further discussed in Appendix E.12).

Consider the other extreme: when  $\beta = 0$ , both methods reduce to vanilla SGD, minimizing momentum-induced bias but retaining the full base variance. These bounds expose a fundamental limitation of conventional optimization paradigms: static choices of  $u$  and  $\beta$  lock the estimator into a rigid, predetermined trade-off, rendering it ill-suited to the dynamic noise and curvature of objective functions.

This analysis reveals an inherent dilemma in momentum methods: structurally reducing variance inevitably amplifies bias, while minimizing bias exposes the estimator to higher variance. This naturally raises a fundamental question: Can we design an adaptive gain that dynamically reduces the dependence on momentum to minimize bias during low-variance phases, while heavily utilizing the momentum update to aggressively filter noise when variance is high?

### 3. Method

In the Sec. 2, we analyzed a challenge in momentum-based methods: how to effectively balance the bias and variance in gradient estimation. The analysis suggests that introducing a variable gain could help mitigate this dilemma by adaptively adjusting the contribution of past and current gradients. Motivated by this, and inspired by the minimum mean square error (MMSE) principle [37] in Optimal Linear Filter [36], we design a novel online gradient estimator tailored for stochastic optimization. In the following, we describe the estimator’s design and theoretical grounding.

---

#### Algorithm 1 SGDF: Online Filter Estimate Gradient (element-wise).

---

**Input:**  $\theta_0$ : initial parameter,  $f(\theta)$ : stochastic objective function

**Parameter:**  $\{\alpha_t\}_{t=1}^T$ : step size,  $\{\beta_1, \beta_2\}$ : attenuation coefficients,  $\{\varepsilon\}$ : numerical stability,  $\{\gamma\}$ : power scaling.

**Output:**  $\theta_T$ : resulting parameters.

```

1: Initialize:  $m_0 \leftarrow 0, s_0 \leftarrow 0$ 
2: while  $t \leq T$  do
3:    $g_t \leftarrow \nabla f_t(\theta_{t-1})$ 
4:    $m_t \leftarrow \beta_1 m_{t-1} + (1 - \beta_1) g_t$ 
5:    $s_t \leftarrow \beta_2 s_{t-1} + (1 - \beta_2)(g_t - m_t)^2$ 
6:    $\hat{m}_t \leftarrow \frac{m_t}{1 - \beta_1^t}, \hat{s}_t \leftarrow \frac{(1 - \beta_1)(1 - \beta_1^{2t}) s_t}{(1 + \beta_1)(1 - \beta_1^t)}$ 
7:    $K_t \leftarrow \frac{\hat{s}_t}{\hat{s}_t + (g_t - \hat{m}_t)^2 + \varepsilon}$ 
8:    $\hat{g}_t \leftarrow \hat{m}_t + K_t^\gamma (g_t - \hat{m}_t)$ 
9:    $\theta_t \leftarrow \theta_{t-1} - \alpha_t \hat{g}_t$ 
10: end while
11: return  $\theta_T$ 

```

---

### 3.1. SGDF General Introduction

In this subsection, we introduce the SGDF by building on principles of optimal gradient estimation. The detailed derivation of the SGDF is provided in Appendix B.1. The complete algorithm is summarized in Algorithm 1. Below, we summarize its key steps and motivation.

In stochastic gradient descent (SGD), the core challenge is to estimate a reliable gradient direction under noise. Suppose we are given a sequence of stochastic gradients  $\{g_i\}_{i=1}^t$ , our goal is to estimate a smoothed direction  $\hat{g}_t$  that effectively combines the current observation  $g_t$  and past gradients.

Inspired by the principle of minimum mean squared error (MMSE), we begin with a naive average:

$$\hat{g}_t = \frac{1}{t} \sum_{i=1}^{t-1} g_i + \frac{1}{t} g_t = \left(1 - \frac{1}{t}\right) \bar{g}_{1:t-1} + \frac{1}{t} g_t, \quad (5)$$

where  $\bar{g}_{1:t-1} = \frac{1}{t-1} \sum_{i=1}^{t-1} g_i$  denotes the averaging of the gradient under different model parameters. Then, we rewrite this as a linear interpolation:

$$\hat{g}_t = (1 - K_t) \bar{g}_{1:t-1} + K_t g_t, \quad \text{where } K_t = \frac{1}{t}. \quad (6)$$

To enable efficient computation, we replace  $\bar{g}_{1:t-1}$  with a bias-corrected momentum estimate  $\hat{m}_t$ , giving:

$$\hat{g}_t = \hat{m}_t + K_t (g_t - \hat{m}_t). \quad (7)$$

This form mirrors the update structure of an Optimal Linear Filter, which recursively refines estimates by weighting

prediction and observation with gain derived from their respective uncertainties. Here,  $K_t$  acts as a gain to balance trust between the prior  $\hat{m}_t$  and the observation  $g_t$ .

To find an optimal gain, we minimize the variance of  $\hat{g}_t$ , assuming  $\hat{m}_t$  and  $g_t$  are independent:

$$\text{Var}(\hat{g}_t) = (1 - K_t)^2 \text{Var}(\hat{m}_t) + K_t^2 \text{Var}(g_t). \quad (8)$$

Solving  $\frac{d}{dK_t} \text{Var}(\hat{g}_t) = 0$  yields the optimal gain:

$$K_t^* = \frac{\text{Var}(\hat{m}_t)}{\text{Var}(\hat{m}_t) + \text{Var}(g_t)}. \quad (9)$$

This form naturally down-weights noisy gradients and shifts the estimate toward the more reliable direction.

To estimate  $\text{Var}(\hat{m}_t)$  in practice, we follow [88] and compute the second-order moment  $s_t$  as the exponential moving average of  $(g_t - m_t)^2$ , applying Adam's bias correction [40] to obtain  $\hat{m}_t$  and  $\hat{s}_t$ . To further refine this estimate, we introduce a variance correction factor  $(1 - \beta_1)(1 - \beta_1^{2t})/(1 + \beta_1)$ , derived in Appendix B.2, which improves  $\hat{s}_t$  under independent gradients with bounded variance. The Fig. 11 in Appendix E.10 compares the performance with and without this correction factor, showing that this correction improves performance and supports our theoretical framework. Finally, to improve responsiveness in noisy regimes, we scale  $K_t$  by  $\gamma = \frac{1}{2}$ , an operation we formally justify in Appendix B.4 as mathematically equivalent to modulating the effective observation variance.

### 3.2. Fusion of Gaussian Distributions

Building on the MMSE-based principle in Sec. 3.1, we now seek a deeper statistical view of the SGDF. Specifically, we interpret the gain-controlled interpolation between the momentum estimate  $\hat{m}_t$  and the current gradient  $g_t$  as the fusion of two uncertain sources. This subsection presents both a variance-weighted linear view and a Bayesian interpretation, showing that SGDF performs optimal Gaussian fusion under the assumption of independent noise.

**Linear combination view.** Starting from the interpolation formula Eq. (7), we write the following:

$$\hat{g}_t = (1 - K_t)\hat{m}_t + K_t g_t. \quad (10)$$

We assume that the stochastic gradients can be modeled as Gaussian distributions [3, 49], i.e.,  $\hat{m}_t \sim \mathcal{N}(\mu_m, \sigma_m^2)$  and  $g_t \sim \mathcal{N}(\mu_g, \sigma_g^2)$ , with independence between the two sources.

Under these assumptions, the fused mean and variance are

$$\mathbb{E}[\hat{g}_t] = (1 - K_t)\mu_m + K_t\mu_g = \frac{\sigma_g^2\mu_m + \sigma_m^2\mu_g}{\sigma_m^2 + \sigma_g^2}, \quad (11)$$

$$\text{Var}(\hat{g}_t) = (1 - K_t)^2\sigma_m^2 + K_t^2\sigma_g^2 = \frac{\sigma_m^2\sigma_g^2}{\sigma_m^2 + \sigma_g^2}. \quad (12)$$

**Bayesian fusion view.** An equivalent result is obtained by multiplying the two Gaussian densities and normalising [22]:

$$p(\hat{g}_t) \propto \exp\left[-\frac{(\hat{g}_t - \mu_m)^2}{2\sigma_m^2} - \frac{(\hat{g}_t - \mu_g)^2}{2\sigma_g^2}\right], \quad (13)$$

which yields the posterior

$$\hat{g}_t \sim \mathcal{N}\left(\frac{\sigma_g^2\mu_m + \sigma_m^2\mu_g}{\sigma_m^2 + \sigma_g^2}, \frac{\sigma_m^2\sigma_g^2}{\sigma_m^2 + \sigma_g^2}\right). \quad (14)$$

The fused mean  $\mu_{\hat{g}_t}$  is a variance-weighted average of  $\mu_m$  and  $\mu_g$ , assigning greater weight to the source with lower variance to reflect higher confidence in more stable estimates. Similarly, the fused variance  $\sigma_{\hat{g}_t}^2$  is smaller than both  $\sigma_m^2$  and  $\sigma_g^2$ , indicating reduced uncertainty in the gradient estimate. This reduction results from the Optimal Linear Filter's optimality in minimizing the mean squared error. The full derivation is provided in Appendix B.3.

### 3.3. Convex and Non-convex Convergence Analysis

Finally, we provide the convergence property of SGDF as shown in Theorem 3.1 and Theorem 3.2. The assumptions are common and standard when analyzing the convergence of convex and non-convex functions via SGD-based methods [9, 40]. Proofs for convergence in convex and non-convex cases are provided in Appendix C and Appendix D, respectively.

**Theorem 3.1** (Convergence in Convex Optimization). *Assume that the objective functions  $f_t$  are convex. Let the gradients be bounded such that  $\|\nabla f_t\|_\infty \leq G_\infty$ , and the optimization domain be bounded with  $\|\theta_m - \theta_n\|_\infty \leq D_\infty$ . Suppose the momentum coefficient  $\beta_1, \beta_2 \in [0, 1)$  is constant, the power scaling factor follows  $\gamma_t = \gamma_0/\sqrt{t}$  for some  $\gamma_0 > 0$ . For a learning rate  $\alpha_t = \alpha/\sqrt{t}$ , SGDF achieves the following cumulative regret bound for all  $T \geq 1$ :*

$$R(T) \leq \sum_{i=1}^d \left( \frac{D_\infty^2}{2\alpha} + \alpha G_\infty^2 \frac{1 + \beta_1}{1 - \beta_1} \right) \sqrt{T} + \sum_{i=1}^d \frac{\beta_1 G_\infty D_\infty}{1 - \beta_1} \left( 2 + \sum_{t=1}^{T-1} |K_{t,i} - K_{t+1,i}| \right) \quad (15)$$

In Adam-type optimizers, decaying  $\beta_{1,t}$  to zero is crucial for convex analysis [40, 88]. By contrast, SGDF maintains constant coefficients  $(\beta_1, \beta_2)$  and delegates the stabilization role to the dynamic power-scaled gain  $K_t^{\gamma_t}$ . With  $\gamma_t = \mathcal{O}(1/\sqrt{t})$  that  $\sum |K_{t,i} - K_{t+1,i}| \leq \mathcal{O}(1) + \mathcal{O}(\sqrt{T})$ . Therefore, in the convex case, Theorem 3.1 establishes that the regret of SGDF is upper bounded by  $\mathcal{O}(\sqrt{T})$ .

**Theorem 3.2.** (Convergence for Non-convex Stochastic Optimization) *Assume Assumptions 1–4 hold and the step size is  $\alpha_t = \alpha/\sqrt{t}$ . For all  $T \geq 1$ , SGDF satisfies:*

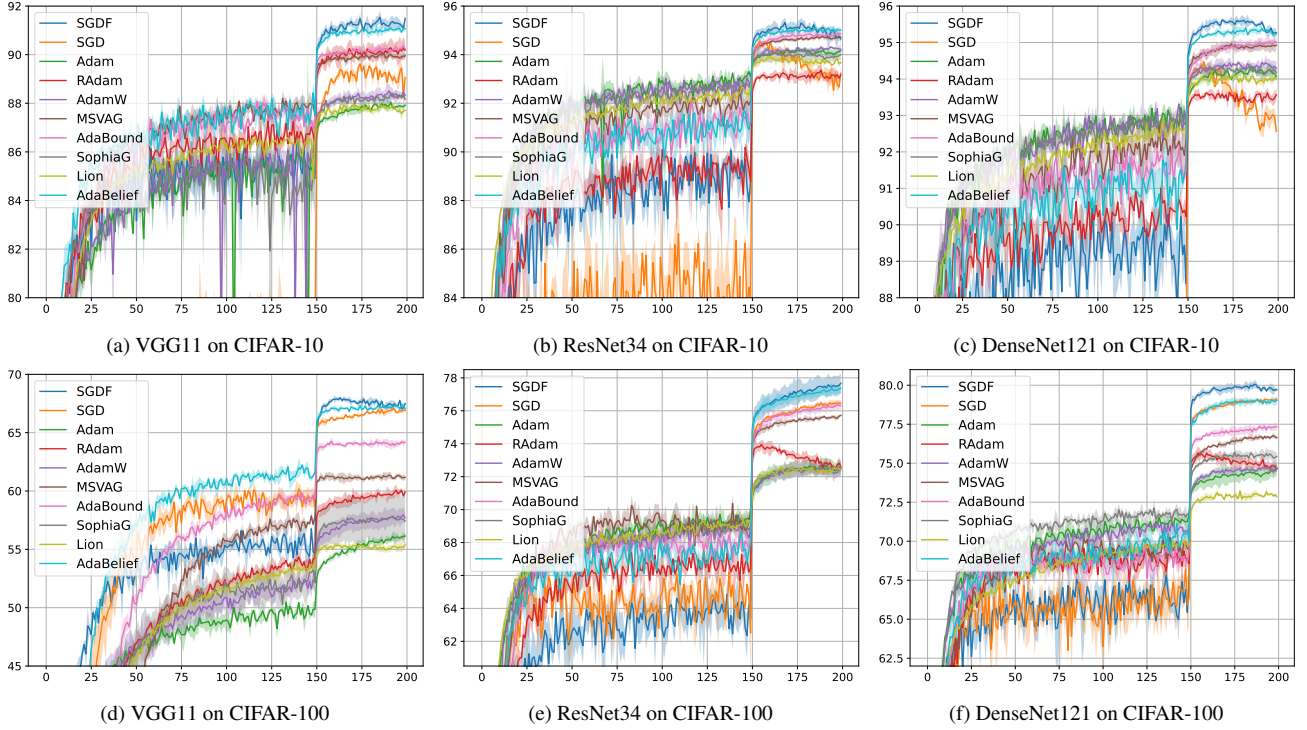


Figure 1. Test accuracy ( $[\mu \pm \sigma]$ ) on CIFAR.

1. **Bounded Variables:**  $\|\theta - \theta^*\|_2 \leq D$  (or  $\|\theta_i - \theta_i^*\|_2 \leq D_i$  for each dimension  $i$ ) for all  $\theta, \theta^*$ .
2. **Unbiased Noise:** The noise  $\zeta_t = g_t - \nabla f(\theta_t)$  satisfies  $\mathbb{E}[\zeta_t] = 0$ ,  $\mathbb{E}[\|\zeta_t\|_2^2] \leq \sigma^2$ , and  $\zeta_{t_1}, \zeta_{t_2}$  are independent for  $t_1 \neq t_2$ .
3. **Bounded Gradients:** Both the true and noisy gradients are uniformly bounded, i.e.,  $\|\nabla f(\theta_t)\|_2 \leq G$  and  $\|g_t\|_2 \leq G$  for all  $t \geq 1$ .
4. **Function Properties:**  $f$  is differentiable, lower bounded, and  $L$ -smooth, i.e.,  $\|\nabla f(x) - \nabla f(y)\|_2 \leq L\|x - y\|_2$  for all  $x, y$ .

The convergence guarantee is given by:

$$\mathbb{E}(T) \leq \frac{C_7 \alpha^2 (\log T + 1) + C_8}{\alpha \sqrt{T}}, \quad (16)$$

where  $\mathbb{E}(T) = \min_{t=1, \dots, T} \mathbb{E}_{t-1}[\|\nabla f(\theta_t)\|_2^2]$  is the minimum expected squared gradient norm,  $\alpha$  is the initial learning rate, and  $C_7, C_8$  are constants independent of  $T$  ( $C_7$  also independent of  $d$ ). The expectation is taken over all randomness in  $\{g_t\}$ .

Theorem 3.2 shows that the convergence rate of SGDF in the non-convex setting is  $\mathcal{O}(\log T / \sqrt{T})$ , which matches the rates established for Adam-type optimizers [9, 64]. In our analysis, the terms involving the estimated gain  $K_t$  were upper bounded by their maximal possible values to simplify the derivation of the final bound. We adopted the general

$L$ -smoothness assumption to obtain this rate. Furthermore, if a fixed decay schedule  $\alpha / \sqrt{T}$  is used, where  $T$  represents the total number of iterations, instead of  $\alpha / \sqrt{t}$  for infinite iterations, the convergence rate improves to  $\mathcal{O}(1 / \sqrt{T})$  [73].

## 4. Experiments

### 4.1. Empirical Evaluation

In this study, we focus on the following tasks: **Image Classification.** We employed the VGG [69], ResNet [30], and DenseNet [33] models for image classification tasks on the CIFAR dataset [41]. The major difference between these three network architectures is the residual connectivity, which we will discuss in Sec. 4.2. We evaluated and compared the performance of SGDF with other optimizers such as SGD, Adam, RAdam [49], AdamW [50], MSVAG [1], Adabound [52], Sophia [48], Lion [10], and AdaBelief [88], all of which were implemented based on the official PyTorch. Additionally, we further tested the performance of SGDF on the ImageNet dataset [15] using the ResNet model. **Object Detection.** Object detection was performed on the PASCAL VOC dataset [21] using Faster-RCNN [65] integrated with FPN. **Post-training in ViT.** We test the performance of transformer architecture networks by post-training ViT [16] on six benchmark dataset. **More experimental results are summarized in Appendix E.**

Table 2. Top-1, 5 accuracy (%) of ResNet18 on ImageNet. \* † ‡ is reported in [8, 49, 88].

Method	SGDF	SGD	AdaBelief	PAdam	AdaBound	Yogi	MSVAG	Adam	RAdam	AdamW
Top-1	<b>70.51</b> $\pm 0.05$	70.23 <sup>†</sup>	70.08*	70.07 <sup>†</sup>	68.13 <sup>†</sup>	68.23 <sup>†</sup>	65.99*	63.79 <sup>†</sup> (66.54 <sup>‡</sup> )	67.62 <sup>‡</sup>	67.93 <sup>†</sup>
Top-5	<b>89.69</b> $\pm 0.16$	89.40 <sup>†</sup>	-	89.47 <sup>†</sup>	88.55 <sup>†</sup>	88.59 <sup>†</sup>	-	85.61 <sup>†</sup>	-	88.47 <sup>†</sup>

Table 3. Comparison of top-1 accuracy (%) across different model variants and optimizers on the ImageNet classification.

Model	VGG11	VGG13	ResNet34	ResNet50	DenseNet121	DenseNet161
SGD <sup>1</sup>	70.37	71.58	73.31	76.13	74.43	77.13
SGDF	<b>71.34</b> $\pm 0.21$	<b>72.74</b> $\pm 0.07$	<b>74.07</b> $\pm 0.21$	<b>76.72</b> $\pm 0.09$	<b>75.75</b> $\pm 0.09$	<b>78.34</b> $\pm 0.08$

**Hyperparameter tuning.** Following [88], we delved deep into the optimal hyperparameter settings for our experiments.

- *SGDF*: We followed to Adam’s original parameter values except learning rate:  $\alpha = 0.5$ ,  $\beta_1 = 0.9$ ,  $\beta_2 = 0.999$ ,  $\epsilon = 10^{-8}$ . The learning rate was searched same as SGD research set.
- *SGD*: We set the momentum 0.9, which is the default for networks like ResNet and DenseNet. The learning rate was searched in the set  $\{10.0, 1.0, 0.5, 0.1, 0.01, 0.001\}$ .
- *Adam, RAdam, MSVAG, AdaBound, AdaBelief*: Exploring the hyperparameter space, we tested  $\beta_1$  values in  $\{0.5, 0.6, 0.7, 0.8, 0.9\}$ , examined  $\alpha$  as in SGD, while keeping other parameters to their literary defaults.
- *AdamW, SophiaG, Lion*: Following Adam’s parameter search pattern, we fixed weight decay at  $5 \times 10^{-4}$ ; yet for AdamW, whose optimal decay often exceeds norms [50], we ranged weight decay over  $\{10^{-4}, 5 \times 10^{-4}, 10^{-3}, 10^{-2}, 10^{-1}\}$ .
- *SophiaG, Lion*: We searched for the learning rate among  $\{10^{-3}, 10^{-4}, 10^{-5}\}$  and adjusted Lion’s learning rate [48]. Following [10, 48], we set  $\beta_1=0.965$ , 0.9 and default parameters  $\beta_2=0.99$ .

**CIFAR-10/100 Experiments.** We trained on the CIFAR-10 and CIFAR-100 datasets using the VGG, ResNet and DenseNet models and access the performance of the SGDF optimizer. In these experiments, we employ basic data augmentation techniques such as random horizontal flip and random cropping. The results represent the mean and standard deviation of 3 runs by fixing random seeds  $\{0, 1, 2\}$ .

As Fig. 1 shows, it is evident that the SGDF optimizer exhibited convergence speeds comparable to adaptive optimization algorithms. Additionally, SGDF’s final test set accuracy was better than others. These consistent results across multiple architectures indicate that SGDF can effectively adapt to networks of varying depths and complexities. We summarize the numerical results for the mean best test accuracies, standard deviations, and parameter details in Appendix E.1 (Tab. 8 and Tab. 9).

**ImageNet Experiments.** We applied standard data augmentation techniques, including random cropping and random horizontal flipping [88], using random seeds  $\{0, 1, 2\}$ . To eliminate the effect of stepwise learning rate schedules, we adopted cosine learning rate decay as suggested by [10, 86]. Following [8, 88], ResNet18 was trained for 100 epochs to compare with popular optimizers using their best-reported results [8, 49, 88].

We further trained additional architectures for 90 epochs following the experimental setup of GAM [86] to benchmark against SGD, including VGG11/13 (with BN), ResNet34/50, and DenseNet121/161. Our results in Tab. 2 and Tab. 3 show that SGDF consistently outperforms SGD. These results highlight SGDF’s robustness and scalability across networks of different capacities. Moreover, the optimizer maintained smooth convergence behavior throughout training, demonstrating strong generalization on large-scale datasets. Detailed training/test curves and hyperparameter settings are provided in Appendix E.2 (Fig. 6 and Tab. 10).

Table 4. The mAP on PASCAL VOC. \* † is reported in [81, 88].

Method	SGDF	AdaBelief	EAdam	SGD	Adam	AdamW	RAdam
mAP	<b>83.81</b>	81.02*	80.62 <sup>†</sup>	80.43	78.67	78.48	75.21

**Object Detection.** We conducted object detection experiments on the PASCAL VOC dataset [21]. The model used in these experiments was pre-trained on the COCO dataset [47], obtained from the official website. We trained this model on the VOC2007 and VOC2012 train-val dataset (17K) and evaluated it on the VOC2007 test dataset (5K). The utilized model was Faster-RCNN [65] with FPN, and the backbone was ResNet50 [30]. Results are summarized in Tab. 4. To facilitate result reproduction, we provide the parameter table for this subpart in Appendix E.3 Tab. 11. As expected, SGDF outperforms other methods in detection accuracy and stability. These results demonstrate the efficiency and robustness of our method in complex detection tasks, highlighting its consistent optimization behavior across vision architectures.

<sup>1</sup>Results from PyTorch official pre-trained models.

Table 5. Post-training in ViT. We report Top-1 accuracy (%).

Model	Method	CIFAR-10	CIFAR-100	Oxford-IIIT-Pets	Oxford Flowers-102	Food101	ImageNet
ViT-B/32	SGD	98.71 $\pm$ 0.03	90.62 $\pm$ 0.07	89.71 $\pm$ 0.32	96.79 $\pm$ 0.29	88.56 $\pm$ 0.05	81.42 $\pm$ 0.04
	SGDF	<b>98.74</b> $\pm$ 0.10	<b>91.44</b> $\pm$ 0.13	<b>92.68</b> $\pm$ 0.04	<b>97.17</b> $\pm$ 0.47	<b>89.35</b> $\pm$ 0.09	<b>81.52</b> $\pm$ 0.02
ViT-L/32	SGD	98.73 $\pm$ 0.05	91.30 $\pm$ 0.17	85.21 $\pm$ 0.39	96.52 $\pm$ 0.15	89.13 $\pm$ 0.20	81.28 $\pm$ 0.04
	SGDF	<b>98.83</b> $\pm$ 0.04	<b>92.20</b> $\pm$ 0.14	<b>91.96</b> $\pm$ 0.18	<b>96.79</b> $\pm$ 0.12	<b>90.04</b> $\pm$ 0.08	<b>81.38</b> $\pm$ 0.01

**Post-training in ViT.** To evaluate SGDF, we conducted ViT post-training by following the standard protocol in [16], which serves as a critical benchmark where SGD with momentum sets the state-of-the-art. We tested on six datasets (CIFAR-10/100, Oxford-IIIT-Pets [61], Oxford Flowers-102 [59], Food101 [5], ImageNet-1K) using ViT-B/32 and ViT-L/32 that were pre-trained on ImageNet-21K. Consistent with ViT’s original setup, the MLP classification head was replaced to match dataset categories, while backbone weights remained frozen to preserve pre-trained representations. We up-sized images to  $384 \times 384$  with 2D-interpolated position encodings and used cosine learning rate decay, no weight decay, batch size 512, and gradient clipping (norm 1), all of which faithfully replicate ViT’s training details. All runs were trained for 10 epochs with seed  $\{0, 1, 2\}$ . Results in Tab. 5 and hyperparameters to Appendix E.6 Tab. 15 validate SGDF’s performance against the established SGD.

## 4.2. Extensibility of Filter-Estimated Gradients

Beyond vanilla SGD, our optimal linear filter serves as a plug-and-play module that enhances first-moment gradient estimates across diverse optimization frameworks. To demonstrate its broad compatibility, we integrate it with Adam, Sign-based optimizers [3], and the Muon [35].

Table 6. Accuracy comparison between Adam and Filter-Adam.

Model	VGG11	ResNet34	DenseNet121
Filter-Adam	<b>62.64</b>	<b>73.98</b>	<b>74.89</b>
Vanilla-Adam	56.73	72.34	<b>74.89</b>

**Integration with Adam.** We first evaluated our filter’s integration with Adam by substituting the first-moment gradient estimates in the vanilla optimizer with our filtered counterparts. As shown in Tab. 6 (with detailed test curves in Appendix E.11 Fig. 14), experiments on the CIFAR-100 dataset reveal distinct behaviors across network architectures. For networks without Batch Normalization (BN) like VGG, the filter significantly improves performance by providing more accurate gradient estimates and reducing noise-induced errors. For architectures like ResNet and DenseNet that inherently promote stable gradient updates through BN and residual/dense connections, the filter still maintains highly competitive performance, albeit with less pronounced marginal gains. This structural dynamic effectively explains the variance in improvements across architectures.

**Extension to Sign-based Optimizers.** To further evaluate the robustness of our gradient estimation in different update paradigms, we tested a sign-based variant. Specifically, we updated the parameters using the sign of our filtered gradient ( $\text{sign}(\hat{g}_t)$ ) [3]. We evaluated this *Sign SGDF* on diffusion models, specifically DiT/SiT-Base (130M parameters) [54, 62] in ImageNet. For a fair comparison, we aligned all hyperparameters with Adam and used an unscaled  $K_t$ . As shown in Fig. 2, Sign SGDF converges significantly faster and achieves a better FID score than the Adam baseline, proving that our filter effectively captures the true gradient direction even when the magnitude is discarded.

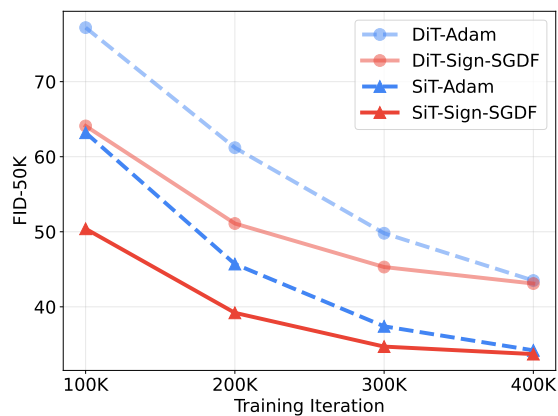


Figure 2. Convergence comparison between Sign SGDF and Adam.

**Compatibility with Muon.** Finally, we explored the compatibility of our filter with Muon, a recently proposed optimizer that relies on orthogonal momentum. We conducted a preliminary experiment on DiT-B/4 by replacing Muon’s standard momentum formulation with our filter-estimated gradient. As presented in Tab. 7, this integration yields superior results compared to the standard Adam baseline across multiple generation metrics at 400K training iterations. This underscores the potential of our optimal linear filter to serve as a fundamental gradient refinement step for state-of-the-art training recipes.

Table 7. Compatibility of filter-estimated gradient with Muon.

Method	FID↓	sFID↓	IS↑	Pre.↑	Rec.↑
Adam	68.32	13.63	20.51	0.36	0.53
Muon + SGDF	<b>64.24</b>	<b>12.43</b>	<b>22.26</b>	<b>0.37</b>	<b>0.59</b>

### 4.3. Top Eigenvalues of Hessian and Hessian Trace

The success of optimization algorithms in deep learning depends on both minimizing training loss and the quality of the solutions they find. So we numerically verified the hessian matrix properties between the different methods. We computed the Hessian spectrum of ResNet-18 trained on the CIFAR-100 dataset for 200 epochs. These experiments ensure that all methods achieve similar results on the training set. We employed power iteration [78] to compute the top eigenvalues of Hessian and Hutchinson’s method [79] to compute the Hessian trace. Histograms illustrating the distribution of the top 50 Hessian eigenvalues for each optimization method are presented in Fig. 3. SGDF brings lower eigenvalue and trace of the hessian matrix, which explains the fact that SGDF demonstrates better performance than SGD as the categorization category increases.

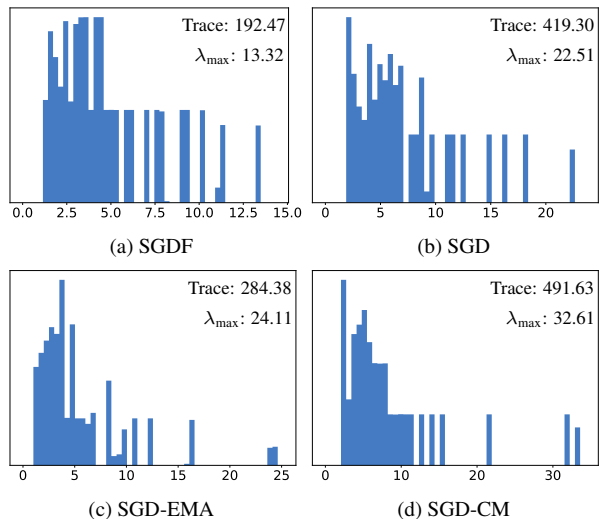


Figure 3. Histogram of Top 50 Hessian Eigenvalues. Lower values indicate better performance on the test dataset.

## 5. Related Works

Early optimization efforts focused on variance reduction [1, 14, 34, 68] and adaptive learning rates [17, 19, 83]. However, standard adaptive optimizers often converge to sharp minima with weak generalization in high-dimensional non-convex landscapes [12, 29, 51, 74, 75]. This motivated geometry-aware regularization, such as Sharpness-Aware Minimization (SAM) and its variants [23, 86, 89], alongside momentum tuning strategies like Adaptive Inertia [76], to explicitly penalize sharpness and escape sharp basins.

Beyond loss geometry, recent studies highlight the critical role of dynamically balancing gradient bias and variance for stable learning [25, 28]. To achieve this, parallel works manipulate updates directly: Quasi-Hyperbolic Momentum (QHM) [53] introduces a static interpolation between cur-

rent gradients and momentum, while Grokfast [44] heuristically amplifies low-frequency gradient signals. Alternatively, methods based on second-order approximations or Kalman filtering [13, 26, 36, 48, 60, 72, 80] refine updates using local curvature or Fisher information. While principled, these techniques significantly inflate computational overhead and parameter complexity, limiting their practical scalability.

In contrast, we formulate momentum fundamentally as an online filtering process to rigorously resolve the bias-variance dilemma without the heavy overhead of curvature estimation. Unlike QHM’s static interpolation or Grokfast’s heuristic frequency scaling, SGDF fuses past and current gradients via an optimal, time-varying gain that adaptively minimizes mean-squared estimation error. Consequently, SGDF achieves noise-aware, stable updates through a lightweight statistical design, ensuring principled gradient refinement at no additional computational cost.

## 6. Discussion and Future Work

Our SDE framework readily accommodates existing continuous-time analyses [46, 70, 76]. A compelling theoretical direction is coupling first-order gradient statistics with zeroth-order loss moments via Itô’s lemma, establishing unified bounds that link local stability to global generalization in non-convex settings. Practically, while SGDF currently requires a memory footprint comparable to standard Adam, integrating block-wise or reduced-state approximations, which are inspired by recent memory-efficient designs like Adam-mini [87], presents a highly promising avenue to minimize overhead. Together, these theoretical and empirical extensions will rigorously refine adaptive optimization for large-scale learning systems.

## 7. Conclusion

In this work, we introduced SGDF, a novel optimizer rooted in statistical signal processing. By dynamically minimizing the mean-squared estimation error, SGDF balances gradient bias and variance, overcoming the suboptimal tradeoffs of traditional momentum to yield highly accurate first-moment estimates. Extensive experiments across diverse architectures confirm that this principled approach achieves a superior tradeoff between convergence speed and generalization compared to current state-of-the-art optimizers.

## Acknowledgement

The authors gratefully acknowledge the financial support provided by the Scientific Research Project of Liaoning Provincial Department of Education under Grant LJ212510149013. Rui Yu received no funding in support of this work. Zhipeng Yao thanks to Aram Davtyan and Prof. Dr. Paolo Favaro in the Computer Vision Group at the University of Bern for discussing and improving the paper.

## References

- [1] Lukas Balles and Philipp Hennig. Dissecting adam: The sign, magnitude and variance of stochastic gradients. In *International Conference on Machine Learning*, pages 404–413. PMLR, 2018. 5, 8
- [2] Yoshua Bengio and Yann Lecun. Scaling learning algorithms towards ai. 2007. 1
- [3] Jeremy Bernstein, Yu-Xiang Wang, Kamyar Azizzadenesheli, and Animashree Anandkumar. signsgd: Compressed optimisation for non-convex problems. In *International Conference on Machine Learning*, pages 560–569. PMLR, 2018. 4, 7, 44
- [4] Jeremy Bernstein, Arash Vahdat, Yisong Yue, and Ming-Yu Liu. On the distance between two neural networks and the stability of learning. *Advances in Neural Information Processing Systems*, 33:21370–21381, 2020. 38
- [5] Lukas Bossard, Matthieu Guillaumin, and Luc Van Gool. Food-101—mining discriminative components with random forests. In *Computer vision—ECCV 2014: 13th European conference, Zurich, Switzerland, September 6–12, 2014, proceedings, part VI 13*, pages 446–461. Springer, 2014. 7, 40
- [6] Léon Bottou, Frank E Curtis, and Jorge Nocedal. Optimization methods for large-scale machine learning. *SIAM review*, 60(2):223–311, 2018. 1, 44
- [7] Nisha Chandramoorthy, Andreas Loukas, Khashayar Gatmiry, and Stefanie Jegelka. On the generalization of learning algorithms that do not converge. *Advances in Neural Information Processing Systems*, 35:34241–34257, 2022. 1
- [8] Jinghui Chen, Dongruo Zhou, Yiqi Tang, Ziyang Yang, Yuan Cao, and Quanquan Gu. Closing the generalization gap of adaptive gradient methods in training deep neural networks. *arXiv preprint arXiv:1806.06763*, 2018. 1, 6
- [9] Xiangyi Chen, Sijia Liu, Ruoyu Sun, and Mingyi Hong. On the convergence of a class of adam-type algorithms for non-convex optimization. In *International Conference on Learning Representations*, 2019. 4, 5
- [10] Xiangning Chen, Chen Liang, Da Huang, Esteban Real, Kaiyuan Wang, Yao Liu, Hieu Pham, Xuanyi Dong, Thang Luong, Cho-Jui Hsieh, et al. Symbolic discovery of optimization algorithms. *arXiv preprint arXiv:2302.06675*, 2023. 5, 6
- [11] Ashok Cutkosky and Harsh Mehta. Momentum improves normalized sgd. In *International conference on machine learning*, pages 2260–2268. PMLR, 2020. 2, 44
- [12] Yann Dauphin, Razvan Pascanu, Caglar Gulcehre, Kyunghyun Cho, Surya Ganguli, and Yoshua Bengio. Identifying and attacking the saddle point problem in high-dimensional non-convex optimization. *MIT Press*, 2014. 8
- [13] Aram Davtyan, Sepehr Sameni, Llukman Cerkezi, Givi Meishvili, Adam Bielski, and Paolo Favaro. Koala: A kalman optimization algorithm with loss adaptivity. In *Proceedings of the AAAI Conference on Artificial Intelligence*, pages 6471–6479, 2022. 8
- [14] Aaron Defazio, Francis Bach, and Simon Lacoste-Julien. Saga: A fast incremental gradient method with support for non-strongly convex composite objectives. In *Advances in Neural Information Processing Systems*, pages 1646–1654, 2014. 8
- [15] Jia Deng, Wei Dong, Richard Socher, Li-Jia Li, Kai Li, and Li Fei-Fei. Imagenet: A large-scale hierarchical image database. In *IEEE Conference on Computer Vision and Pattern Recognition*, 2009. 5, 35
- [16] Alexey Dosovitskiy, Lucas Beyer, Alexander Kolesnikov, Dirk Weissenborn, Xiaohua Zhai, Thomas Unterthiner, Mostafa Dehghani, Matthias Minderer, Georg Heigold, Sylvain Gelly, et al. An image is worth 16x16 words: Transformers for image recognition at scale. *arXiv preprint arXiv:2010.11929*, 2020. 5, 7, 40
- [17] Timothy Dozat. Incorporating nesterov momentum into adam. *International Conference on Learning Representations Workshop, 2016*, 2016. 1, 8, 43
- [18] Simon Du and Jason Lee. On the power of overparametrization in neural networks with quadratic activation. In *International conference on machine learning*, pages 1329–1338. PMLR, 2018. 1
- [19] Duchi, John, Hazan, Elad, Singer, and Yoram. Adaptive subgradient methods for online learning and stochastic optimization. *Journal of Machine Learning Research*, 2011. 8
- [20] John Duchi and Hongseok Namkoong. Variance-based regularization with convex objectives. *Journal of Machine Learning Research*, 20(68):1–55, 2019. 1
- [21] Mark Everingham, Luc Van Gool, Christopher KI Williams, John Winn, and Andrew Zisserman. The pascal visual object classes (voc) challenge. *International journal of computer vision*, 88(2):303–338, 2010. 5, 6, 36
- [22] Ramsey Faragher. Understanding the basis of the kalman filter via a simple and intuitive derivation [lecture notes]. *IEEE Signal processing magazine*, 29(5):128–132, 2012. 4, 20
- [23] Pierre Foret et al. Sharpness-aware minimization for efficiently improving generalization. In *ICLR*, 2021. spotlight. 8
- [24] Stuart Geman, Elie Bienenstock, and René Doursat. Neural networks and the bias/variance dilemma. *Neural Computation*, 4(1):1–58, 2014. 1
- [25] Arna Ghosh, Yuhua Helena Liu, Guillaume Lajoie, Konrad Kording, and Blake Aaron Richards. How gradient estimator variance and bias impact learning in neural networks. In *The Eleventh International Conference on Learning Representations*, 2022. 8
- [26] Damien Martins Gomes, Yanlei Zhang, Eugene Belilovsky, Guy Wolf, and Mahdi S Hosseini. Adafisher: Adaptive second order optimization via fisher information. *arXiv preprint arXiv:2405.16397*, 2024. 8
- [27] Ian Goodfellow, Yoshua Bengio, and Aaron Courville. *Deep learning*. MIT Press, 2016. 1
- [28] Mingming Ha, Xuwen Tao, Wenfang Lin, Qiongxu Ma, Wujiang Xu, and Linxun Chen. Fine-grained dynamic framework for bias-variance joint optimization on data missing not at random. *Advances in Neural Information Processing Systems*, 37:104010–104034, 2024. 8
- [29] Moritz Hardt, Benjamin Recht, and Yoram Singer. Train faster, generalize better: Stability of stochastic gradient descent. *Mathematics*, 2015. 8

- [30] Kaiming He, Xiangyu Zhang, Shaoqing Ren, and Jian Sun. Deep residual learning for image recognition. In *Proceedings of the IEEE conference on computer vision and pattern recognition*, pages 770–778, 2016. [5](#), [6](#), [35](#), [36](#)
- [31] Martin Heusel, Hubert Ramsauer, Thomas Unterthiner, Bernhard Nessler, and Sepp Hochreiter. Gans trained by a two time-scale update rule converge to a local nash equilibrium. *Advances in neural information processing systems*, 30, 2017. [38](#)
- [32] Geoffrey Hinton, Nitish Srivastava, and Kevin Swersky. Neural networks for machine learning lecture 6a overview of mini-batch gradient descent. *Cited on*, 14(8):2, 2012. [1](#)
- [33] Gao Huang, Zhuang Liu, Laurens Van Der Maaten, and Kilian Q Weinberger. Densely connected convolutional networks. In *Proceedings of the IEEE conference on computer vision and pattern recognition*, pages 4700–4708, 2017. [5](#), [35](#)
- [34] Rie Johnson and Tong Zhang. Accelerating stochastic gradient descent using predictive variance reduction. *Advances in neural information processing systems*, 26, 2013. [8](#)
- [35] Keller Jordan, Yuchen Jin, Vlado Boza, Jiacheng You, Franz Cesista, Laker Newhouse, and Jeremy Bernstein. Muon: An optimizer for hidden layers in neural networks, 2024. [7](#)
- [36] R. E. Kalman. A new approach to linear filtering and prediction problems. *Journal of Basic Engineering*, 1960. [3](#), [8](#)
- [37] Steven M Kay. *Fundamentals of Statistical Signal Processing: Estimation Theory*. Prentice-Hall, Inc., 1993. [3](#)
- [38] Nitish Shirish Keskar and Richard Socher. Improving generalization performance by switching from adam to sgd. *arXiv preprint arXiv:1712.07628*, 2017. [1](#)
- [39] Nitish Shirish Keskar, Dheevatsa Mudigere, Jorge Nocedal, Mikhail Smelyanskiy, and Ping Tak Peter Tang. On large-batch training for deep learning: Generalization gap and sharp minima. In *International Conference on Learning Representations*, 2022. [1](#)
- [40] Diederik P Kingma and Jimmy Ba. Adam: A method for stochastic optimization. *arXiv preprint arXiv:1412.6980*, 2014. [1](#), [2](#), [4](#), [35](#)
- [41] Alex Krizhevsky, Geoffrey Hinton, et al. Learning multiple layers of features from tiny images. 2009. [5](#), [35](#)
- [42] Frederik Kunstner, Jacques Chen, Jonathan Wilder Lavington, and Mark Schmidt. Noise is not the main factor behind the gap between sgd and adam on transformers, but sign descent might be. *arXiv preprint arXiv:2304.13960*, 2023. [44](#)
- [43] Guillaume Leclerc and Aleksander Madry. The two regimes of deep network training. *arXiv preprint arXiv:2002.10376*, 2020. [44](#)
- [44] Jaerin Lee, Bong Gyun Kang, Kihoon Kim, and Kyoung Mu Lee. Grokfast: Accelerated grokking by amplifying slow gradients. *arXiv preprint arXiv:2405.20233*, 2024. [8](#)
- [45] Hao Li, Zheng Xu, Gavin Taylor, Christoph Studer, and Tom Goldstein. Visualizing the loss landscape of neural nets. *Advances in neural information processing systems*, 31, 2018. [41](#)
- [46] Qianxiao Li, Cheng Tai, and E Weinan. Stochastic modified equations and dynamics of stochastic gradient algorithms i: Mathematical foundations. *Journal of Machine Learning Research*, 20(40):1–47, 2019. [8](#), [13](#)
- [47] Tsung-Yi Lin, Michael Maire, Serge Belongie, James Hays, Pietro Perona, Deva Ramanan, Piotr Dollár, and C. Lawrence Zitnick. Microsoft coco: Common objects in context. *European Conference on Computer Vision (ECCV)*, 2014. [6](#), [36](#)
- [48] Hong Liu, Zhiyuan Li, David Hall, Percy Liang, and Tengyu Ma. Sophia: A scalable stochastic second-order optimizer for language model pre-training. *arXiv preprint arXiv:2305.14342*, 2023. [5](#), [6](#), [8](#)
- [49] Liyuan Liu, Haoming Jiang, Pengcheng He, Weizhu Chen, Xiaodong Liu, Jianfeng Gao, and Jiawei Han. On the variance of the adaptive learning rate and beyond. In *International Conference on Learning Representations*, 2020. [1](#), [4](#), [5](#), [6](#), [35](#), [36](#), [44](#)
- [50] Ilya Loshchilov and Frank Hutter. Decoupled weight decay regularization. *arXiv preprint arXiv:1711.05101*, 2017. [5](#), [6](#), [35](#)
- [51] Aurelien Lucchi, Frank Proske, Antonio Orvieto, Francis Bach, and Hans Kersting. On the theoretical properties of noise correlation in stochastic optimization. *Advances in Neural Information Processing Systems*, 35:14261–14273, 2022. [8](#)
- [52] Liangchen Luo, Yuanhao Xiong, Yan Liu, and Xu Sun. Adaptive gradient methods with dynamic bound of learning rate. *arXiv preprint arXiv:1902.09843*, 2019. [1](#), [5](#)
- [53] Jerry Ma and Denis Yarats. Quasi-hyperbolic momentum and adam for deep learning. *arXiv preprint arXiv:1810.06801*, 2018. [8](#)
- [54] Nanye Ma, Mark Goldstein, Michael S Albergo, Nicholas M Boffi, Eric Vanden-Eijnden, and Saining Xie. Sit: Exploring flow and diffusion-based generative models with scalable interpolant transformers. In *European Conference on Computer Vision*, pages 23–40. Springer, 2024. [7](#)
- [55] Xiaolei Ma, Zhimin Tao, Yin Hai Wang, Haiyang Yu, and Yunpeng Wang. Long short-term memory neural network for traffic speed prediction using remote microwave sensor data. *Transportation Research Part C: Emerging Technologies*, 54: 187–197, 2015. [39](#)
- [56] Mary Ann Marcinkiewicz. Building a large annotated corpus of english: The penn treebank. *Using Large Corpora*, 273: 31, 1994. [39](#)
- [57] Robbins Sutton Monro. a stochastic approximation method. *Annals of Mathematical Statistics*, 22(3):400–407, 1951. [1](#), [35](#)
- [58] Han Nguyen, Hai Pham, Sashank J Reddi, and Barnabás Póczos. On the algorithmic stability and generalization of adaptive optimization methods. *arXiv preprint arXiv:2211.03970*, 2022. [1](#)
- [59] Maria-Elena Nilsback and Andrew Zisserman. Automated flower classification over a large number of classes. In *2008 Sixth Indian conference on computer vision, graphics & image processing*, pages 722–729. IEEE, 2008. [7](#), [40](#)
- [60] Yann Ollivier. The extended kalman filter is a natural gradient descent in trajectory space. *arXiv: Optimization and Control*, 2019. [8](#)
- [61] Omkar M Parkhi, Andrea Vedaldi, Andrew Zisserman, and CV Jawahar. Cats and dogs. In *2012 IEEE conference on*

- computer vision and pattern recognition*, pages 3498–3505. IEEE, 2012. 7, 40
- [62] William Peebles and Saining Xie. Scalable diffusion models with transformers. In *Proceedings of the IEEE/CVF International Conference on Computer Vision*, pages 4195–4205, 2023. 7
- [63] Boris T Polyak. Some methods of speeding up the convergence of iteration methods. *Ussr computational mathematics and mathematical physics*, 4(5):1–17, 1964. 1, 2, 12
- [64] Sashank J Reddi, Satyen Kale, and Sanjiv Kumar. On the convergence of adam and beyond. In *International Conference on Learning Representations*, 2018. 5
- [65] Shaoqing Ren, Kaiming He, Ross Girshick, and Jian Sun. Faster r-cnn: Towards real-time object detection with region proposal networks. *Neural Information Processing Systems (NIPS)*, 2015. 5, 6, 36
- [66] Sebastian Ruder. An overview of gradient descent optimization algorithms. *arXiv preprint arXiv:1609.04747*, 2016. 1
- [67] Tim Salimans, Ian Goodfellow, Wojciech Zaremba, Vicki Cheung, Alec Radford, and Xi Chen. Improved techniques for training gans. *Advances in neural information processing systems*, 29, 2016. 38
- [68] Mark Schmidt, Nicolas Le Roux, and Francis Bach. Minimizing finite sums with the stochastic average gradient. *Mathematical Programming*, 162(1):83–112, 2017. 8
- [69] Karen Simonyan and Andrew Zisserman. Very deep convolutional networks for large-scale image recognition. *Computer Science*, 2014. 5, 35, 42
- [70] Mandt Stephan, Matthew D Hoffman, David M Blei, et al. Stochastic gradient descent as approximate bayesian inference. *Journal of Machine Learning Research*, 18(134):1–35, 2017. 2, 8, 12, 13
- [71] Ilya Sutskever, James Martens, George Dahl, and Geoffrey Hinton. On the importance of initialization and momentum in deep learning. In *International conference on machine learning*, pages 1139–1147. PMLR, 2013. 1, 2, 12
- [72] James Vuckovic. Kalman gradient descent: Adaptive variance reduction in stochastic optimization. *ArXiv*, 2018. 8
- [73] Bohan Wang, Jingwen Fu, Huishuai Zhang, Nanning Zheng, and Wei Chen. Closing the gap between the upper bound and lower bound of adam’s iteration complexity. *Advances in Neural Information Processing Systems*, 36:39006–39032, 2023. 5
- [74] Ashia C Wilson, Rebecca Roelofs, Mitchell Stern, Nati Srebro, and Benjamin Recht. The marginal value of adaptive gradient methods in machine learning. *Advances in neural information processing systems*, 30, 2017. 8
- [75] Zeke Xie, Qian Yuan Tang, Yunfeng Cai, Mingming Sun, and Ping Li. On the power-law spectrum in deep learning: A bridge to protein science. *arXiv preprint arXiv:2201.13011*, 2, 2022. 8
- [76] Zeke Xie, Xinrui Wang, Huishuai Zhang, Issei Sato, and Masashi Sugiyama. Adaptive inertia: Disentangling the effects of adaptive learning rate and momentum. In *International conference on machine learning*, pages 24430–24459. PMLR, 2022. 8
- [77] Ning Yang, Chao Tang, and Yuhai Tu. Stochastic gradient descent introduces an effective landscape-dependent regularization favoring flat solutions. *Physical Review Letters*, 130(23):237101, 2023. 1, 44
- [78] Zhewei Yao, Amir Gholami, Qi Lei, Kurt Keutzer, and Michael W Mahoney. Hessian-based analysis of large batch training and robustness to adversaries. *Advances in Neural Information Processing Systems*, 31, 2018. 8, 40
- [79] Zhewei Yao, Amir Gholami, Kurt Keutzer, and Michael W. Mahoney. Pyhessian: Neural networks through the lens of the hessian. In *International Conference on Big Data*, 2020. 8, 40
- [80] Zhewei Yao, Amir Gholami, Sheng Shen, Kurt Keutzer, and Michael W Mahoney. Adahessian: An adaptive second order optimizer for machine learning. *arXiv preprint arXiv:2006.00719*, 2020. 8
- [81] Wei Yuan and Kai-Xin Gao. Eadam optimizer: How  $\epsilon$  impact adam. *arXiv preprint arXiv:2011.02150*, 2020. 6
- [82] Manzil Zaheer, Sashank Reddi, Devendra Sachan, Satyen Kale, and Sanjiv Kumar. Adaptive methods for nonconvex optimization. *Advances in neural information processing systems*, 31, 2018. 38
- [83] Matthew D. Zeiler. Adadelta: An adaptive learning rate method. *arXiv e-prints*, 2012. 8
- [84] Chiyuan Zhang, Samy Bengio, Moritz Hardt, Benjamin Recht, and Oriol Vinyals. Understanding deep learning (still) requires rethinking generalization. *Communications of the ACM*, 64(3):107–115, 2021. 1
- [85] Jian Zhang and Ioannis Mitliagkas. Yellowfin and the art of momentum tuning. *arXiv preprint arXiv:1706.03471*, 2017. 1, 43
- [86] Xingxuan Zhang, Renzhe Xu, Han Yu, Hao Zou, and Peng Cui. Gradient norm aware minimization seeks first-order flatness and improves generalization. *IEEE/CVF Conference on Computer Vision and Pattern Recognition (CVPR)*, 2023. 6, 8
- [87] Yushun Zhang, Congliang Chen, Ziniu Li, Tian Ding, Chenwei Wu, Diederik P Kingma, Yinyu Ye, Zhi-Quan Luo, and Ruoyu Sun. Adam-mini: Use fewer learning rates to gain more. *arXiv preprint arXiv:2406.16793*, 2024. 8
- [88] Juntang Zhuang, Tommy Tang, Yifan Ding, Sekhar C Tatikonda, Nicha Dvornek, Xenophon Papademetris, and James Duncan. Adabelief optimizer: Adapting stepsizes by the belief in observed gradients. *Advances in neural information processing systems*, 33:18795–18806, 2020. 1, 4, 5, 6, 38
- [89] Juntang Zhuang, Boqing Gong, Liangzhe Yuan, Yin Cui, Hartwig Adam, Nicha Dvornek, Sekhar Tatikonda, James Duncan, and Ting Liu. Surrogate gap minimization improves sharpness-aware training. *arXiv preprint arXiv:2203.08065*, 2022. 8

# Dynamic Momentum Recalibration in Online Gradient Learning

## Appendix

### A. Bias-Variance Decomposition (Section 2 in main paper)

**Definition A.1.** The unified momentum update rule is defined as:

$$m_t = \beta m_{t-1} + u g_t, \quad \theta_t = \theta_{t-1} - \alpha m_t, \quad (17)$$

where  $\beta \in [0, 1)$  denotes the momentum (decay) coefficient, and  $u \geq 1 - \beta$  is a scaling parameter controlling the contribution of the current gradient. The stochastic gradient is given by  $g_t = \nabla f_t(\theta_t) + \epsilon_t$ ,  $\epsilon_t \sim \mathcal{N}(0, \sigma^2 I)$ , where  $f_t(\theta) = f(\theta; \xi_t)$  denotes the stochastic objective at iteration  $t$  with  $\xi_t$  sampled from the data distribution  $\mathcal{D}$ . Specific cases include:

- $u = 1 - \beta$ : Exponential Moving Average (EMA),
- $u = 1$ : Classical Momentum (CM) [63, 71].

**Assumption A.2.** We make the following assumptions on the smoothness and stochasticity of the objective function  $f$ :

1. **Lipschitz continuity:** There exists a constant  $L > 0$  such that, for any  $\theta$  and  $\phi$ ,  $\|\nabla f(\theta) - \nabla f(\phi)\| \leq L\|\theta - \phi\|$ .
2. **Bounded gradients:** There exists a constant  $G > 0$  such that, for all  $t$ ,  $\|\nabla f(\theta_t)\| \leq G$ .
3. **Bounded gradient noise:** The stochastic gradient noise  $\epsilon_t$  is temporally uncorrelated with zero mean, i.e.,  $\mathbb{E}[\epsilon_t] = \mathbf{0}$ , for all  $t$ . Furthermore, the variance of the stochastic gradients is uniformly bounded, meaning there exists a constant  $\sigma > 0$  such that  $\mathbb{E}[\|g_t - \nabla f(\theta_t)\|^2] \leq \sigma^2$ .

**Lemma A.3** (Bias-Variance Decomposition). *Let the stochastic gradient be given by  $g_t = \nabla f(\theta_t) + \epsilon_t$ ,  $\epsilon_t \sim \mathcal{N}(0, \sigma^2 I)$ , where  $\nabla f(\theta_t)$  denotes the true gradient and  $\epsilon_t$  represents zero-mean Gaussian noise. For any gradient estimator  $\hat{g}_t = \mathcal{A}(g_1, \dots, g_t)$  produced by an arbitrary algorithm  $\mathcal{A}$ , the mean squared error (MSE) satisfies the bias-variance decomposition:*

$$\mathbb{E}[\|\hat{g}_t - \nabla f(\theta_t)\|^2] = \underbrace{\|\mathbb{E}[\hat{g}_t] - \nabla f(\theta_t)\|^2}_{\text{Bias}^2} + \underbrace{\mathbb{E}[\|\hat{g}_t - \mathbb{E}[\hat{g}_t]\|^2]}_{\text{Variance}}. \quad (18)$$

*Proof.*

$$\begin{aligned} \mathbb{E}[\|\hat{g}_t - \nabla f(\theta_t)\|^2] &= \mathbb{E}[\|\hat{g}_t - \mathbb{E}[\hat{g}_t] + \mathbb{E}[\hat{g}_t] - \nabla f(\theta_t)\|^2] \\ &= \mathbb{E}[\|\hat{g}_t - \mathbb{E}[\hat{g}_t]\|^2] + \|\mathbb{E}[\hat{g}_t] - \nabla f(\theta_t)\|^2 + 2\mathbb{E}[\langle \hat{g}_t - \mathbb{E}[\hat{g}_t], \mathbb{E}[\hat{g}_t] - \nabla f(\theta_t) \rangle] \\ &= \text{Var}(\hat{g}_t) + \text{Bias}^2(\hat{g}_t) + 2 \underbrace{\langle \mathbb{E}[\hat{g}_t - \mathbb{E}[\hat{g}_t]], \mathbb{E}[\hat{g}_t] - \nabla f(\theta_t) \rangle}_{=0} \\ &= \text{Var}(\hat{g}_t) + \text{Bias}^2(\hat{g}_t). \end{aligned} \quad (19)$$

**Lemma A.4.** *Refer to the SDEs of vanilla SGD [70], the Definition A.1 with learning rate  $\alpha$  can be represented in continuous time as the stochastic differential equation (SDE):*

$$\begin{cases} dm(t) = [-(1 - \beta)m(t) + u\nabla f(\theta(t))] dt + u\sigma dW(t), \\ d\theta(t) = -\alpha m(t) dt, \end{cases} \quad (20)$$

where  $m(t)$  is the momentum,  $\theta(t)$  is the parameter,  $\beta \in [0, 1)$  is the momentum coefficient,  $u \geq 1 - \beta$  is the gradient scaling factor,  $\alpha > 0$  is the learning rate,  $\nabla f(\theta(t))$  is the gradient of the objective function,  $\sigma$  is the noise standard deviation, and  $W(t)$  is a standard  $d$ -dimensional Wiener process. This approximation holds when the learning rate  $\alpha$  is sufficiently small.

*Proof.* Start with the discrete momentum update rule from Definition A.1:

$$m_{n+1} = \beta m_n + u g(t_n), \quad \theta_{n+1} = \theta_n - \alpha m_{n+1}, \quad (21)$$

where  $m_n = m(t_n)$  is the momentum,  $\theta_n = \theta(t_n)$  is the parameter,  $g(t_n) = \nabla f(\theta_n) + \epsilon_n$  with  $\epsilon_n \sim \mathcal{N}(0, \sigma^2 I)$ , and  $\alpha > 0$  is the learning rate.

Rewrite the momentum update in terms of the increment:

$$\begin{aligned}
m_{n+1} - m_n &= \beta m_n + ug(t_n) - m_n \\
&= -(1 - \beta)m_n + ug(t_n) \\
&= -(1 - \beta)m_n + u\nabla f(\theta_n) + u\epsilon_n.
\end{aligned} \tag{22}$$

For the parameter:

$$\theta_{n+1} - \theta_n = -\alpha m_{n+1}. \tag{23}$$

To model this as a continuous-time SDE, assume the learning rate  $\alpha$  is sufficiently small, controlling the step size of the discrete updates. Define  $t_n = n$  to index discrete iterations, each corresponding to a unit time step  $dt = 1$ . The learning rate  $\alpha$  controls the update magnitude but does not rescale time.

For the momentum, interpret the increment as the rate of change over one iteration:

$$m_{n+1} - m_n \approx [-(1 - \beta)m_n + u\nabla f(\theta_n)] dt + u\epsilon_n, \quad dt = 1. \tag{24}$$

For small constant step sizes  $\alpha$ , this yields the drift:

$$dm(t) = [-(1 - \beta)m(t) + u\nabla f(\theta(t))] dt. \tag{25}$$

For the stochastic part, assume  $\epsilon_n = \sigma Z_n$ ,  $Z_n \sim \mathcal{N}(0, I)$ , so that the stochastic increment  $u\epsilon_n$  has variance  $u^2\sigma^2$  per iteration, matching the Brownian term  $u\sigma dW(t)$  under the step-time scaling  $dt = 1$ .

Therefore, in the SDE limit, the momentum dynamics can be written as:

$$dm(t) = [-(1 - \beta)m(t) + u\nabla f(\theta(t))] dt + u\sigma dW(t). \tag{26}$$

For the parameter update:

$$\theta_{n+1} - \theta_n = -\alpha m_{n+1} \approx -\alpha m(t) \cdot (\text{time step}), \tag{27}$$

where the time step is implicitly  $dt$  in the continuous limit, yielding:

$$d\theta(t) = -\alpha m(t) dt. \tag{28}$$

Combining both, when  $\alpha$  is small, the discrete updates approximate:

$$\begin{cases} dm(t) = [-(1 - \beta)m(t) + u\nabla f(\theta(t))] dt + u\sigma dW(t), \\ d\theta(t) = -\alpha m(t) dt. \end{cases} \tag{29}$$

This SDE captures the dynamics of the momentum and parameter updates, with  $\alpha$  as the learning rate driving the continuous approximation. ■

*Remark A.5 (Step-time scaling).* Our continuous-time formulation adopts the *step-time* scaling of Mandt et al. [70]. An alternative is the *slow-time* scaling  $t = n\alpha$ , often used in stochastic modified equations [46]. In that regime, one typically sets  $1 - \beta = \Theta(\alpha)$ , and the diffusion term scales with  $\sqrt{\alpha}$ . We do not adopt this scaling here, since doing so would modify both the drift and diffusion coefficients, as well as the form of  $d\theta$ .

**Lemma A.6.** *Under Lemma A.4, the solution to the stochastic differential equation (SDE), with initial conditions  $m(0) = 0$  and  $\theta(0) = \theta_0$ , is given by:*

$$\begin{cases} m(t) = u \int_0^t e^{-(1-\beta)(t-s)} \nabla f(\theta(s)) ds + u\sigma \int_0^t e^{-(1-\beta)(t-s)} dW(s), \\ \theta(t) = \theta_0 - \alpha \int_0^t m(s) ds, \end{cases} \tag{30}$$

where  $W(t)$  is a standard Wiener process, and the integrals represent the stochastic evolution driven by the gradient  $\nabla f(\theta(t))$  and noise.

*Proof.* We solve the coupled stochastic differential equation (SDE) system step-by-step:

$$\begin{cases} dm(t) = [-(1 - \beta)m(t) + u\nabla f(\theta(t))] dt + u\sigma dW(t), \\ d\theta(t) = -\alpha m(t) dt, \end{cases} \quad (31)$$

with initial conditions  $m(0) = 0$  and  $\theta(0) = \theta_0$ .

The  $\theta(t)$  dynamics have drift only (no explicit diffusion term), but  $\theta(t)$  is still random because  $m(t)$  is random. Integrate:

$$\begin{aligned} d\theta(t) &= -\alpha m(t) dt, \\ \theta(t) - \theta(0) &= -\alpha \int_0^t m(s) ds. \end{aligned} \quad (32)$$

Since  $\theta(0) = \theta_0$ , we obtain:

$$\theta(t) = \theta_0 - \alpha \int_0^t m(s) ds. \quad (33)$$

This expresses  $\theta(t)$  as a functional of  $m(t)$ , which we now determine.

Consider the linear SDE for  $m(t)$  with a time-dependent forcing term:

$$dm(t) = [-(1 - \beta)m(t) + u\nabla f(\theta(t))] dt + u\sigma dW(t). \quad (34)$$

Rewrite it in standard form:

$$dm(t) + (1 - \beta)m(t) dt = u\nabla f(\theta(t)) dt + u\sigma dW(t). \quad (35)$$

To solve this, apply the integrating factor  $e^{\int_0^t (1-\beta) ds} = e^{(1-\beta)t}$ . Multiply through by  $e^{(1-\beta)t}$ :

$$e^{(1-\beta)t} dm(t) + (1 - \beta)e^{(1-\beta)t} m(t) dt = ue^{(1-\beta)t} \nabla f(\theta(t)) dt + u\sigma e^{(1-\beta)t} dW(t). \quad (36)$$

Recognize the left-hand side as the differential of a product:

$$\begin{aligned} d[e^{(1-\beta)t} m(t)] &= e^{(1-\beta)t} dm(t) + (1 - \beta)e^{(1-\beta)t} m(t) dt \\ &= ue^{(1-\beta)t} \nabla f(\theta(t)) dt + u\sigma e^{(1-\beta)t} dW(t). \end{aligned} \quad (37)$$

Integrate both sides from 0 to  $t$ , with  $m(0) = 0$ , this simplifies to:

$$\begin{aligned} e^{(1-\beta)t} m(t) - e^{(1-\beta) \cdot 0} m(0) &= u \int_0^t e^{(1-\beta)s} \nabla f(\theta(s)) ds + u\sigma \int_0^t e^{(1-\beta)s} dW(s), \\ e^{(1-\beta)t} m(t) &= u \int_0^t e^{(1-\beta)s} \nabla f(\theta(s)) ds + u\sigma \int_0^t e^{(1-\beta)s} dW(s), \\ m(t) &= u \int_0^t e^{-(1-\beta)(t-s)} \nabla f(\theta(s)) ds + u\sigma \int_0^t e^{-(1-\beta)(t-s)} dW(s), \end{aligned} \quad (38)$$

where the exponent is adjusted using  $e^{(1-\beta)s} / e^{(1-\beta)t} = e^{-(1-\beta)(t-s)}$ .

The expression for  $m(t)$  depends on  $\theta(s)$  via  $\nabla f(\theta(s))$ , where:

$$\theta(s) = \theta_0 - \alpha \int_0^s m(\tau) d\tau. \quad (39)$$

Thus, the complete solution is:

$$\begin{cases} m(t) = u \int_0^t e^{-(1-\beta)(t-s)} \nabla f(\theta(s)) ds + u\sigma \int_0^t e^{-(1-\beta)(t-s)} dW(s), \\ \theta(t) = \theta_0 - \alpha \int_0^t m(s) ds. \end{cases} \quad (40)$$

This integral form encapsulates the coupled dynamics, with  $\nabla f(\theta(t))$  linking the equations and the stochastic term  $\int e^{-(1-\beta)(t-s)} dW(s)$  as an Itô integral. ■

**Theorem A.7.** Consider the unified momentum estimator  $m(t)$  defined by the stochastic differential equation (SDE) from Lemma A.4, with solution given in Lemma A.6. Let the bias be defined relative to the expected true gradient:  $\text{Bias}(m(t)) = \mathbb{E}[m(t)] - \mathbb{E}[\nabla f(\theta(t))]$ . Assuming that the gradient  $\nabla f(\theta(t))$  is bounded and Lipschitz continuous, the asymptotic bounds (as  $t \rightarrow \infty$ ) for the bias and variance of  $m(t)$  as an estimator are given by:

$$\|\text{Bias}(m(t))\|^2 \leq \left( \frac{u^2 \alpha L G}{(1-\beta)^3} + \frac{u^2 \alpha L \sigma}{\sqrt{2}(1-\beta)^{2.5}} + \left( \frac{u}{1-\beta} - 1 \right) G \right)^2, \quad (41)$$

where  $L$  is the Lipschitz constant,  $G$  bounds the gradient norm  $\|\nabla f(\theta(t))\|$ , and the second term inside the parenthesis explicitly captures the parameter-shift bias induced by the stochastic noise  $\sigma$ .

$$\text{Var}(m(t)) \leq \frac{u^2 \sigma^2}{1-\beta} + \frac{2u^2 V^2}{(1-\beta)^2}, \quad (42)$$

where  $\sigma^2$  is the total variance of the stochastic gradient noise, and  $V^2$  conservatively bounds the variance of the true gradient sequence, i.e.,  $\text{Var}(\nabla f(\theta(t))) \leq V^2$ .

*Proof.* We compute the bias and variance of  $m(t)$  relative to  $\mathbb{E}[\nabla f(\theta(t))]$ .

### 1. Bias Calculation

Consider the unified momentum update rule:

$$m_t = \beta m_{t-1} + u g_t, \quad \theta_t = \theta_{t-1} - \alpha m_t, \quad (43)$$

where  $\beta \in [0, 1)$  represents the decay or momentum factor,  $u \in [1 - \beta, 1]$  is a scaling parameter controlling the gradient contribution,  $\alpha > 0$  is the learning rate, and  $g_t = \nabla f(\theta_t) + \epsilon_t$  with  $\epsilon_t \sim \mathcal{N}(0, \sigma^2 I)$ .

In continuous time, the expectation of  $m(t)$  is:

$$\mathbb{E}[m(t)] = u \int_0^t e^{-(1-\beta)(t-s)} \mathbb{E}[\nabla f(\theta(s))] ds, \quad (44)$$

since the stochastic term has zero mean:

$$\mathbb{E} \left[ u \sigma \int_0^t e^{-(1-\beta)(t-s)} dW(s) \right] = 0. \quad (45)$$

The squared bias is defined as:

$$\begin{aligned} (\text{Bias}(m(t)))^2 &= (\mathbb{E}[m(t)] - \mathbb{E}[\nabla f(\theta(t))])^2 \\ &= \left( u \int_0^t e^{-(1-\beta)(t-s)} \mathbb{E}[\nabla f(\theta(s))] ds - \mathbb{E}[\nabla f(\theta(t))] \right)^2. \end{aligned} \quad (46)$$

We assume  $\nabla f$  is Lipschitz continuous with constant  $L > 0$ :

$$\|\nabla f(\theta) - \nabla f(\phi)\| \leq L \|\theta - \phi\|, \quad \forall \theta, \phi. \quad (47)$$

Given  $u \geq 1 - \beta$ , so  $\frac{u}{1-\beta} \geq 1$ . From the continuous-time dynamics  $\frac{d\theta}{dt} = -\alpha m(t)$ , integrating from  $s$  to  $t$  ( $s < t$ ) yields:

$$\theta(s) - \theta(t) = \alpha \int_s^t m(u) du. \quad (48)$$

To bound  $\mathbb{E}[\|\theta(s) - \theta(t)\|]$ , we must first bound the magnitude of the momentum  $\mathbb{E}[\|m(u)\|]$  considering both the gradient drift and the noise diffusion:

$$m(u) = u \int_0^u e^{-(1-\beta)(u-v)} \nabla f(\theta(v)) dv + u \sigma \int_0^u e^{-(1-\beta)(u-v)} dW(v). \quad (49)$$

Taking the expectation of the norm and applying Jensen's inequality to the stochastic term:

$$\begin{aligned}\mathbb{E}[\|m(u)\|] &\leq u \int_0^u e^{-(1-\beta)(u-v)} \mathbb{E}[\|\nabla f(\theta(v))\|] dv + \mathbb{E}\left[\left\|u\sigma \int_0^u e^{-(1-\beta)(u-v)} dW(v)\right\|\right] \\ &\leq \frac{uG}{1-\beta} + \sqrt{u^2\sigma^2 \frac{1-e^{-2(1-\beta)u}}{2(1-\beta)}} \\ &\leq \frac{uG}{1-\beta} + \frac{u\sigma}{\sqrt{2(1-\beta)}} := M.\end{aligned}\tag{50}$$

Thus, taking the expected norm for the parameter difference:

$$\mathbb{E}[\|\theta(s) - \theta(t)\|] \leq \alpha \int_s^t \mathbb{E}[\|m(u)\|] du \leq \alpha M(t-s).\tag{51}$$

Rewrite the bias by splitting the integral:

$$\begin{aligned}\text{Bias}(m(t)) &= u \int_0^t e^{-(1-\beta)(t-s)} (\mathbb{E}[\nabla f(\theta(s))] - \mathbb{E}[\nabla f(\theta(t))]) ds \\ &\quad + \mathbb{E}[\nabla f(\theta(t))] \left( u \int_0^t e^{-(1-\beta)(t-s)} ds - 1 \right).\end{aligned}\tag{52}$$

Compute the second integral:

$$u \int_0^t e^{-(1-\beta)(t-s)} ds = u \frac{1 - e^{-(1-\beta)t}}{1-\beta}.\tag{53}$$

Apply the triangle inequality and the bounded gradient assumption:

$$\|\text{Bias}(m(t))\| \leq \underbrace{\left\| u \int_0^t e^{-(1-\beta)(t-s)} (\mathbb{E}[\nabla f(\theta(s))] - \mathbb{E}[\nabla f(\theta(t))]) ds \right\|}_{:=I_1} + \left| u \frac{1 - e^{-(1-\beta)t}}{1-\beta} - 1 \right| G.\tag{54}$$

Bound  $I_1$  using Lipschitz continuity and our bound  $M$ :

$$\begin{aligned}\|I_1\| &\leq u \int_0^t e^{-(1-\beta)(t-s)} \mathbb{E}[\|\nabla f(\theta(s)) - \nabla f(\theta(t))\|] ds \\ &\leq uL\alpha M \int_0^t e^{-(1-\beta)(t-s)} (t-s) ds.\end{aligned}\tag{55}$$

Evaluate the integral:

$$\begin{aligned}\int_0^t e^{-(1-\beta)(t-s)} (t-s) ds &= \int_0^t e^{-(1-\beta)\tau} \tau d\tau \\ &= \frac{1}{(1-\beta)^2} - \left( \frac{t}{1-\beta} + \frac{1}{(1-\beta)^2} \right) e^{-(1-\beta)t} \leq \frac{1}{(1-\beta)^2},\end{aligned}\tag{56}$$

thus  $\|I_1\| \leq \frac{u\alpha LM}{(1-\beta)^2}$ . Then:

$$\|\text{Bias}(m(t))\| \leq \frac{u\alpha LM}{(1-\beta)^2} + \left| u \frac{1 - e^{-(1-\beta)t}}{1-\beta} - 1 \right| G.\tag{57}$$

As  $t \rightarrow \infty$ ,  $e^{-(1-\beta)t} \rightarrow 0$ , giving  $\left| u \frac{1 - e^{-(1-\beta)t}}{1-\beta} - 1 \right| \rightarrow \frac{u}{1-\beta} - 1$ . Substitute  $M = \frac{uG}{1-\beta} + \frac{u\sigma}{\sqrt{2(1-\beta)}}$  and square the bound:

$$\begin{aligned}\|\text{Bias}(m(t))\|^2 &\leq \left( \frac{u\alpha LM}{(1-\beta)^2} + \left( u \frac{1 - e^{-(1-\beta)t}}{1-\beta} - 1 \right) G \right)^2 \\ &\leq \left( \frac{u\alpha L}{(1-\beta)^2} \left( \frac{uG}{1-\beta} + \frac{u\sigma}{\sqrt{2(1-\beta)}} \right) + \left( \frac{u}{1-\beta} - 1 \right) G \right)^2 \\ &= \left( \frac{u^2\alpha LG}{(1-\beta)^3} + \frac{u^2\alpha L\sigma}{\sqrt{2}(1-\beta)^{2.5}} + \left( \frac{u}{1-\beta} - 1 \right) G \right)^2.\end{aligned}\tag{58}$$

## 2. Variance Calculation

The fluctuation  $m(t) - \mathbb{E}[m(t)]$  is:

$$m(t) - \mathbb{E}[m(t)] = \underbrace{u \int_0^t e^{-(1-\beta)(t-s)} [\nabla f(\theta(s)) - \mathbb{E}[\nabla f(\theta(s))]] ds}_{\mathcal{T}_{\text{Grad Diff}}} + \underbrace{u\sigma \int_0^t e^{-(1-\beta)(t-s)} dW(s)}_{\mathcal{T}_{\text{Noise Diff}}}. \quad (59)$$

Using the inequality  $\|a + b\|^2 \leq 2\|a\|^2 + 2\|b\|^2$ , the variance becomes:

$$\begin{aligned} \text{Var}(m(t)) &= \mathbb{E} \left[ \|m(t) - \mathbb{E}[m(t)]\|^2 \right] \\ &\leq 2 \mathbb{E} [\|\mathcal{T}_{\text{Grad Diff}}\|^2] + 2 \mathbb{E} [\|\mathcal{T}_{\text{Noise Diff}}\|^2]. \end{aligned} \quad (60)$$

The noise variance term is derived using the Itô isometry:

$$\begin{aligned} 2 \mathbb{E} [\|\mathcal{T}_{\text{Noise Diff}}\|^2] &= 2u^2\sigma^2 \mathbb{E} \left[ \left( \int_0^t e^{-(1-\beta)(t-s)} dW(s) \right)^2 \right] \\ &= 2u^2\sigma^2 \int_0^t e^{-2(1-\beta)(t-s)} ds \quad (\text{Itô isometry}) \\ &= 2u^2\sigma^2 \frac{1 - e^{-2(1-\beta)t}}{2(1-\beta)} \leq \frac{u^2\sigma^2}{1-\beta}. \end{aligned} \quad (61)$$

For the gradient variance term, we apply the Cauchy-Schwarz inequality to properly bound the squared norm of the integral:

$$\begin{aligned} 2 \mathbb{E} [\|\mathcal{T}_{\text{Grad Diff}}\|^2] &= 2u^2 \mathbb{E} \left[ \left\| \int_0^t e^{-(1-\beta)(t-s)/2} \cdot e^{-(1-\beta)(t-s)/2} [\nabla f(\theta(s)) - \mathbb{E}[\nabla f(\theta(s))]] ds \right\|^2 \right] \\ &\leq 2u^2 \mathbb{E} \left[ \left( \int_0^t e^{-(1-\beta)(t-s)} ds \right) \left( \int_0^t e^{-(1-\beta)(t-s)} \|\nabla f(\theta(s)) - \mathbb{E}[\nabla f(\theta(s))]\|^2 ds \right) \right] \\ &\leq \frac{2u^2}{1-\beta} \int_0^t e^{-(1-\beta)(t-s)} \text{Var}(\nabla f(\theta(s))) ds. \end{aligned} \quad (62)$$

By Assumption A.2,  $\text{Var}(\nabla f(\theta(s))) \leq V^2$ , yielding:

$$\begin{aligned} 2 \mathbb{E} [\|\mathcal{T}_{\text{Grad Diff}}\|^2] &\leq \frac{2u^2V^2}{1-\beta} \int_0^t e^{-(1-\beta)(t-s)} ds \\ &\leq \frac{2u^2V^2}{1-\beta} \left( \frac{1}{1-\beta} \right) = \frac{2u^2V^2}{(1-\beta)^2}. \end{aligned} \quad (63)$$

Combining both bounds, the total variance is bounded by:

$$\text{Var}(m(t)) \leq \frac{u^2\sigma^2}{1-\beta} + \frac{2u^2V^2}{(1-\beta)^2}. \quad (64)$$

■

## B. Method Derivation (Section 3 in main paper)

### B.1. Optimal Linear Filter Derivation for Gradient Estimation (Main paper Section 3.1)

In the stochastic gradient descent (SGD) process, given the sequence of gradients  $\{g_i\}_{i=1}^t$ , our objective is to estimate  $\hat{g}_t$ , which incorporates information from both historical gradients and the current gradient. The Optimal Linear Filter provides a mechanism to minimize the mean squared error in this estimation. We start by constructing  $\hat{g}_t$  as a simple average and then refine it using the properties of the Optimal Linear Filter.

$$\begin{aligned}\hat{g}_t &= \frac{1}{t} \sum_{i=1}^t g_i = \frac{1}{t} \left( \sum_{i=1}^{t-1} g_i + g_t \right) = \frac{1}{t} \sum_{i=1}^{t-1} g_i + \frac{1}{t} g_t \\ &= \frac{1}{t} \left[ (t-1) \cdot \frac{1}{t-1} \sum_{i=1}^{t-1} g_i \right] + \frac{1}{t} g_t \\ &= \frac{t-1}{t} \bar{g}_{1:t-1} + \frac{1}{t} g_t,\end{aligned}\tag{65}$$

where  $\bar{g}_{1:t-1} = \frac{1}{t-1} \sum_{i=1}^{t-1} g_i$  denoting the averaging of the gradient under different  $\theta_t$  to differentiate  $\bar{g}_t$  which in fixed parameter  $\theta$ .

To better capture historical information, we replace the arithmetic mean  $\bar{g}_{1:t-1}$  with the momentum term  $\hat{m}_t$ . Here we substitute the iteration  $m_{t-1}$  with  $m_t$  because of the absence of  $m_0$  and the ease of implementation. Thus, we rewrite  $\hat{g}_t$  as follows:

$$\begin{aligned}\hat{g}_t &\approx \frac{t-1}{t} \hat{m}_t + \frac{1}{t} g_t \\ &= \left( 1 - \frac{1}{t} \right) \hat{m}_t + \frac{1}{t} g_t \\ &= \hat{m}_t - K_t \hat{m}_t + K_t g_t \\ &= \hat{m}_t + K_t (g_t - \hat{m}_t),\end{aligned}\tag{66}$$

where  $K_t = \frac{1}{t}$  serves as an initial estimation gain that balances the influence of  $\hat{m}_t$  and  $g_t$ .

To achieve an optimal balance, we define  $\hat{g}_t$  as a weighted combination of  $\hat{m}_t$  and  $g_t$ , aiming to minimize the variance of  $\hat{g}_t$ . Assuming independence between  $\hat{m}_t$  and  $g_t$ , we express the variance as:

$$\begin{aligned}\text{Var}(\hat{g}_t) &= \text{Var}((1 - K_t)\hat{m}_t + K_t g_t) \\ &= (1 - K_t)^2 \text{Var}(\hat{m}_t) + K_t^2 \text{Var}(g_t).\end{aligned}\tag{67}$$

To find the optimal  $K_t$ , we take the derivative of  $\text{Var}(\hat{g}_t)$  with respect to  $K_t$  and set it to zero:

$$\begin{aligned}\frac{d\text{Var}(\hat{g}_t)}{dK_t} &= -2(1 - K_t)\text{Var}(\hat{m}_t) + 2K_t\text{Var}(g_t) = 0, \\ (1 - K_t)\text{Var}(\hat{m}_t) &= K_t\text{Var}(g_t),\end{aligned}\tag{68}$$

solving for  $K_t$  gives:

$$K_t = \frac{\text{Var}(\hat{m}_t)}{\text{Var}(\hat{m}_t) + \text{Var}(g_t)}.\tag{69}$$

The final expression for  $K_t$  indicates that the optimal interpolation coefficient is the ratio of the variance of the momentum term to the total variance. This embodies the Optimal Linear Filter's principle: optimally combining historical estimates with new observations to minimize estimation error due to stochastic noise in the gradient signal.

### B.2. Variance Correction (Correction factor in main paper Section 3.1)

The momentum term  $m_t$  in stochastic gradient descent is defined as:

$$m_t = (1 - \beta_1) \sum_{i=1}^t \beta_1^{t-i} g_i,\tag{70}$$

which means that  $m_t$  is a weighted sum of past gradients, where the weights decrease exponentially over time according to the factor  $\beta_1$ .

To accurately estimate the variance of  $m_t$  using the variance of  $g_t$ , we derive a correction factor under the assumption that the stochastic gradients  $g_t$  are independent with bounded variance  $\sigma_g^2$ .

Each weighted gradient term  $\beta_1^{t-i} g_i$  has a variance of  $\beta_1^{2(t-i)} \sigma_g^2$ , because the variance scaling factor becomes  $\beta_1^{2(t-i)}$  in the variance computation due to the quadratic nature of the variance operator.

Given that  $m_t$  is a sum of these weighted terms and assuming independence among  $g_i$ , the variance of  $m_t$  is the sum of the variances of all weighted gradients:

$$\sigma_{m_t}^2 = (1 - \beta_1)^2 \sigma_g^2 \sum_{i=1}^t \beta_1^{2(t-i)}. \quad (71)$$

The factor  $(1 - \beta_1)^2$  appears from the multiplication factor  $(1 - \beta_1)$  in the definition of  $m_t$ , which also applies to the variance calculation.

The summation  $\sum_{i=1}^t \beta_1^{2(t-i)}$  forms a geometric series:

$$\sum_{i=1}^t \beta_1^{2(t-i)} = \frac{1 - \beta_1^{2t}}{1 - \beta_1^2}. \quad (72)$$

As  $t \rightarrow \infty$  and given that  $\beta_1 < 1$ , we find that  $\beta_1^{2t} \rightarrow 0$ , so the series converges to:

$$\sum_{i=1}^t \beta_1^{2(t-i)} \approx \frac{1}{1 - \beta_1^2}. \quad (73)$$

Substituting back, we obtain the long-term variance of  $m_t$  as:

$$\sigma_{m_t}^2 = \frac{(1 - \beta_1)^2}{1 - \beta_1^2} \sigma_g^2 = \frac{1 - \beta_1}{1 + \beta_1} \sigma_g^2. \quad (74)$$

Thus, the correction factor we derived is:

$$\left( \frac{1 - \beta_1}{1 + \beta_1} \right) \cdot (1 - \beta_1^{2t}). \quad (75)$$

This correction factor  $\left( \frac{1 - \beta_1}{1 + \beta_1} \right) \cdot (1 - \beta_1^{2t})$  allows us to adjust the variance of the EMA gradient to accurately estimate the variance of the momentum gradient  $m_t$  using the original variance  $\sigma_g^2$ . This adjustment reflects the effect of exponentially decaying weights in  $m_t$ , yielding a more stable gradient estimate with reduced noise over time.

### B.3. Fusion of Gaussian Distributions (Main paper Section 3.2)

In this section, we address the fusion of two Gaussian distributions to produce a more reliable gradient estimate in the stochastic gradient descent (SGD) process. This fusion combines information from both the historical momentum term  $\hat{m}_t$  and the current gradient  $g_t$ , resulting in an estimate with reduced uncertainty. Here, "fusion" refers to finding an optimal combined distribution that minimizes mean-square error by utilizing both sources of information.

Consider the following two Gaussian distributions:

- The momentum term  $\hat{m}_t$  follows a normal distribution with mean  $\mu_m$  and variance  $\sigma_m^2$ , denoted as  $\hat{m}_t \sim \mathcal{N}(\mu_m, \sigma_m^2)$ .
- The current gradient  $g_t$  follows a normal distribution with mean  $\mu_g$  and variance  $\sigma_g^2$ , denoted as  $g_t \sim \mathcal{N}(\mu_g, \sigma_g^2)$ .

**Linear estimator perspective.** Before presenting the probability density product approach, we first derive the fused estimate  $\hat{g}_t$  from a weighted linear combination perspective. We define  $\hat{g}_t$  as:

$$\hat{g}_t = (1 - K_t) \hat{m}_t + K_t g_t, \quad (76)$$

where  $K_t$  is a variance-based weighting coefficient:

$$K_t = \frac{\sigma_m^2}{\sigma_m^2 + \sigma_g^2}, \quad \text{thus} \quad 1 - K_t = \frac{\sigma_g^2}{\sigma_m^2 + \sigma_g^2}. \quad (77)$$

Assuming independence between  $\hat{m}_t$  and  $g_t$ , the expectation of  $\hat{g}_t$  is:

$$\mathbb{E}[\hat{g}_t] = (1 - K_t)\mu_m + K_t\mu_g = \frac{\sigma_g^2\mu_m + \sigma_m^2\mu_g}{\sigma_m^2 + \sigma_g^2}. \quad (78)$$

The variance of  $\hat{g}_t$  becomes:

$$\begin{aligned} \text{Var}(\hat{g}_t) &= (1 - K_t)^2\sigma_m^2 + K_t^2\sigma_g^2 \\ &= \left(\frac{\sigma_g^2}{\sigma_m^2 + \sigma_g^2}\right)^2 \sigma_m^2 + \left(\frac{\sigma_m^2}{\sigma_m^2 + \sigma_g^2}\right)^2 \sigma_g^2 \\ &= \frac{\sigma_g^4\sigma_m^2 + \sigma_m^4\sigma_g^2}{(\sigma_m^2 + \sigma_g^2)^2} = \frac{\sigma_m^2\sigma_g^2}{\sigma_m^2 + \sigma_g^2}. \end{aligned} \quad (79)$$

**Probability density product derivation.** We now show that the same fused Gaussian distribution arises from multiplying the two individual Gaussian probability densities:

$$N(\hat{m}_t; \mu_m, \sigma_m) \cdot N(g_t; \mu_g, \sigma_g) = \frac{1}{2\pi\sigma_m\sigma_g} \exp\left(-\frac{(\hat{g}_t - \mu_m)^2}{2\sigma_m^2} - \frac{(\hat{g}_t - \mu_g)^2}{2\sigma_g^2}\right). \quad (80)$$

To derive the fused form, we simplify the exponent by completing the square:

$$\begin{aligned} \text{Exponent} &= -\frac{(\hat{g}_t - \mu_m)^2}{2\sigma_m^2} - \frac{(\hat{g}_t - \mu_g)^2}{2\sigma_g^2} \\ &= -\frac{\sigma_g^2(\hat{g}_t - \mu_m)^2 + \sigma_m^2(\hat{g}_t - \mu_g)^2}{2\sigma_m^2\sigma_g^2} \\ &= -\frac{\left(\hat{g}_t - \frac{\sigma_g^2\mu_m + \sigma_m^2\mu_g}{\sigma_m^2 + \sigma_g^2}\right)^2}{\frac{2\sigma_m^2\sigma_g^2}{\sigma_m^2 + \sigma_g^2}} + \frac{(\mu_m - \mu_g)^2}{2(\sigma_m^2 + \sigma_g^2)}. \end{aligned} \quad (81)$$

Ignoring constant terms, we identify the resulting fused distribution:

$$\mu_{\hat{g}_t} = \frac{\sigma_g^2\mu_m + \sigma_m^2\mu_g}{\sigma_m^2 + \sigma_g^2}, \quad \sigma_{\hat{g}_t}^2 = \frac{\sigma_m^2\sigma_g^2}{\sigma_m^2 + \sigma_g^2}. \quad (82)$$

**Equivalence and insight.** This demonstrates that the PDF product view yields the same fused mean and variance as the minimum mean-square error (MMSE) linear estimator. The fused mean  $\mu_{\hat{g}_t}$  is closer to the distribution with smaller variance, indicating greater trust in more certain estimates [22]. The fused variance  $\sigma_{\hat{g}_t}^2$  is always less than either original variance, demonstrating the variance reduction benefit of fusion.

This equivalence between statistical estimation and probabilistic fusion confirms the theoretical soundness of the SGDF method. It validates the fusion-based formulation from both a Bayesian and a signal processing perspective.

#### B.4. Modulating Observation Variance through Power Scaling

The preceding analysis yields the optimal linear fusion gain under the MMSE criterion

$$K_t = \frac{\sigma_m^2}{\sigma_m^2 + \sigma_g^2}, \quad (83)$$

which balances the historical momentum estimate and the instantaneous stochastic gradient according to their uncertainties.

In practice, the variance estimates (especially  $\sigma_g^2$ ) can be noisy or biased due to mini-batch stochasticity and nonstationarity. To improve robustness while remaining consistent with our convergence analysis, we adopt a power-scaled gain

$$\tilde{K}_t = K_t^\gamma, \quad \gamma = \frac{1}{2}, \quad (84)$$

since  $K_t \in [0, 1]$  element-wise, the scaled gain still satisfies  $\|\tilde{K}_t\|_\infty \leq 1$ , which is the sole requirement for our convergence guarantees; therefore, the theoretical results remain unchanged.

With  $K_t = \frac{\sigma_m^2}{\sigma_m^2 + \sigma_g^2}$ , the choice  $\gamma = \frac{1}{2}$  gives

$$\tilde{K}_t = \sqrt{K_t} = \sqrt{\frac{\sigma_m^2}{\sigma_m^2 + \sigma_g^2}}. \quad (85)$$

We show that  $\tilde{K}_t$  can be written in the same variance-fusion form as  $K_t$  by introducing an *effective* observation variance  $\tilde{\sigma}_g^2$  such that

$$\tilde{K}_t = \frac{\sigma_m^2}{\sigma_m^2 + \tilde{\sigma}_g^2}. \quad (86)$$

Equating the two expressions and solving for  $\tilde{\sigma}_g^2$ :

$$\begin{aligned} \frac{\sigma_m^2}{\sigma_m^2 + \tilde{\sigma}_g^2} &= \sqrt{\frac{\sigma_m^2}{\sigma_m^2 + \sigma_g^2}}, \\ \frac{\sigma_m^2 + \tilde{\sigma}_g^2}{\sigma_m^2} &= \sqrt{\frac{\sigma_m^2 + \sigma_g^2}{\sigma_m^2}} = \sqrt{1 + \frac{\sigma_g^2}{\sigma_m^2}}, \\ 1 + \frac{\tilde{\sigma}_g^2}{\sigma_m^2} &= \sqrt{1 + \frac{\sigma_g^2}{\sigma_m^2}}, \\ \frac{\tilde{\sigma}_g^2}{\sigma_m^2} &= \sqrt{1 + \frac{\sigma_g^2}{\sigma_m^2}} - 1. \end{aligned} \quad (87)$$

Therefore, according to Eq. (87), we have:

$$\tilde{\sigma}_g^2 = \sigma_m^2 \left( \sqrt{1 + \frac{\sigma_g^2}{\sigma_m^2}} - 1 \right).$$

Therefore, the scaled gain  $\tilde{K}_t = \sqrt{K_t}$  is equivalently a standard variance-based fusion gain with a reparameterized (effective) observation variance:

$$\tilde{K}_t = \frac{\sigma_m^2}{\sigma_m^2 + \tilde{\sigma}_g^2}, \quad \tilde{\sigma}_g^2 = \sigma_m^2 \left( \sqrt{1 + \frac{\sigma_g^2}{\sigma_m^2}} - 1 \right). \quad (88)$$

This view shows that power-scaling preserves the fusion structure while introducing a controlled regularization against overconfident (noisy) instantaneous gradient observations.

### C. Convergence analysis in convex online learning case (Theorem 3.2 in main paper).

**Assumption C.1.** Variables are bounded:  $\exists D, D_\infty$  such that  $\forall t, \|\theta_t - \theta^*\|_2 \leq D, \|\theta_t - \theta^*\|_\infty \leq D_\infty$ . Gradients are bounded:  $\exists G, G_\infty$  such that  $\forall t, \|g_t\|_2 \leq G, \|g_t\|_\infty \leq G_\infty$ . The interpolation parameter satisfies  $K_{t,i} \in [0, 1]$ . Furthermore, we assume the interpolation parameter sequence has sublinear total variation, i.e.,  $\sum_{t=1}^{T-1} |K_{t,i} - K_{t+1,i}| \leq \mathcal{O}(\sqrt{T})$ .

**Definition C.2.** Let  $f_t(\theta_t)$  be the loss at time  $t$  and  $f_t(\theta^*)$  be the loss of the best possible strategy at the same time. The cumulative regret  $R(T)$  at time  $T$  is defined as:

$$R(T) = \sum_{t=1}^T (f_t(\theta_t) - f_t(\theta^*)) \quad (89)$$

**Definition C.3.** A function  $f : \mathbb{R}^d \rightarrow \mathbb{R}$  is convex if for all  $x, y \in \mathbb{R}^d$  and for all  $\lambda \in [0, 1]$ ,

$$\lambda f(x) + (1 - \lambda)f(y) \geq f(\lambda x + (1 - \lambda)y) \quad (90)$$

Also, notice that a convex function can be lower bounded by a hyperplane at its tangent.

**Lemma C.4.** If a function  $f : \mathbb{R}^d \rightarrow \mathbb{R}$  is convex, then for all  $x, y \in \mathbb{R}^d$ ,

$$f(x) - f(y) \leq \nabla f(x)^T (x - y) \quad (91)$$

The above lemma can be used to upper bound the regret, and our proof for the main theorem is constructed by substituting the hyperplane with SGDF update rules.

We define  $g_t \triangleq \nabla f_t(\theta_t)$  and  $g_{t,i}$  as the  $i^{\text{th}}$  element. Let  $\hat{g}_t$  be the effective update direction.

**Lemma C.5.** Let gradients be bounded by  $|g_{t,i}| \leq G_\infty$ . For any  $T \geq 1$ , the sum of squared bounded elements discounted by  $\sqrt{t}$  is strictly bounded by:

$$\sum_{t=1}^T \frac{g_{t,i}^2}{\sqrt{t}} \leq 2G_\infty^2 \sqrt{T} \quad (92)$$

*Proof.* Since  $g_{t,i}^2 \leq G_\infty^2$ , we can bound the summation using the integral test. Since  $1/\sqrt{t}$  is a monotonically decreasing function for  $t \geq 1$ :

$$\begin{aligned} \sum_{t=1}^T \frac{g_{t,i}^2}{\sqrt{t}} &\leq G_\infty^2 \sum_{t=1}^T \frac{1}{\sqrt{t}} \\ &\leq G_\infty^2 \left( 1 + \int_1^T \frac{1}{\sqrt{t}} dt \right) \\ &= G_\infty^2 (1 + 2\sqrt{T} - 2) \leq 2G_\infty^2 \sqrt{T} \end{aligned} \quad (93)$$

**Lemma C.6.** Let the exponential moving average be  $m_{t,i} = \beta_1 m_{t-1,i} + (1 - \beta_1)g_{t,i}$ , with bias-correction  $\hat{m}_{t,i} = m_{t,i}/(1 - \beta_1^t)$ . Under the update rule  $\hat{g}_{t,i} = \hat{m}_{t,i} + K_{t,i}(g_{t,i} - \hat{m}_{t,i})$ , the effective update direction is bounded by  $|\hat{g}_{t,i}| \leq G_\infty$ .

*Proof.* By mathematical induction, since  $m_{t,i}$  is a convex combination of past bounded gradients, we have  $|m_{t,i}| \leq (1 - \beta_1^t)G_\infty$ . Therefore, the bias-corrected momentum satisfies  $|\hat{m}_{t,i}| \leq G_\infty$ . The update direction is a convex combination  $\hat{g}_{t,i} = K_{t,i}g_{t,i} + (1 - K_{t,i})\hat{m}_{t,i}$ . Since both components are bounded by  $G_\infty$  and  $K_{t,i} \in [0, 1]$ , we rigorously have  $|\hat{g}_{t,i}| \leq G_\infty$ . ■

**Lemma C.7 (Bounded Total Variation).** Assume the gradient sequence is bounded such that  $\|\nabla f_t\|_\infty \leq G_\infty$  for all  $t$ , and the hyperparameters  $\beta_1, \beta_2 \in [0, 1)$  are constants. If the power scaling factor is scheduled as  $\gamma_t = \gamma_0/\sqrt{t}$ , the effective interpolation gain  $\tilde{K}_t = K_t^{\gamma_t}$  satisfies:

$$\sum_{t=1}^{T-1} |K_{t+1}^{\gamma_{t+1}} - K_t^{\gamma_t}| \leq \mathcal{O}(\sqrt{T}) \quad (94)$$

*Proof.* Decomposition of the total variation using the triangle inequality.

$$\begin{aligned}
\sum_{t=1}^{T-1} |K_{t+1}^{\gamma_{t+1}} - K_t^{\gamma_t}| &\leq \sum_{t=1}^{T-1} (|K_{t+1}^{\gamma_{t+1}} - K_{t+1}^{\gamma_t}| + |K_{t+1}^{\gamma_t} - K_t^{\gamma_t}|) \\
&= \underbrace{\sum_{t=1}^{T-1} |K_{t+1}^{\gamma_{t+1}} - K_{t+1}^{\gamma_t}|}_{\text{Part (A)}} + \underbrace{\sum_{t=1}^{T-1} |K_{t+1}^{\gamma_t} - K_t^{\gamma_t}|}_{\text{Part (B)}}
\end{aligned} \tag{95}$$

Bound Part (A) representing the variation in the exponent  $\gamma_t$ . By the Mean Value Theorem for  $f(\gamma) = x^\gamma$  where  $x \in [\delta, 1]$  and  $\delta = \frac{\varepsilon}{G_\infty^2 + \varepsilon}$  (with  $\varepsilon > 0$  being a small constant), there exists  $\xi_t \in [\gamma_{t+1}, \gamma_t]$  such that:

$$\begin{aligned}
|K_{t+1}^{\gamma_{t+1}} - K_{t+1}^{\gamma_t}| &= |K_{t+1}^{\xi_t} \ln(K_{t+1})| \cdot |\gamma_{t+1} - \gamma_t| \\
&\leq C_\varepsilon \cdot \gamma_0 \left( \frac{1}{\sqrt{t}} - \frac{1}{\sqrt{t+1}} \right)
\end{aligned} \tag{96}$$

Summing over  $t$  yields a telescoping series:

$$\begin{aligned}
\sum_{t=1}^{T-1} |K_{t+1}^{\gamma_{t+1}} - K_{t+1}^{\gamma_t}| &\leq C_\varepsilon \gamma_0 \sum_{t=1}^{T-1} \left( \frac{1}{\sqrt{t}} - \frac{1}{\sqrt{t+1}} \right) \\
&= C_\varepsilon \gamma_0 \left( 1 - \frac{1}{\sqrt{T}} \right) = \mathcal{O}(1)
\end{aligned} \tag{97}$$

Bound Part (B) representing the variation in the base  $K_t$ . Assuming  $\gamma_0 \leq 1$ , and using the Lipschitz continuity of  $x^{\gamma_t}$  on  $[\delta, 1]$  with  $\gamma_t \in (0, 1]$ , we observe:

$$\begin{aligned}
|K_{t+1}^{\gamma_t} - K_t^{\gamma_t}| &\leq \left( \sup_{x \in [\delta, 1]} \gamma_t x^{\gamma_t-1} \right) \cdot |K_{t+1} - K_t| \\
&\leq \gamma_t \delta^{\gamma_t-1} \cdot |K_{t+1} - K_t|
\end{aligned} \tag{98}$$

Even if  $|K_{t+1} - K_t| = \mathcal{O}(1)$  due to constant  $\beta_2$  and lack of smoothness, the decay of  $\gamma_t$  ensures:

$$\begin{aligned}
\sum_{t=1}^{T-1} |K_{t+1}^{\gamma_t} - K_t^{\gamma_t}| &\leq \text{Const} \cdot \sum_{t=1}^{T-1} \gamma_t \\
&= \text{Const} \cdot \gamma_0 \sum_{t=1}^{T-1} \frac{1}{\sqrt{t}} \\
&\leq 2 \cdot \text{Const} \cdot \gamma_0 \sqrt{T} = \mathcal{O}(\sqrt{T})
\end{aligned} \tag{99}$$

Combine the bounds to achieve the final sublinear variation.

$$\begin{aligned}
\sum_{t=1}^{T-1} |K_{t+1}^{\gamma_{t+1}} - K_t^{\gamma_t}| &\leq \mathcal{O}(1) + \mathcal{O}(\sqrt{T}) \\
&= \mathcal{O}(\sqrt{T})
\end{aligned} \tag{100}$$

**Theorem C.8.** Assume that Assumption C.1 holds, and  $\beta_1 \in [0, 1)$ . Let the learning rate be  $\alpha_t = \alpha/\sqrt{t}$ . For all  $T \geq 1$ , SGDF achieves the following cumulative regret bound:

$$R(T) \leq \sum_{i=1}^d \left( \frac{D_\infty^2}{2\alpha} + \alpha G_\infty^2 \frac{1 + \beta_1}{1 - \beta_1} \right) \sqrt{T} + \sum_{i=1}^d \frac{\beta_1 G_\infty D_\infty}{1 - \beta_1} \left( 2 + \sum_{t=1}^{T-1} |K_{t,i} - K_{t+1,i}| \right) \tag{101}$$

Under the assumption that the total variation of the interpolation parameter is sublinear, i.e.,  $\sum_{t=1}^{T-1} |K_{t,i} - K_{t+1,i}| \leq \mathcal{O}(\sqrt{T})$ , we have  $R(T) \leq \mathcal{O}(\sqrt{T})$ . Consequently, the average regret converges to zero:  $\lim_{T \rightarrow \infty} \frac{R(T)}{T} = 0$ .

*Proof.* Using Lemma C.4, we lower bound the convex functions to establish the regret connection:

$$f_t(\theta_t) - f_t(\theta^*) \leq \langle g_t, \theta_t - \theta^* \rangle = \sum_{i=1}^d g_{t,i}(\theta_{t,i} - \theta_i^*) \quad (102)$$

From Algorithm 1, the update direction incorporates bias correction and interpolation:

$$\hat{g}_{t,i} = K_{t,i}g_{t,i} + (1 - K_{t,i})\hat{m}_{t,i} \implies g_{t,i} = \hat{g}_{t,i} + (1 - K_{t,i})(g_{t,i} - \hat{m}_{t,i}) \quad (103)$$

Recall the momentum definition  $m_{t,i} = \beta_1 m_{t-1,i} + (1 - \beta_1)g_{t,i}$ , giving  $g_{t,i} - m_{t,i} = \frac{\beta_1}{1 - \beta_1}(m_{t,i} - m_{t-1,i})$ . Also,  $\hat{m}_{t,i} = m_{t,i}/(1 - \beta_1^t)$ . Expanding the difference accurately yields:

$$\begin{aligned} g_{t,i} - \hat{m}_{t,i} &= (g_{t,i} - m_{t,i}) + \left( m_{t,i} - \frac{m_{t,i}}{1 - \beta_1^t} \right) \\ &= \frac{\beta_1}{1 - \beta_1}(m_{t,i} - m_{t-1,i}) - \frac{\beta_1^t}{1 - \beta_1^t} m_{t,i} \end{aligned} \quad (104)$$

Substituting this back, we decompose the inner product into three parts:

$$\sum_{t=1}^T g_{t,i}(\theta_{t,i} - \theta_i^*) = \underbrace{\sum_{t=1}^T \hat{g}_{t,i}(\theta_{t,i} - \theta_i^*)}_{(A)} + \underbrace{\frac{\beta_1}{1 - \beta_1} \sum_{t=1}^T (1 - K_{t,i})(m_{t,i} - m_{t-1,i})(\theta_{t,i} - \theta_i^*)}_{(B)} - \underbrace{\sum_{t=1}^T (1 - K_{t,i}) \frac{\beta_1^t}{1 - \beta_1^t} m_{t,i}(\theta_{t,i} - \theta_i^*)}_{(C)} \quad (105)$$

For part (A), using the parameter update rule  $\theta_{t+1,i} = \theta_{t,i} - \alpha_t \hat{g}_{t,i}$ , we have:

$$\hat{g}_{t,i}(\theta_{t,i} - \theta_i^*) = \frac{(\theta_{t,i} - \theta_i^*)^2 - (\theta_{t+1,i} - \theta_i^*)^2}{2\alpha_t} + \frac{\alpha_t}{2} \hat{g}_{t,i}^2 \quad (106)$$

Summing over  $T$  and noting  $\alpha_t = \alpha/\sqrt{t}$ , we get a telescoping sum:

$$\begin{aligned} \sum_{t=1}^T \hat{g}_{t,i}(\theta_{t,i} - \theta_i^*) &\leq \frac{D_\infty^2}{2\alpha_1} + \sum_{t=2}^T \frac{D_\infty^2}{2} \left( \frac{1}{\alpha_t} - \frac{1}{\alpha_{t-1}} \right) + \frac{\alpha}{2} \sum_{t=1}^T \frac{\hat{g}_{t,i}^2}{\sqrt{t}} \\ &\leq \frac{D_\infty^2 \sqrt{T}}{2\alpha} + \alpha G_\infty^2 \sqrt{T} \quad (\text{Using Lemma C.5 and C.6}) \end{aligned} \quad (107)$$

For part (B), let  $C_{t,i} = 1 - K_{t,i}$ . We apply Summation by Parts (Abel transformation):

$$\begin{aligned} &\sum_{t=1}^T C_{t,i}(m_{t,i} - m_{t-1,i})(\theta_{t,i} - \theta_i^*) \\ &= C_{T,i}m_{T,i}(\theta_{T,i} - \theta_i^*) - C_{1,i}m_{0,i}(\theta_{1,i} - \theta_i^*) - \sum_{t=1}^{T-1} m_{t,i} [C_{t+1,i}(\theta_{t+1,i} - \theta_i^*) - C_{t,i}(\theta_{t,i} - \theta_i^*)] \end{aligned} \quad (108)$$

Since  $m_{0,i} = 0$ , the boundary term is bounded by  $G_\infty D_\infty$ . We rigorously expand the difference inside the summation:

$$\begin{aligned} &C_{t+1,i}(\theta_{t+1,i} - \theta_i^*) - C_{t,i}(\theta_{t,i} - \theta_i^*) \\ &= C_{t+1,i}(\theta_{t+1,i} - \theta_{t,i}) + (C_{t+1,i} - C_{t,i})(\theta_{t,i} - \theta_i^*) \\ &= -(1 - K_{t+1,i})\alpha_t \hat{g}_{t,i} + (K_{t,i} - K_{t+1,i})(\theta_{t,i} - \theta_i^*) \end{aligned} \quad (109)$$

Taking the absolute value and substituting back, we obtain:

$$\begin{aligned} |\text{(B)}| &\leq \frac{\beta_1}{1 - \beta_1} \left( G_\infty D_\infty + \sum_{t=1}^{T-1} |m_{t,i}| \cdot |1 - K_{t+1,i}| \alpha_t |\hat{g}_{t,i}| + \sum_{t=1}^{T-1} |m_{t,i}| \cdot |K_{t,i} - K_{t+1,i}| \cdot |\theta_{t,i} - \theta_i^*| \right) \\ &\leq \frac{\beta_1}{1 - \beta_1} \left( G_\infty D_\infty + \alpha G_\infty^2 \sum_{t=1}^{T-1} \frac{1}{\sqrt{t}} + G_\infty D_\infty \sum_{t=1}^{T-1} |K_{t,i} - K_{t+1,i}| \right) \\ &\leq \frac{\beta_1}{1 - \beta_1} \left( G_\infty D_\infty + 2\alpha G_\infty^2 \sqrt{T} + G_\infty D_\infty \sum_{t=1}^{T-1} |K_{t,i} - K_{t+1,i}| \right) \end{aligned} \quad (110)$$

For part (C), the bias correction residual can be tightly bounded. Recall from Lemma C.6 that  $|m_{t,i}| \leq (1 - \beta_1^t)G_\infty$ . Substituting this into the expression allows us to exactly cancel the denominator:

$$\begin{aligned}
|(\text{C})| &\leq \sum_{t=1}^T |1 - K_{t,i}| \frac{\beta_1^t}{1 - \beta_1^t} |m_{t,i}| |\theta_{t,i} - \theta_i^*| \\
&\leq \sum_{t=1}^T 1 \cdot \frac{\beta_1^t}{1 - \beta_1^t} (1 - \beta_1^t) G_\infty D_\infty \\
&= G_\infty D_\infty \sum_{t=1}^T \beta_1^t \leq \frac{\beta_1}{1 - \beta_1} G_\infty D_\infty
\end{aligned} \tag{111}$$

Summing parts (A), (B), and (C) over all  $d$  dimensions and grouping the terms by  $\sqrt{T}$  and the interpolation total variation, we obtain the highly condensed cumulative regret:

$$R(T) \leq \sum_{i=1}^d \left[ \left( \frac{D_\infty^2}{2\alpha} + \alpha G_\infty^2 \frac{1 + \beta_1}{1 - \beta_1} \right) \sqrt{T} + \frac{\beta_1 G_\infty D_\infty}{1 - \beta_1} \left( 2 + \sum_{t=1}^{T-1} |K_{t,i} - K_{t+1,i}| \right) \right] \tag{112}$$

Given Lemma C.7 that  $\sum |K_{t,i} - K_{t+1,i}| \leq \mathcal{O}(\sqrt{T})$ , the cumulative regret satisfies  $R(T) \leq \mathcal{O}(\sqrt{T})$ . To prove convergence, we evaluate the average regret as  $T \rightarrow \infty$ :

$$\lim_{T \rightarrow \infty} \frac{R(T)}{T} \leq \lim_{T \rightarrow \infty} \frac{\mathcal{O}(\sqrt{T})}{T} = \lim_{T \rightarrow \infty} \mathcal{O}\left(\frac{1}{\sqrt{T}}\right) = 0 \tag{113}$$

■

## D. Convergence analysis for non-convex stochastic optimization (Theorem 3.3 in main paper).

We have relaxed the assumption on the objective function, allowing it to be non-convex, and adjusted the criterion for convergence from the statistic  $R(T)$  to  $\mathbb{E}(T)$ . Let's briefly review the assumptions and the criterion for convergence after relaxing the assumption:

### Assumption D.1.

- A1 Bounded variables (same as convex).  $\|\theta - \theta^*\|_2 \leq D$ ,  $\forall \theta, \theta^*$  or for any dimension  $i$  of the variable,  $\|\theta_i - \theta_i^*\|_2 \leq D_i$ ,  $\forall \theta_i, \theta_i^*$
- A2 The noisy gradient is unbiased. For  $\forall t$ , the random variable  $\zeta_t$  is defined as  $\zeta_t = g_t - \nabla f(\theta_t)$ ,  $\zeta_t$  satisfy  $\mathbb{E}[\zeta_t] = 0$ ,  $\mathbb{E}[\|\zeta_t\|_2^2] \leq \sigma^2$ , and when  $t_1 \neq t_2$ ,  $\zeta_{t_1}$  and  $\zeta_{t_2}$  are statistically independent, i.e.,  $\zeta_{t_1} \perp \zeta_{t_2}$ .
- A3 Bounded gradient and noisy gradient. At step  $t$ , the algorithm can access a bounded noisy gradient, and the true gradient is also bounded. i.e.  $\|\nabla f(\theta_t)\| \leq G$ ,  $\|g_t\| \leq G$ ,  $\forall t > 1$ .
- A4 The property of function. The objective function  $f(\theta)$  is a global loss function, defined as  $f(\theta) = \lim_{T \rightarrow \infty} \frac{1}{T} \sum_{t=1}^T f_t(\theta)$ . Although  $f(\theta)$  is no longer a convex function, it must still be a  $L$ -smooth function, i.e., it satisfies (1)  $f$  is differentiable,  $\nabla f$  exists everywhere in the domain; (2) there exists  $L > 0$  such that for any  $\theta_1$  and  $\theta_2$  in the domain, (first definition)

$$f(\theta_2) \leq f(\theta_1) + \langle \nabla f(\theta_1), \theta_2 - \theta_1 \rangle + \frac{L}{2} \|\theta_2 - \theta_1\|_2^2 \quad (114)$$

or (second definition)

$$\|\nabla f(\theta_1) - \nabla f(\theta_2)\|_2 \leq L \|\theta_1 - \theta_2\|_2 \quad (115)$$

This condition is also known as  $L$ -Lipschitz.

**Definition D.2.** The criterion for convergence is the statistic  $\mathbb{E}(T)$ :

$$\mathbb{E}(T) = \min_{t=1,2,\dots,T} \mathbb{E}_t \left[ \|\nabla f(\theta_t)\|_2^2 \right] \quad (116)$$

When  $T \rightarrow \infty$ , if the amortized value of  $\mathbb{E}(T)$ ,  $\mathbb{E}(T)/T \rightarrow 0$ , we consider such an algorithm to be convergent, and generally, the slower  $\mathbb{E}(T)$  grows with  $T$ , the faster the algorithm converges.

**Definition D.3.** Define  $\xi_t$  as

$$\xi_t = \begin{cases} \theta_t & t = 1 \\ \theta_t + \frac{\beta_1}{1-\beta_1} (\theta_t - \theta_{t-1}) & t \geq 2 \end{cases} \quad (117)$$

**Lemma D.4.** Let  $f$  be an  $L$ -smooth function. Then, for any points  $\xi_t$  and  $\theta_t$ , the following inequality holds:

$$f(\xi_{t+1}) - f(\xi_t) \leq \frac{L}{2} \|\xi_t - \theta_t\|_2^2 + L \|\xi_{t+1} - \xi_t\|_2^2 + \langle \nabla f(\theta_t), \xi_{t+1} - \xi_t \rangle \quad (118)$$

*Proof.* Since  $f$  is an  $L$ -smooth function,

$$\|\nabla f(\xi_t) - \nabla f(\theta_t)\|_2^2 \leq L^2 \|\xi_t - \theta_t\|_2^2 \quad (119)$$

Thus,

$$\begin{aligned}
& f(\xi_{t+1}) - f(\xi_t) \\
& \leq \langle \nabla f(\xi_t), \xi_{t+1} - \xi_t \rangle + \frac{L}{2} \|\xi_{t+1} - \xi_t\|_2^2 \\
& = \left\langle \frac{1}{\sqrt{L}} (\nabla f(\xi_t) - \nabla f(\theta_t)), \sqrt{L} (\xi_{t+1} - \xi_t) \right\rangle + \langle \nabla f(\theta_t), \xi_{t+1} - \xi_t \rangle + \frac{L}{2} \|\xi_{t+1} - \xi_t\|_2^2 \\
& \leq \frac{1}{2} \left( \frac{1}{L} \|\nabla f(\xi_t) - \nabla f(\theta_t)\|_2^2 + L \|\xi_{t+1} - \xi_t\|_2^2 \right) + \langle \nabla f(\theta_t), \xi_{t+1} - \xi_t \rangle + \frac{L}{2} \|\xi_{t+1} - \xi_t\|_2^2 \\
& \leq \frac{1}{2L} \|\nabla f(\xi_t) - \nabla f(\theta_t)\|_2^2 + L \|\xi_{t+1} - \xi_t\|_2^2 + \langle \nabla f(\theta_t), \xi_{t+1} - \xi_t \rangle \\
& \leq \frac{1}{2L} L^2 \|\xi_t - \theta_t\|_2^2 + L \|\xi_{t+1} - \xi_t\|_2^2 + \langle \nabla f(\theta_t), \xi_{t+1} - \xi_t \rangle \\
& = \frac{L}{2} \underbrace{\|\xi_t - \theta_t\|_2^2}_{(1)} + L \underbrace{\|\xi_{t+1} - \xi_t\|_2^2}_{(2)} + \underbrace{\langle \nabla f(\theta_t), \xi_{t+1} - \xi_t \rangle}_{(3)}
\end{aligned} \tag{120}$$

■

**Theorem D.5.** Consider a non-convex optimization problem. Suppose Assumption D.1 are satisfied, and let  $\alpha_t = \alpha/\sqrt{t}$ . For all  $T \geq 1$ , SGDF achieves the following guarantee:

$$\mathbb{E}(T) \leq \frac{C_7 \alpha^2 (\log T + 1) + C_8}{\alpha \sqrt{T}} \tag{121}$$

where  $\mathbb{E}(T) = \min_{t=1,2,\dots,T} \mathbb{E}_{t-1} \left[ \|\nabla f(\theta_t)\|_2^2 \right]$  denotes the minimum of the squared-paradigm expectation of the gradient,  $\alpha$  is the learning rate at the 1-th step,  $C_7$  are constants independent of  $d$  and  $T$ ,  $C_8$  is a constant independent of  $T$ , and the expectation is taken w.r.t all randomness corresponding to  $g_t$ .

*Proof.* According to Lemma D.4, we deal with the three terms (1), (2), and (3) separately.

**Bounding Term (1):** When  $t = 1$ ,  $\|\xi_t - \theta_t\|_2^2 = 0$

When  $t \geq 2$ ,

$$\begin{aligned}
\|\xi_t - \theta_t\|_2^2 &= \left\| \frac{\beta_1}{1 - \beta_1} (\theta_t - \theta_{t-1}) \right\|_2^2 \\
&= \frac{\beta_1^2}{(1 - \beta_1)^2} \alpha_{t-1}^2 \|\hat{g}_{t-1}\|_2^2 \\
&= \frac{\beta_1^2}{(1 - \beta_1)^2} \alpha_{t-1}^2 \sum_{i=1}^d \left( (1 - K_{t-1,i}) (\hat{m}_{t-1,i})^2 + K_{t-1,i} g_{t-1,i}^2 \right) \\
&\stackrel{(a)}{\leq} \frac{\beta_1^2}{(1 - \beta_1)^2} \alpha_{t-1}^2 \sum_{i=1}^d G_i^2
\end{aligned} \tag{122}$$

Where (a) holds because for any  $t$ :

1.  $|\hat{m}_{t,i}| \leq \frac{1}{1 - \beta_1^t} \sum_{s=1}^t (1 - \beta_1) \beta_1^{t-s} |g_{s,i}| \leq \frac{1}{1 - \beta_1^t} \sum_{s=1}^t (1 - \beta_1) \beta_1^{t-s} G_i = G_i$ .
2.  $\|g_t\|_2 \leq G$ ,  $\forall t$ , or for any dimension of the variable  $i$ :  $\|g_{t,i}\|_2 \leq G_i$ ,  $\forall t$

**Bounding Term (2):** For the initial iteration  $t = 1$ , we have:

$$\begin{aligned}
\xi_2 - \xi_1 &= \theta_2 + \frac{\beta_1}{1 - \beta_1} (\theta_2 - \theta_1) - \theta_1 \\
&= \frac{1}{1 - \beta_1} (\theta_2 - \theta_1) \\
&= -\frac{\alpha_1}{1 - \beta_1} (\hat{g}_1) \\
&= -\frac{\alpha_1}{1 - \beta_1} \left( \frac{1 - K_1}{1 - \beta_1} m_1 + K_1 g_1 \right) \\
&= -\frac{\alpha_1}{1 - \beta_1} \frac{1 - K_1}{1 - \beta_1} \left( \beta_1 m_0 + (1 - \beta_1) g_1 \right) - \frac{\alpha_1}{1 - \beta_1} K_1 g_1 \\
&= -\frac{\alpha_1 (1 - K_1)}{1 - \beta_1} g_1 - \frac{\alpha_1 K_1}{1 - \beta_1} g_1 \\
&= -\frac{\alpha_1}{1 - \beta_1} g_1
\end{aligned} \tag{123}$$

Consequently, the squared  $\ell_2$ -norm can be bounded as follows:

$$\begin{aligned}
\|\xi_2 - \xi_1\|_2^2 &= \left\| -\frac{\alpha_1}{1 - \beta_1} g_1 \right\|_2^2 \\
&= \frac{\alpha_1^2}{(1 - \beta_1)^2} \|g_1\|_2^2 \\
&= \frac{\alpha_1^2}{(1 - \beta_1)^2} \sum_{i=1}^d g_{1,i}^2 \\
&\leq \frac{\alpha_1^2}{(1 - \beta_1)^2} \sum_{i=1}^d G_i^2
\end{aligned} \tag{124}$$

For subsequent iterations  $t \geq 2$ , the difference between consecutive auxiliary variables expands as:

$$\begin{aligned}
\xi_{t+1} - \xi_t &= \theta_{t+1} + \frac{\beta_1}{1 - \beta_1} (\theta_{t+1} - \theta_t) - \theta_t - \frac{\beta_1}{1 - \beta_1} (\theta_t - \theta_{t-1}) \\
&= \frac{1}{1 - \beta_1} (\theta_{t+1} - \theta_t) - \frac{\beta_1}{1 - \beta_1} (\theta_t - \theta_{t-1})
\end{aligned} \tag{125}$$

Recalling the parameter update rule, the difference  $\theta_{t+1} - \theta_t$  is given by:

$$\begin{aligned}
\theta_{t+1} - \theta_t &= -\alpha_t \hat{g}_t \\
&= -\frac{\alpha_t (1 - K_t)}{1 - \beta_1^t} m_t - \alpha_t K_t g_t \\
&= -\frac{\alpha_t (1 - K_t)}{1 - \beta_1^t} (\beta_1 m_{t-1} + (1 - \beta_1) g_t) - \alpha_t K_t g_t
\end{aligned} \tag{126}$$

Substituting this expression back into the expansion of  $\xi_{t+1} - \xi_t$  and rearranging the terms, we obtain:

$$\begin{aligned}
& \xi_{t+1} - \xi_t \\
&= \frac{1}{1 - \beta_1} \left( -\frac{\alpha_t(1 - K_t)}{1 - \beta_1^t} (\beta_1 m_{t-1} + (1 - \beta_1) g_t) - \alpha_t K_t g_t \right) \\
&\quad - \frac{\beta_1}{1 - \beta_1} \left( -\frac{\alpha_{t-1}(1 - K_{t-1})}{1 - \beta_1^{t-1}} m_{t-1} - \alpha_{t-1} K_{t-1} g_{t-1} \right) \\
&= -\frac{\beta_1}{1 - \beta_1} m_{t-1} \odot \left( \frac{\alpha_t(1 - K_t)}{1 - \beta_1^t} - \frac{\alpha_{t-1}(1 - K_{t-1})}{1 - \beta_1^{t-1}} \right) \\
&\quad - \left( \frac{\alpha_t(1 - K_t)}{1 - \beta_1^t} + \frac{\alpha_t K_t}{1 - \beta_1} \right) g_t + \frac{\beta_1 \alpha_{t-1} K_{t-1}}{1 - \beta_1} g_{t-1}
\end{aligned} \tag{127}$$

Using the general inequality  $\|A + B + C\|_2^2 \leq 3\|A\|_2^2 + 3\|B\|_2^2 + 3\|C\|_2^2$ , we have:

$$\begin{aligned}
\|\xi_{t+1} - \xi_t\|_2^2 &\leq 3 \left\| -\frac{\beta_1}{1 - \beta_1} m_{t-1} \odot \left( \frac{\alpha_t(1 - K_t)}{1 - \beta_1^t} - \frac{\alpha_{t-1}(1 - K_{t-1})}{1 - \beta_1^{t-1}} \right) \right\|_2^2 \\
&\quad + 3 \left\| -\left( \frac{\alpha_t(1 - K_t)}{1 - \beta_1^t} + \frac{\alpha_t K_t}{1 - \beta_1} \right) g_t \right\|_2^2 + 3 \left\| \frac{\beta_1 \alpha_{t-1} K_{t-1}}{1 - \beta_1} g_{t-1} \right\|_2^2
\end{aligned} \tag{128}$$

To properly decouple the step size decay from the dynamic mask flipping, let  $\eta_t = \frac{\alpha_t}{1 - \beta_1^t}$ . We can decompose the mask difference algebraically by adding and subtracting  $\eta_{t-1} K_t$ :

$$\begin{aligned}
\eta_t(1 - K_t) - \eta_{t-1}(1 - K_{t-1}) &= \eta_t - \eta_t K_t - \eta_{t-1} + \eta_{t-1} K_{t-1} \\
&= (\eta_t - \eta_{t-1}) - \eta_t K_t + \eta_{t-1} K_t - \eta_{t-1} K_t + \eta_{t-1} K_{t-1} \\
&= (\eta_t - \eta_{t-1})(1 - K_t) + \eta_{t-1}(K_{t-1} - K_t)
\end{aligned} \tag{129}$$

Using the inequality  $\|A + B\|_2^2 \leq 2\|A\|_2^2 + 2\|B\|_2^2$ , we bound the squared  $\ell_2$  norm of this difference. Since  $K_{t,i} \in \{0, 1\}$ , we have  $(1 - K_{t,i})^2 \leq 1$  and  $(K_{t-1,i} - K_{t,i})^2 = |K_{t-1,i} - K_{t,i}|$ :

$$\begin{aligned}
\left\| \frac{\alpha_t(1 - K_t)}{1 - \beta_1^t} - \frac{\alpha_{t-1}(1 - K_{t-1})}{1 - \beta_1^{t-1}} \right\|_2^2 &= \sum_{i=1}^d ((\eta_t - \eta_{t-1})(1 - K_{t,i}) + \eta_{t-1}(K_{t-1,i} - K_{t,i}))^2 \\
&\leq 2 \sum_{i=1}^d (\eta_{t-1} - \eta_t)^2 (1 - K_{t,i})^2 + 2 \sum_{i=1}^d \eta_{t-1}^2 (K_{t-1,i} - K_{t,i})^2 \\
&\leq 2 \sum_{i=1}^d (\eta_{t-1} - \eta_t)^2 + 2\eta_{t-1}^2 \sum_{i=1}^d |K_{t-1,i} - K_{t,i}|
\end{aligned} \tag{130}$$

Since  $\eta_t$  is monotonically decreasing,  $\eta_{t-1} - \eta_t \geq 0$ , and thus  $(\eta_{t-1} - \eta_t)^2 \leq \eta_1(\eta_{t-1} - \eta_t)$ . Let  $F_t = \sum_{i=1}^d |K_{t-1,i} - K_{t,i}|$  denote the total number of flipped mask bits at step  $t$ . To maintain a tight bound, we retain  $F_t$ :

$$\begin{aligned}
\left\| \frac{\alpha_t(1 - K_t)}{1 - \beta_1^t} - \frac{\alpha_{t-1}(1 - K_{t-1})}{1 - \beta_1^{t-1}} \right\|_2^2 &\leq 2d\eta_1(\eta_{t-1} - \eta_t) + 2\eta_{t-1}^2 F_t \\
&\leq 2d\eta_1 \left( \frac{\alpha_{t-1}}{1 - \beta_1^{t-1}} - \frac{\alpha_t}{1 - \beta_1^t} \right) + 2F_t \left( \frac{\alpha_{t-1}}{1 - \beta_1^{t-1}} \right)^2
\end{aligned} \tag{131}$$

Now, bounding the three terms of  $\|\xi_{t+1} - \xi_t\|_2^2$  respectively. For the first term, since  $|m_{t-1,i}| \leq G_i$ :

$$\begin{aligned}
& 3 \left\| \frac{\beta_1}{1-\beta_1} m_{t-1} \odot \left( \frac{\alpha_t(1-K_t)}{1-\beta_1^t} - \frac{\alpha_{t-1}(1-K_{t-1})}{1-\beta_1^{t-1}} \right) \right\|_2^2 \\
& \leq 3 \frac{\beta_1^2}{(1-\beta_1)^2} \left( \max_i G_i \right)^2 \left( 2d\eta_1 \left( \frac{\alpha_{t-1}}{1-\beta_1^{t-1}} - \frac{\alpha_t}{1-\beta_1^t} \right) + 2F_t \left( \frac{\alpha_{t-1}}{1-\beta_1^{t-1}} \right)^2 \right) \\
& = 6d \frac{\beta_1^2 \eta_1}{(1-\beta_1)^2} \left( \max_i G_i \right)^2 \left( \frac{\alpha_{t-1}}{1-\beta_1^{t-1}} - \frac{\alpha_t}{1-\beta_1^t} \right) + 6F_t \frac{\beta_1^2}{(1-\beta_1)^2} \left( \max_i G_i \right)^2 \left( \frac{\alpha_{t-1}}{1-\beta_1^{t-1}} \right)^2
\end{aligned} \tag{132}$$

For the second term, notice that  $1 - \beta_1 \leq 1 - \beta_1^t$ , which implies  $\frac{1}{1-\beta_1} \geq \frac{1}{1-\beta_1^t}$ . Since the dimensions masked by  $K_t$  and  $1 - K_t$  are completely disjoint, we safely bound the disjoint coefficients using the globally larger denominator  $\frac{1}{1-\beta_1}$ :

$$\begin{aligned}
& 3 \left\| \left( \frac{\alpha_t(1-K_t)}{1-\beta_1^t} + \frac{\alpha_t K_t}{1-\beta_1} \right) g_t \right\|_2^2 = 3 \sum_{i=1}^d \left( \frac{\alpha_t(1-K_{t,i})}{1-\beta_1^t} + \frac{\alpha_t K_{t,i}}{1-\beta_1} \right)^2 g_{t,i}^2 \\
& \leq 3 \left( \frac{\alpha_t}{1-\beta_1} \right)^2 \sum_{i=1}^d G_i^2
\end{aligned} \tag{133}$$

For the third term, we maintain the exact  $\beta_1$  constant multiplier to prevent invalid bounding:

$$3 \left\| \frac{\beta_1 \alpha_{t-1} K_{t-1}}{1-\beta_1} g_{t-1} \right\|_2^2 \leq 3 \frac{\beta_1^2 \alpha_{t-1}^2}{(1-\beta_1)^2} \sum_{i=1}^d G_i^2 \tag{134}$$

Therefore, bringing everything together, we obtain the corrected upper bound:

$$\begin{aligned}
\|\xi_{t+1} - \xi_t\|_2^2 & \leq 6d \frac{\beta_1^2 \eta_1}{(1-\beta_1)^2} \left( \max_i G_i \right)^2 \left( \frac{\alpha_{t-1}}{1-\beta_1^{t-1}} - \frac{\alpha_t}{1-\beta_1^t} \right) \\
& \quad + 6F_t \frac{\beta_1^2}{(1-\beta_1)^2} \left( \max_i G_i \right)^2 \left( \frac{\alpha_{t-1}}{1-\beta_1^{t-1}} \right)^2 \\
& \quad + 3 \left( \frac{\alpha_t}{1-\beta_1} \right)^2 \sum_{i=1}^d G_i^2 + 3 \frac{\beta_1^2 \alpha_{t-1}^2}{(1-\beta_1)^2} \sum_{i=1}^d G_i^2
\end{aligned} \tag{135}$$

**Bounding Term (3):** When  $t = 1$ , referring to the case of  $t = 1$  in the previous subsection, we expand the inner product:

$$\begin{aligned}
\langle \nabla f(\theta_1), \xi_2 - \xi_1 \rangle & = \left\langle \nabla f(\theta_1), -\frac{\alpha_1}{1-\beta_1} g_1 \right\rangle \\
& = \left\langle \nabla f(\theta_1), -\frac{\alpha_1}{1-\beta_1} \nabla f(\theta_1) \right\rangle + \left\langle \nabla f(\theta_1), -\frac{\alpha_1}{1-\beta_1} \zeta_1 \right\rangle \\
& = -\frac{\alpha_1}{1-\beta_1} \|\nabla f(\theta_1)\|_2^2 + \left\langle \nabla f(\theta_1), -\frac{\alpha_1}{1-\beta_1} \zeta_1 \right\rangle
\end{aligned} \tag{136}$$

Note that we leave the inner product with the zero-mean noise  $\zeta_1$  exactly as it is, because it will vanish when taking the conditional expectation later.

When  $t \geq 2$ ,

$$\begin{aligned}
& \langle \nabla f(\theta_t), \xi_{t+1} - \xi_t \rangle \\
& = \left\langle \nabla f(\theta_t), -\frac{\beta_1}{1-\beta_1} m_{t-1} \odot \left( \frac{\alpha_t(1-K_t)}{1-\beta_1^t} - \frac{\alpha_{t-1}(1-K_{t-1})}{1-\beta_1^{t-1}} \right) \right\rangle \\
& \quad + \left\langle \nabla f(\theta_t), -\left( \frac{\alpha_t(1-K_t)}{1-\beta_1^t} + \frac{\alpha_t K_t}{1-\beta_1} \right) \nabla f(\theta_t) \right\rangle + \left\langle \nabla f(\theta_t), -\left( \frac{\alpha_t(1-K_t)}{1-\beta_1^t} + \frac{\alpha_t K_t}{1-\beta_1} \right) \zeta_t \right\rangle \\
& \quad + \left\langle \nabla f(\theta_t), \frac{\beta_1 \alpha_{t-1} K_{t-1}}{1-\beta_1} \nabla f(\theta_{t-1}) \right\rangle + \left\langle \nabla f(\theta_t), \frac{\beta_1 \alpha_{t-1} K_{t-1}}{1-\beta_1} \zeta_{t-1} \right\rangle
\end{aligned} \tag{137}$$

Let us deal with the terms after the equal sign separately.

Start by looking at the first term. We decouple the step size decay and dynamic mask flipping using the identity  $\eta_t(1 - K_t) - \eta_{t-1}(1 - K_{t-1}) = (\eta_t - \eta_{t-1})(1 - K_t) + \eta_{t-1}(K_{t-1} - K_t)$  and Hölder's inequality ( $|\langle A, B \rangle| \leq \|A\|_\infty \|B\|_1$ ):

$$\begin{aligned}
& \left\langle \nabla f(\theta_t), -\frac{\beta_1}{1-\beta_1} m_{t-1} \odot \left( \frac{\alpha_t(1-K_t)}{1-\beta_1^t} - \frac{\alpha_{t-1}(1-K_{t-1})}{1-\beta_1^{t-1}} \right) \right\rangle \\
& \leq \frac{\beta_1}{1-\beta_1} \|\nabla f(\theta_t)\|_\infty \|m_{t-1}\|_\infty \left\| \frac{\alpha_t(1-K_t)}{1-\beta_1^t} - \frac{\alpha_{t-1}(1-K_{t-1})}{1-\beta_1^{t-1}} \right\|_1 \\
& \leq \frac{\beta_1}{1-\beta_1} \left( \max_i G_i \right)^2 \left( \sum_{i=1}^d \left( \frac{\alpha_{t-1}}{1-\beta_1^{t-1}} - \frac{\alpha_t}{1-\beta_1^t} \right) (1-K_{t,i}) + \sum_{i=1}^d \frac{\alpha_{t-1}}{1-\beta_1^{t-1}} |K_{t-1,i} - K_{t,i}| \right) \\
& \leq \frac{\beta_1}{1-\beta_1} \left( \max_i G_i \right)^2 \cdot d \left( \frac{\alpha_{t-1}}{1-\beta_1^{t-1}} - \frac{\alpha_t}{1-\beta_1^t} \right) + \frac{\beta_1}{1-\beta_1} \left( \max_i G_i \right)^2 \frac{\alpha_{t-1}}{1-\beta_1^{t-1}} F_t
\end{aligned} \tag{138}$$

where  $F_t = \sum_{i=1}^d |K_{t-1,i} - K_{t,i}|$  represents the number of indices where the mask changes at step  $t$ .

For the second and third terms, notice that since  $1 - \beta_1^t \geq 1 - \beta_1$ , we have  $\frac{\alpha_t(1-K_t)}{1-\beta_1^t} + \frac{\alpha_t K_t}{1-\beta_1} \geq \frac{\alpha_t}{1-\beta_1^t} (1 - K_t + K_t) = \frac{\alpha_t}{1-\beta_1^t}$ :

$$\begin{aligned}
& \left\langle \nabla f(\theta_t), -\left( \frac{\alpha_t(1-K_t)}{1-\beta_1^t} + \frac{\alpha_t K_t}{1-\beta_1} \right) \nabla f(\theta_t) \right\rangle + \left\langle \nabla f(\theta_t), -\left( \frac{\alpha_t(1-K_t)}{1-\beta_1^t} + \frac{\alpha_t K_t}{1-\beta_1} \right) \zeta_t \right\rangle \\
& \leq -\frac{\alpha_t}{1-\beta_1^t} \|\nabla f(\theta_t)\|_2^2 + \left\langle \nabla f(\theta_t), -\left( \frac{\alpha_t(1-K_t)}{1-\beta_1^t} + \frac{\alpha_t K_t}{1-\beta_1} \right) \zeta_t \right\rangle
\end{aligned} \tag{139}$$

For the fourth term (the cross-gradient term), applying Hölder's inequality directly would yield an un-decaying  $\mathcal{O}(\alpha_{t-1})$  penalty. Instead, we use the basic inequality  $2\langle a, b \rangle \leq \|a\|_2^2 + \|b\|_2^2$ . Since  $K_{t-1,i} \in \{0, 1\}$ , we have:

$$\begin{aligned}
\left\langle \nabla f(\theta_t), \frac{\beta_1 \alpha_{t-1} K_{t-1}}{1-\beta_1} \nabla f(\theta_{t-1}) \right\rangle &= \frac{\beta_1 \alpha_{t-1}}{1-\beta_1} \sum_{i=1}^d K_{t-1,i} \nabla f(\theta_t)_i \nabla f(\theta_{t-1})_i \\
&\leq \frac{\beta_1 \alpha_{t-1}}{2(1-\beta_1)} \sum_{i=1}^d K_{t-1,i} (\nabla f(\theta_t)_i^2 + \nabla f(\theta_{t-1})_i^2) \\
&\leq \frac{\beta_1 \alpha_{t-1}}{2(1-\beta_1)} \left( \|\nabla f(\theta_t)\|_2^2 + \|\nabla f(\theta_{t-1})\|_2^2 \right)
\end{aligned} \tag{140}$$

For the fifth term (the noise term involving  $\zeta_{t-1}$ ), taking the absolute value would similarly result in an  $\mathcal{O}(\alpha_{t-1})$  error bound. To properly bound it, we decompose the inner product to leverage the expectation later:

$$\begin{aligned}
\left\langle \nabla f(\theta_t), \frac{\beta_1 \alpha_{t-1} K_{t-1}}{1-\beta_1} \zeta_{t-1} \right\rangle &= \frac{\beta_1 \alpha_{t-1}}{1-\beta_1} \langle \nabla f(\theta_{t-1}), K_{t-1} \odot \zeta_{t-1} \rangle \\
&+ \frac{\beta_1 \alpha_{t-1}}{1-\beta_1} \langle \nabla f(\theta_t) - \nabla f(\theta_{t-1}), K_{t-1} \odot \zeta_{t-1} \rangle
\end{aligned} \tag{141}$$

Notice that when taking the expectation, the first part satisfies  $\mathbb{E}_{t-2} [\langle \nabla f(\theta_{t-1}), K_{t-1} \odot \zeta_{t-1} \rangle] = 0$  because both  $\theta_{t-1}$  and  $K_{t-1}$  are independent of the noise realization  $\zeta_{t-1}$ . For the second part, we apply the Cauchy-Schwarz inequality and utilize the  $L$ -smoothness of the objective function. Given that  $\|\theta_t - \theta_{t-1}\|_2 \leq \alpha_{t-1} \|\hat{g}_{t-1}\|_2 \leq \alpha_{t-1} \sqrt{\sum_{i=1}^d G_i^2}$  and

$\|\zeta_{t-1}\|_2 \leq 2\sqrt{\sum_{i=1}^d G_i^2}$ , we can bound this term strictly by  $\mathcal{O}(\alpha_{t-1}^2)$ :

$$\begin{aligned}
\frac{\beta_1 \alpha_{t-1}}{1-\beta_1} \langle \nabla f(\theta_t) - \nabla f(\theta_{t-1}), K_{t-1} \odot \zeta_{t-1} \rangle &\leq \frac{\beta_1 \alpha_{t-1}}{1-\beta_1} \|\nabla f(\theta_t) - \nabla f(\theta_{t-1})\|_2 \|\zeta_{t-1}\|_2 \\
&\leq \frac{\beta_1 \alpha_{t-1}}{1-\beta_1} L \|\theta_t - \theta_{t-1}\|_2 \|\zeta_{t-1}\|_2 \\
&\leq \frac{\beta_1 \alpha_{t-1}}{1-\beta_1} L \left( \alpha_{t-1} \sqrt{\sum_{i=1}^d G_i^2} \right) \left( 2 \sqrt{\sum_{i=1}^d G_i^2} \right) \\
&= \frac{2L\beta_1}{1-\beta_1} \alpha_{t-1}^2 \sum_{i=1}^d G_i^2
\end{aligned} \tag{142}$$

Finally, combining everything together:

$$\begin{aligned}
&\langle \nabla f(\theta_t), \xi_{t+1} - \xi_t \rangle \\
&\leq \frac{\beta_1 d}{1-\beta_1} \left( \max_i G_i \right)^2 \left( \frac{\alpha_{t-1}}{1-\beta_1^{t-1}} - \frac{\alpha_t}{1-\beta_1^t} \right) + \frac{\beta_1}{1-\beta_1} \left( \max_i G_i \right)^2 \frac{\alpha_{t-1}}{1-\beta_1^{t-1}} F_t \\
&\quad - \left( \frac{\alpha_t}{1-\beta_1^t} - \frac{\beta_1 \alpha_{t-1}}{2(1-\beta_1)} \right) \|\nabla f(\theta_t)\|_2^2 + \frac{\beta_1 \alpha_{t-1}}{2(1-\beta_1)} \|\nabla f(\theta_{t-1})\|_2^2 \\
&\quad + \left\langle \nabla f(\theta_t), - \left( \frac{\alpha_t(1-K_t)}{1-\beta_1^t} + \frac{\alpha_t K_t}{1-\beta_1} \right) \zeta_t \right\rangle \\
&\quad + \frac{\beta_1 \alpha_{t-1}}{1-\beta_1} \langle \nabla f(\theta_{t-1}), K_{t-1} \odot \zeta_{t-1} \rangle + \frac{2L\beta_1}{1-\beta_1} \alpha_{t-1}^2 \sum_{i=1}^d G_i^2
\end{aligned} \tag{143}$$

**Summarizing the results** Since we have already rigorously bounded the cross-inner product terms and the noise components in the previous subsection, we can proceed directly to summarizing the results.

First, taking the expectation  $\mathbb{E}_t$  over the random distribution of  $\zeta_1, \zeta_2, \dots, \zeta_t$  on both sides of the inequality. Since the value of  $\theta_t$  is independent of  $g_t$ , they are statistically independent of  $\zeta_t$ , and  $\mathbb{E}_t[\zeta_t] = 0$ . Therefore, all inner products with  $\zeta_t$  perfectly vanish:

$$\begin{aligned}
&\mathbb{E}_t \left[ \left\langle \nabla f(\theta_t), - \left( \frac{\alpha_t(1-K_t)}{1-\beta_1^t} + \frac{\alpha_t K_t}{1-\beta_1} \right) \zeta_t \right\rangle \right] \\
&= \left\langle - \left( \frac{\alpha_t(1-K_t)}{1-\beta_1^t} + \frac{\alpha_t K_t}{1-\beta_1} \right) \nabla f(\theta_t), \mathbb{E}_t[\zeta_t] \right\rangle = 0
\end{aligned} \tag{144}$$

Combining the bounds from Term (1), Term (2), and the refined Term (3), for  $t \geq 2$ , we have:

$$\begin{aligned}
&\mathbb{E}_t [f(\xi_{t+1}) - f(\xi_t)] \\
&\leq \frac{L\beta_1^2}{2(1-\beta_1)^2} \alpha_{t-1}^2 \sum_{i=1}^d G_i^2 + 6dL \frac{\beta_1^2 \eta_1}{(1-\beta_1)^2} (\max_i G_i)^2 \left( \frac{\alpha_{t-1}}{1-\beta_1^{t-1}} - \frac{\alpha_t}{1-\beta_1^t} \right) \\
&\quad + \left( 6F_t \frac{\beta_1^2}{(1-\beta_1)^2} (\max_i G_i)^2 + 3L \sum_{i=1}^d G_i^2 \right) \left( \frac{\alpha_{t-1}}{1-\beta_1^{t-1}} \right)^2 + 3L \left( \frac{\alpha_t}{1-\beta_1} \right)^2 \sum_{i=1}^d G_i^2 \\
&\quad + \frac{\beta_1 d}{1-\beta_1} (\max_i G_i)^2 \left( \frac{\alpha_{t-1}}{1-\beta_1^{t-1}} - \frac{\alpha_t}{1-\beta_1^t} \right) + \frac{\beta_1}{(1-\beta_1)^2} (\max_i G_i)^2 \left( \frac{\alpha_{t-1}}{1-\beta_1^{t-1}} \right) F_t \\
&\quad - \left( \frac{\alpha_t}{1-\beta_1^t} - \frac{\beta_1 \alpha_{t-1}}{2(1-\beta_1)} \right) \mathbb{E}_t \|\nabla f(\theta_t)\|_2^2 + \frac{\beta_1 \alpha_{t-1}}{2(1-\beta_1)} \mathbb{E}_{t-1} \|\nabla f(\theta_{t-1})\|_2^2 \\
&\quad + \frac{2L\beta_1}{1-\beta_1} \alpha_{t-1}^2 \sum_{i=1}^d G_i^2
\end{aligned} \tag{145}$$

To maintain the inequality and simplify the notation, we define the following iteration-independent constants. Note that  $\frac{1}{1-\beta_1^t} \leq \frac{1}{1-\beta_1}$ , and we absorb the new noise bound into  $C_1$ :

1. For  $\alpha_{t-1}^2$ :  $C_1 \triangleq \frac{L\beta_1^2}{2(1-\beta_1)^2} \sum_{i=1}^d G_i^2 + \frac{3L}{(1-\beta_1)^2} \sum_{i=1}^d G_i^2 + \frac{2L\beta_1}{1-\beta_1} \sum_{i=1}^d G_i^2$
  2. For  $\alpha_t^2$ :  $C_2 \triangleq \frac{3L}{(1-\beta_1)^2} \sum_{i=1}^d G_i^2$
  3. For the telescoping difference:  $C_3 \triangleq \frac{6dL\beta_1^2\alpha_1}{(1-\beta_1)^3} (\max_i G_i)^2 + \frac{\beta_1 d}{1-\beta_1} (\max_i G_i)^2$
  4. For the dynamic mask flipping terms (both linear and squared):  $C_4 \triangleq \frac{\beta_1}{(1-\beta_1)^2} (\max_i G_i)^2 + \frac{6\beta_1^2}{(1-\beta_1)^4} (\max_i G_i)^2 \alpha_1$
- For  $t = 1$ :

$$\mathbb{E}_1 [f(\xi_2) - f(\xi_1)] \leq \frac{L}{(1-\beta_1)^2} \alpha_1^2 \sum_{i=1}^d G_i^2 - \frac{\alpha_1}{1-\beta_1} \mathbb{E}_1 \|\nabla f(\theta_1)\|_2^2 \quad (146)$$

Summing up both sides of the inequality for  $t = 1, 2, \dots, T$ :

**Left side of the inequality (LHS)**

$$\begin{aligned} \sum_{t=1}^T \mathbb{E}_t [f(\xi_{t+1}) - f(\xi_t)] &= \mathbb{E}_T [f(\xi_{T+1})] - \mathbb{E}_0 [f(\xi_1)] \\ &\geq f(\theta^*) - f(\theta_1) \end{aligned} \quad (147)$$

**Right side of the inequality (RHS)**

$$\begin{aligned} \sum_{t=1}^T \mathbb{E}_t [\text{RHS}] &\leq \sum_{t=2}^T C_1 \alpha_{t-1}^2 + \sum_{t=2}^T C_2 \alpha_t^2 + \sum_{t=2}^T C_3 \left( \frac{\alpha_{t-1}}{1-\beta_1^{t-1}} - \frac{\alpha_t}{1-\beta_1^t} \right) + \sum_{t=2}^T C_4 \frac{\alpha_{t-1}}{1-\beta_1^{t-1}} F_t \\ &\quad + \sum_{t=2}^T \frac{\beta_1 \alpha_{t-1}}{2(1-\beta_1)} \mathbb{E}_{t-1} \|\nabla f(\theta_{t-1})\|_2^2 - \sum_{t=2}^T \left( \frac{\alpha_t}{1-\beta_1^t} - \frac{\beta_1 \alpha_{t-1}}{2(1-\beta_1)} \right) \mathbb{E}_t \|\nabla f(\theta_t)\|_2^2 \\ &\quad + \frac{L}{(1-\beta_1)^2} \alpha_1^2 \sum_{i=1}^d G_i^2 - \frac{\alpha_1}{1-\beta_1} \mathbb{E}_1 \|\nabla f(\theta_1)\|_2^2 \end{aligned} \quad (148)$$

We rigorously shift the index of the positive gradient expectation term to combine it with the negative counterpart. By shifting  $k = t - 1$ :

$$\begin{aligned} &\sum_{t=2}^T \frac{\beta_1 \alpha_{t-1}}{2(1-\beta_1)} \mathbb{E}_{t-1} \|\nabla f(\theta_{t-1})\|_2^2 - \sum_{t=2}^T \left( \frac{\alpha_t}{1-\beta_1^t} - \frac{\beta_1 \alpha_{t-1}}{2(1-\beta_1)} \right) \mathbb{E}_t \|\nabla f(\theta_t)\|_2^2 \\ &= \frac{\beta_1 \alpha_1}{2(1-\beta_1)} \mathbb{E}_1 \|\nabla f(\theta_1)\|_2^2 + \sum_{t=2}^{T-1} \frac{\beta_1 \alpha_t}{2(1-\beta_1)} \mathbb{E}_t \|\nabla f(\theta_t)\|_2^2 \\ &\quad - \sum_{t=2}^{T-1} \left( \frac{\alpha_t}{1-\beta_1^t} - \frac{\beta_1 \alpha_{t-1}}{2(1-\beta_1)} \right) \mathbb{E}_t \|\nabla f(\theta_t)\|_2^2 - \left( \frac{\alpha_T}{1-\beta_1^T} - \frac{\beta_1 \alpha_{T-1}}{2(1-\beta_1)} \right) \mathbb{E}_T \|\nabla f(\theta_T)\|_2^2 \\ &\leq \frac{\beta_1 \alpha_1}{2(1-\beta_1)} \mathbb{E}_1 \|\nabla f(\theta_1)\|_2^2 - \sum_{t=2}^T \left( \frac{\alpha_t}{1-\beta_1^t} - \frac{\beta_1 (\alpha_{t-1} + \alpha_t)}{2(1-\beta_1)} \right) \mathbb{E}_t \|\nabla f(\theta_t)\|_2^2 \end{aligned} \quad (149)$$

where the inequality holds because we drop the strictly negative term  $-\frac{\beta_1 \alpha_T}{2(1-\beta_1)} \mathbb{E}_T \|\nabla f(\theta_T)\|_2^2$  to upper-bound the expression.

Now, integrating the  $t = 1$  expectation term from the initialization, we observe that since  $\beta_1 < 1$ , the combined coefficient for  $t = 1$  is strictly negative:

$$-\frac{\alpha_1}{1-\beta_1} \mathbb{E}_1 \|\nabla f(\theta_1)\|_2^2 + \frac{\beta_1 \alpha_1}{2(1-\beta_1)} \mathbb{E}_1 \|\nabla f(\theta_1)\|_2^2 = -\frac{\alpha_1(2-\beta_1)}{2(1-\beta_1)} \mathbb{E}_1 \|\nabla f(\theta_1)\|_2^2 \leq -\frac{\alpha_1}{2(1-\beta_1)} \mathbb{E}_1 \|\nabla f(\theta_1)\|_2^2 \quad (150)$$

For  $t \geq 2$ , we assume the effective learning rate is chosen to be small enough such that this coefficient bounds the descent effectively:  $\frac{\alpha_t}{1-\beta_1^t} - \frac{\beta_1(\alpha_{t-1} + \alpha_t)}{2(1-\beta_1)} \geq \frac{\alpha_t}{2(1-\beta_1^t)}$ . Combining this with the bounds for the telescoping difference sum ( $\leq \frac{\alpha_1}{1-\beta_1}$ )

and the mask flipping bounded by  $S_{\text{total}}$ , we have:

$$f(\theta^*) - f(\theta_1) \leq (C_1 + C_2) \sum_{t=1}^T \alpha_t^2 + C_3 \frac{\alpha_1}{1 - \beta_1} + C_4 \frac{\alpha_1}{1 - \beta_1} S_{\text{total}} - \sum_{t=1}^T \frac{\alpha_t}{2(1 - \beta_1^t)} \mathbb{E}_t \left[ \|\nabla f(\theta_t)\|_2^2 \right] \quad (151)$$

Rearranging the terms to isolate the gradient norm:

$$\sum_{t=1}^T \frac{\alpha_t}{2(1 - \beta_1^t)} \mathbb{E}_t \left[ \|\nabla f(\theta_t)\|_2^2 \right] \leq (C_1 + C_2) \sum_{t=1}^T \alpha_t^2 + f(\theta_1) - f(\theta^*) + C_3 \frac{\alpha_1}{1 - \beta_1} + C_4 \frac{\alpha_1}{1 - \beta_1} S_{\text{total}} \quad (152)$$

Let  $C_7 \triangleq 2(C_1 + C_2)$  and let  $C_8$  absorb all the non-decaying initial constants,  $C_8 \triangleq 2 \left( f(\theta_1) - f(\theta^*) + C_3 \frac{\alpha_1}{1 - \beta_1} + C_4 \frac{\alpha_1}{1 - \beta_1} S_{\text{total}} \right)$ . Note that since  $1 - \beta_1^t \leq 1$ , we universally have  $\frac{1}{1 - \beta_1^t} \geq 1$ . Therefore, multiplying both sides by 2 yields:

$$\sum_{t=1}^T \alpha_t \mathbb{E}_t \left[ \|\nabla f(\theta_t)\|_2^2 \right] \leq \sum_{t=1}^T \frac{\alpha_t}{1 - \beta_1^t} \mathbb{E}_t \left[ \|\nabla f(\theta_t)\|_2^2 \right] \leq C_7 \sum_{t=1}^T \alpha_t^2 + C_8 \quad (153)$$

Extracting the minimum over the trajectory  $\mathbb{E}(T) = \min_{t=1, \dots, T} \mathbb{E}_{t-1} \left[ \|\nabla f(\theta_t)\|_2^2 \right]$ :

$$\mathbb{E}(T) \sum_{t=1}^T \alpha_t \leq \sum_{t=1}^T \alpha_t \mathbb{E}_t \left[ \|\nabla f(\theta_t)\|_2^2 \right] \leq C_7 \sum_{t=1}^T \alpha_t^2 + C_8 \implies \mathbb{E}(T) \leq \frac{C_7 \sum_{t=1}^T \alpha_t^2 + C_8}{\sum_{t=1}^T \alpha_t} \quad (154)$$

Since  $\alpha_t = \alpha/\sqrt{t}$ , we apply the standard integral bound for the squared step size summation:

$$\sum_{t=1}^T \alpha_t^2 = \alpha^2 \sum_{t=1}^T \frac{1}{t} \leq \alpha^2 \left( 1 + \int_1^T \frac{1}{x} dx \right) = \alpha^2 (\log T + 1) \quad (155)$$

For the linear step size summation, we can strictly lower bound it by replacing each term with the minimum term in the sequence:

$$\sum_{t=1}^T \alpha_t = \alpha \sum_{t=1}^T \frac{1}{\sqrt{t}} \geq \alpha \sum_{t=1}^T \frac{1}{\sqrt{T}} = \alpha \frac{T}{\sqrt{T}} = \alpha \sqrt{T} \quad (156)$$

Substituting the upper bound of the numerator and the lower bound of the denominator yields the final finite-time convergence bound:

$$\mathbb{E}(T) \leq \frac{C_7 \alpha^2 (\log T + 1) + C_8}{\alpha \sqrt{T}} = \mathcal{O} \left( \frac{\log T}{\sqrt{T}} \right) \quad (157)$$

■

## E. Detailed Experimental Supplement

We performed extensive comparisons with other optimizers, including SGD [57], Adam [40], RAdam [49] and AdamW [50], and so on. The experiments include: (a) image classification on CIFAR dataset [41] with VGG [69], ResNet [30] and DenseNet [33], and image recognition with VGG, ResNet, and DenseNet on ImageNet [15].

### E.1. Image classification with CNNs on CIFAR

For all experiments, the model is trained for 200 epochs with a batch size of 128, and the learning rate is multiplied by 0.1 at epoch 150. We performed extensive hyperparameter search as described in the main paper. Here, we report both training and test accuracy in Fig. 4 and Fig. 5. Detailed experimental parameters we place in Tab. 8. We summarize the mean best test accuracies and their standard deviations for each algorithm in Tab. 9. The best results are highlighted in bold font. SGDF not only achieves the highest test accuracy but also a smaller gap between training and test accuracy compared with other optimizers. We ran each experiment three times with different seeds  $\{0, 1, 2\}$  to ensure the robustness of the results.

Table 8. Hyperparameters used for CIFAR-10 and CIFAR-100 datasets.

Optimizer	Learning Rate	$\beta_1$	$\beta_2$	Epochs	Schedule	Weight Decay	Batch Size	$\epsilon$
SGDF	0.5	0.9	0.999	200	StepLR	0.0005	128	1e-8
SGD	0.1	0.9	-	200	StepLR	0.0005	128	-
Adam	0.001	0.9	0.999	200	StepLR	0.0005	128	1e-8
RAdam	0.001	0.9	0.999	200	StepLR	0.0005	128	1e-8
AdamW	0.001	0.9	0.999	200	StepLR	0.01	128	1e-8
MSVAG	0.1	0.9	0.999	200	StepLR	0.0005	128	1e-8
AdaBound	0.001	0.9	0.999	200	StepLR	0.0005	128	-
Sophia	0.0001	0.965	0.99	200	StepLR	0.1	128	-
Lion	0.00002	0.9	0.99	200	StepLR	0.1	128	-
AdaBound	0.001	0.9	0.999	200	StepLR	0.0005	128	1e-8

Table 9. Test Accuracies for CIFAR-10 and CIFAR-100 across different models and algorithms.

Algorithm	CIFAR-10			CIFAR-100		
	VGG11	ResNet34	DenseNet121	VGG11	ResNet34	DenseNet121
SGDF	<b>91.61</b> $\pm 0.21$	<b>95.33</b> $\pm 0.19$	<b>95.74</b> $\pm 0.06$	<b>68.12</b> $\pm 0.15$	<b>77.69</b> $\pm 0.64$	<b>80.17</b> $\pm 0.19$
SGD	89.83 $\pm 0.05$	94.62 $\pm 0.07$	94.52 $\pm 0.03$	63.48 $\pm 0.39$	76.88 $\pm 0.12$	78.77 $\pm 0.27$
Adam	88.12 $\pm 0.10$	94.30 $\pm 0.06$	94.37 $\pm 0.17$	56.27 $\pm 0.32$	72.81 $\pm 0.45$	74.67 $\pm 0.45$
AdamW	88.59 $\pm 0.20$	94.42 $\pm 0.00$	94.61 $\pm 0.06$	58.09 $\pm 0.69$	72.74 $\pm 0.45$	74.96 $\pm 0.10$
RAdam	90.47 $\pm 0.34$	93.41 $\pm 0.21$	93.75 $\pm 0.04$	60.20 $\pm 0.37$	74.08 $\pm 0.35$	75.82 $\pm 0.28$
MSVAG	90.08 $\pm 0.13$	94.79 $\pm 0.08$	95.01 $\pm 0.12$	61.55 $\pm 0.23$	75.75 $\pm 0.06$	76.84 $\pm 0.13$
Lion	88.04 $\pm 0.06$	93.97 $\pm 0.10$	94.26 $\pm 0.02$	55.59 $\pm 0.15$	72.79 $\pm 0.14$	73.41 $\pm 0.10$
SophiaG	88.53 $\pm 0.04$	94.15 $\pm 0.26$	94.53 $\pm 0.13$	58.01 $\pm 1.85$	72.83 $\pm 0.18$	75.81 $\pm 0.23$
AdaBound	90.41 $\pm 0.12$	94.93 $\pm 0.12$	95.06 $\pm 0.13$	64.51 $\pm 0.15$	76.37 $\pm 0.29$	77.43 $\pm 0.18$
AdaBelief	91.24 $\pm 0.04$	95.18 $\pm 0.01$	95.44 $\pm 0.04$	67.59 $\pm 0.03$	77.47 $\pm 0.34$	79.20 $\pm 0.16$

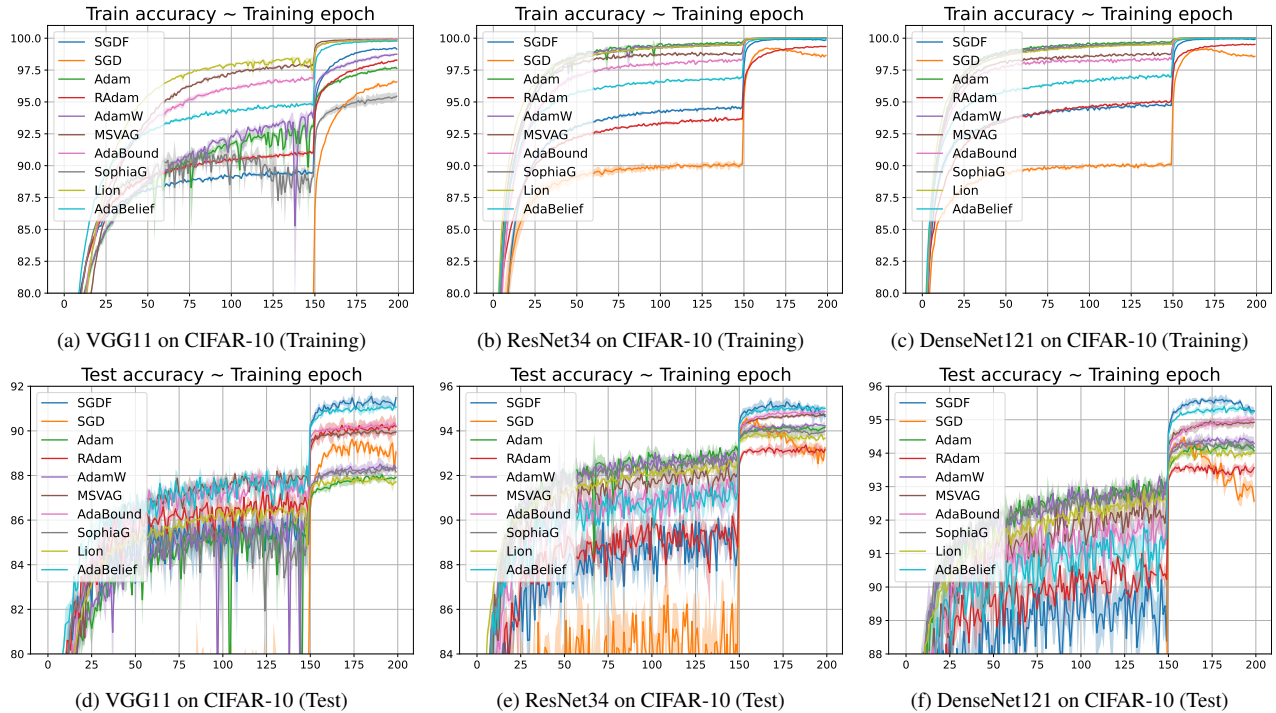


Figure 4. Training (top row) and test (bottom row) accuracy of CNNs on CIFAR-10 dataset. We report confidence interval ( $[\mu \pm \sigma]$ ) of 3 independent runs.

## E.2. Image Classification on ImageNet

We experimented with a VGG / ResNet / DenseNet on ImageNet classification task. For SGDF and SGD, we set the initial learning rate of 0.5 same as CIFAR experiments. The weight decay is set as  $10^{-4}$  for both cases to match the settings in [49]. Here  $\beta_1$  serves to capture the gradient mean. The more closer  $\beta_1$  is to 1, the longer the moving window is and the wider the historical mean is captured. Since ImageNet dataset has more iterations than CIFAR dataset, we directly set  $\beta_1 = 0.5$  to prevent  $K_t$  from being overly influenced by the historical mean gradient. For sure, setting  $\beta_1$  to 0.9, consistent with CIFAR experiments can also be superior to SGD, and adjusting  $\beta_1$  to 0.5 or 0.9 according to the size of the dataset and batch size can bring better results. Detailed experimental parameters we place in Tab. 10. As shown in Fig. 6, SGDF outperformed SGD.

Table 10. Hyperparameters used for ImageNet.

Optimizer	Learning Rate	$\beta_1$	$\beta_2$	Epochs	Schedule	Weight Decay	Batch Size	$\epsilon$
SGDF	0.5	0.5	0.999	100/90	Cosine	0.0001	256	1e-8
SGD	0.1	0.9	-	100/90	Cosine	0.0001	256	-

## E.3. Objective Detection on PASCAL VOC

We conducted object detection experiments on the PASCAL VOC dataset [21]. The model used in these experiments was pre-trained on the COCO dataset [47], obtained from the official website. We trained this model on the VOC2007 and VOC2012 trainval dataset (17K) and evaluated it on the VOC2007 test dataset (5K). The utilized model was Faster-RCNN [65] with FPN, and the backbone was ResNet50 [30]. We train 4 epochs and adjust the learning rate decay by a factor of 0.1 at the last epoch. We show the results on PASCAL VOC [21]. Object detection with a Faster-RCNN model [65]. Detailed experimental parameters we place in Fig. 11. The results are reported in Tab. 4, and detection examples are shown in Fig. 7. These results also illustrate that our method is still efficient in object detection tasks.

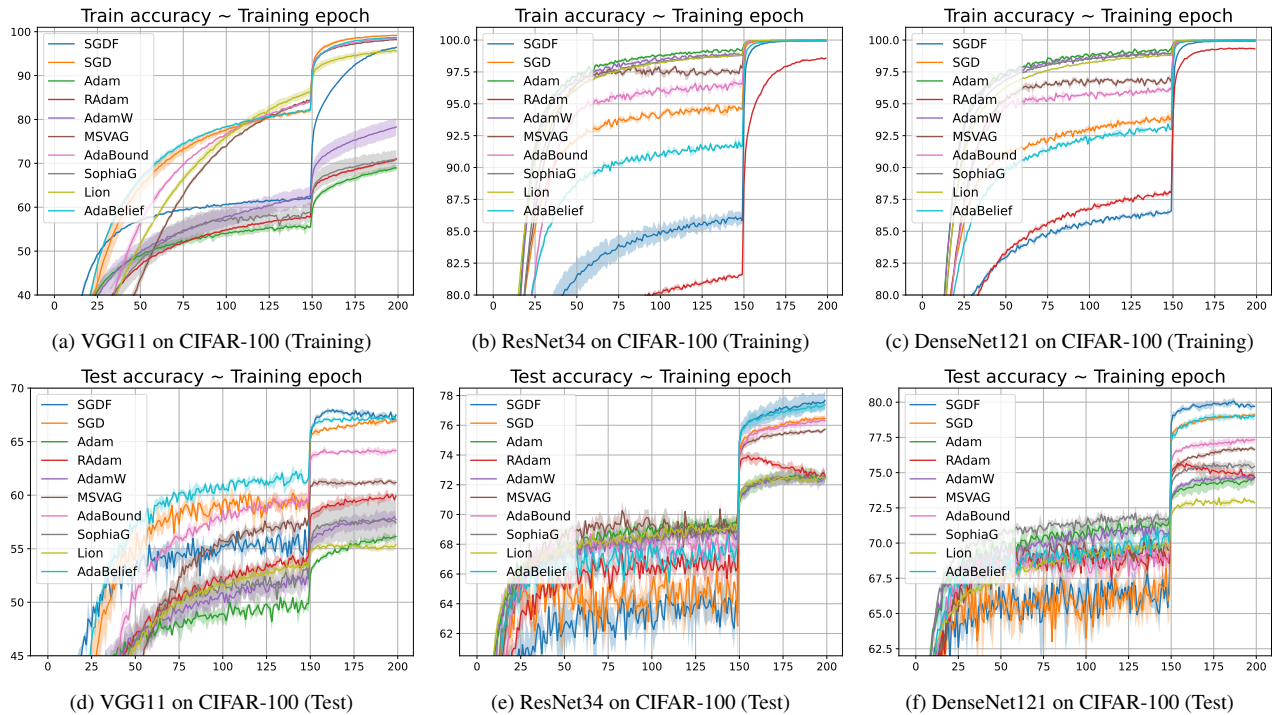


Figure 5. Training (top row) and test (bottom row) accuracy of CNNs on CIFAR-100 dataset. We report confidence interval ( $[\mu \pm \sigma]$ ) of 3 independent runs.



Figure 6. Training and test accuracy (top-1) of ResNet18 on ImageNet.

Table 11. Hyperparameters for object detection on PASCAL VOC using Faster-RCNN+FPN with different optimizers.

Optimizer	Learning Rate	$\beta_1$	$\beta_2$	Epochs	Schedule	Weight Decay	Batch Size	$\epsilon$
SGDF	0.01	0.9	0.999	4	StepLR	0.0001	2	1e-8
SGD	0.01	0.9	-	4	StepLR	0.0001	2	-
Adam	0.0001	0.9	0.999	4	StepLR	0.0001	2	1e-8
AdamW	0.0001	0.9	0.999	4	StepLR	0.0001	2	1e-8
RAdam	0.0001	0.9	0.999	4	StepLR	0.0001	2	1e-8

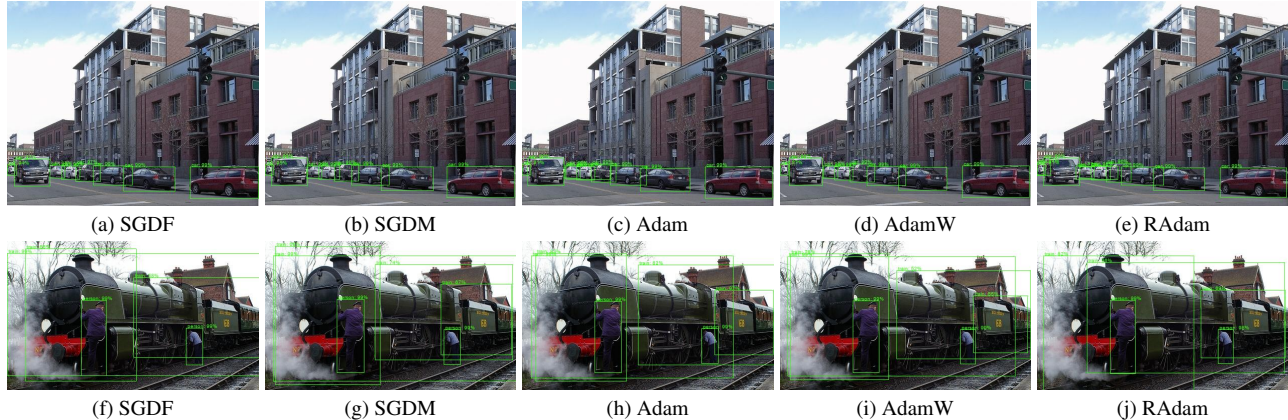


Figure 7. Detection examples using Faster-RCNN + FPN trained on PASCAL VOC.

#### E.4. Image Generation

The stability of optimizers is crucial, especially when training Generative Adversarial Networks (GANs). If the generator and discriminator have mismatched complexities, it can lead to imbalance during GAN training, causing the GAN to fail to converge. This is known as model collapse. For instance, Vanilla SGD frequently causes model collapse, making adaptive optimizers like Adam and RMSProp the preferred choice. Therefore, GAN training provides a good benchmark for assessing optimizer stability. For reproducibility details, please refer to the parameter table in Tab. 13.

We evaluated the Wasserstein-GAN with gradient penalty (WGAN-GP) [67]. Using well-known optimizers [4, 82], the model was trained for 100 epochs. We then calculated the Frechet Inception Distance (FID) [31] which is a metric that measures the similarity between the real image and the generated image distribution and is used to assess the quality of the generated model (lower FID indicates superior performance). Five random runs were conducted, and the outcomes are presented in Tab. 12. Results for SGD and MSVAG were extracted from Zhuang *et al.* [88].

Table 12. FID score of WGAN-GP.

Method	SGDF	Adam	RMSProp	RAdam	Fromage	Yogi	AdaBound	SGD	MSVAG
FID	88.7 ± 4.9	<b>78.6 ± 4.8</b>	109.2 ± 14.5	93.4 ± 8.3	101.5 ± 28.9	138.7 ± 21.2	119.8 ± 24.6	250.3 ± 30.1	239.7 ± 5.2

Experimental results demonstrate that SGDF significantly enhances WGAN-GP model training, achieving a FID score higher than vanilla SGD and outperforming most adaptive optimization methods. The integration of an Optimal Linear Filter in SGDF facilitates smooth gradient updates, mitigating training oscillations and effectively addressing the issue of pattern collapse.

Table 13. Hyperparameters for Image Generation Tasks.

Optimizer	Learning Rate	$\beta_1$	$\beta_2$	Epochs	Batch Size	$\epsilon$
SGDF	0.01	0.5	0.999	100	64	1e-8
SGD	0.01	0.5	-	100	64	-
Adam	0.0002	0.5	0.999	100	64	1e-8
AdamW	0.0002	0.5	0.999	100	64	1e-8
Fromage	0.01	0.5	0.999	100	64	1e-8
RMSProp	0.0002	0.5	0.999	100	64	1e-8
AdaBound	0.0002	0.5	0.999	100	64	1e-8
Yogi	0.01	0.5	0.999	100	64	1e-8
RAdam	0.0002	0.5	0.999	100	64	1e-8

## E.5. LSTM on Language Modeling

We experiment with LSTM [55] on the Penn-TreeBank dataset [56]. For SGDF, we apply gradient clipping with values of 0.1 for the LSTM 1-layer, 0.15 for 2-layer, and 0.25 for 3-layer. The learning rate is decayed by multiplying it by 0.1 at epochs [100, 145] using StepLR scheduling, as detailed in Tab. 14 alongside other hyperparameters. We report the mean and standard deviation across 3 independent runs with random seeds {0, 1, 2} to ensure result robustness. As shown in Fig. 8, which presents both training and test perplexity curves for 1-layer, 2-layer, and 3-layer LSTM architectures, SGDF consistently outperforms other optimizers by achieving the lowest perplexity across all model configurations, highlighting its effectiveness for sequence modeling tasks. Notably, Adabelief performs poorly under standard parameters, failing to match the performance of other optimizers.

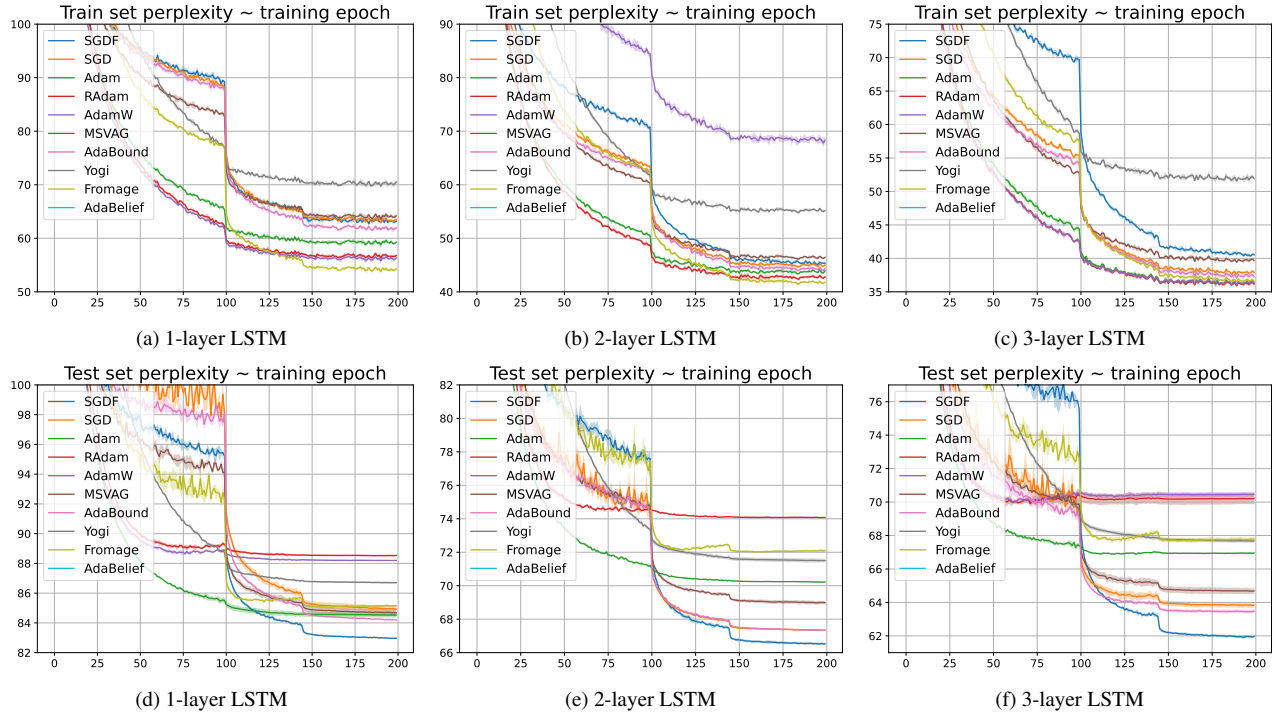


Figure 8. Training (top row) and test (bottom row) perplexity on Penn-TreeBank dataset, lower is better.

Table 14. Hyperparameters used for LSTM.

Optimizer	Learning Rate	$\beta_1$	$\beta_2$	Epochs	Schedule	Weight Decay	Batch Size	$\varepsilon$
SGDF	60	0.9	0.999	200	StepLR	1.2e-6	20	1e-8
SGD	30	0.9	-	200	StepLR	1.2e-6	20	-
Adam	0.001	0.9	0.999	200	StepLR	1.2e-6	20	1e-8
RAdam	0.001	0.9	0.999	200	StepLR	1.2e-6	20	1e-8
AdamW	0.001	0.9	0.999	200	StepLR	1.2e-6	20	1e-8
MSVAG	30	0.9	0.999	200	StepLR	1.2e-6	20	1e-8
AdaBound	0.001	0.9	0.999	200	StepLR	1.2e-6	20	-
Yogi	0.01	0.9	0.999	200	StepLR	1.2e-6	20	1e-3
Fromage	0.01	0.9	0.999	200	StepLR	1.2e-6	20	-
Adabelief	0.001	0.9	0.999	200	StepLR	1.2e-6	20	1e-8

## E.6. Post-training in ViT.

To evaluate SGDF’s performance, we used Vision Transformers (ViT) [16] on six benchmark datasets: CIFAR-10, CIFAR-100, Oxford-IIIT-Pets [61], Oxford Flowers-102 [59], Food101 [5], and ImageNet-1K. Two ViT variants, ViT-B/32 and ViT-L/32, pretrained on ImageNet-21K, were selected. For fine-tuning, we replaced the original MLP classification head with a new fully connected layer, tailored to the dataset categories. All Transformer backbone weights were retained, preserving the rich representations learned from ImageNet-21K. We increased the image resolution (*e.g.*, from  $224 \times 224$  to  $384 \times 384$ ) to improve accuracy, while adjusting positional encoding through 2D interpolation to match the new resolution. For optimization, SGDF was compared to SGD with momentum as a baseline (We research learning set  $\{0.001, 0.003, 0.01, 0.03\}$  same as [16]. For ours method, we’re not tuning and just mirror the hyperparameter in the CIFAR experiments.), using cosine learning rate decay and no weight decay. A batch size of 512 and global gradient clipping (norm of 1) were used to prevent gradient explosion. All experiments were trained uniformly for 10 epochs and the random seed is set as the current year. We set the random seed to  $\{0, 1, 2\}$ . Results are summarized in Tab. 5. We summarized the hyperparameter in Tab. 15.

Table 15. Hyperparameters used for fine-tuning ViT.

Optimizer	Learning Rate	$\beta_1$	$\beta_2$	Epochs	Schedule	Weight Decay	Batch Size	$\epsilon$	Resolution
SGDF	0.5	0.9	0.999	10	Cosine	0	512	1e-8	384
SGD	0.03	0.9	-	10	Cosine	0	512	-	384

## E.7. Top Eigenvalues of Hessian and Hessian Trace

We computed the Hessian spectrum of ResNet-18 trained on the CIFAR-100 dataset for 200 epochs using more optimization methods: SGDF, SGD, SGD-EMA, SGD-CM, Adabelief, Adam, AdamW, and RAdam. We employed power iteration [78] to compute the top eigenvalues of Hessian and Hutchinson’s method [79] to compute the Hessian trace. Histograms illustrating the distribution of the top 50 Hessian eigenvalues for each optimization method are presented in Fig. 9. SGDF brings lower eigenvalue and trace of the hessian matrix, which explains the fact that SGDF demonstrates better performance than SGD as the categorization category increases. Note that Fig. 9g shows that AdamW achieves very low hessian matrix eigenvalues and traces, but the final test set accuracy is about 4% lower than the other methods, and that AdamW’s unique decouple weight decay changes the nature of the converged solution (We apply decoupled weight decay to other algorithms and similar results occur).

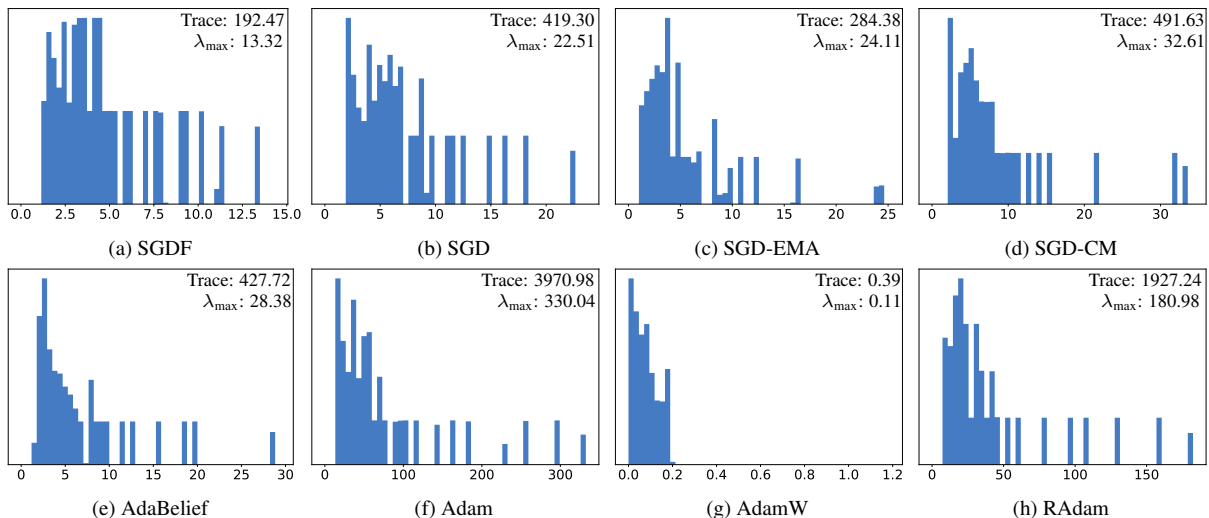


Figure 9. Histogram of Top 50 Hessian Eigenvalues.

## E.8. Visualization of Landscapes

We visualized the loss landscapes of models trained with SGD, SGDM, SGDF, and Adam using the ResNet-18 model on CIFAR-100, following the method in [45]. All models are trained with the same hyperparameters for 200 epochs, as detailed in Sec. 4.1. As shown in Fig. 10, SGDF finds flatter minima. Notably, the visualization reveals that Adam is more prone to converge to sharper minima.

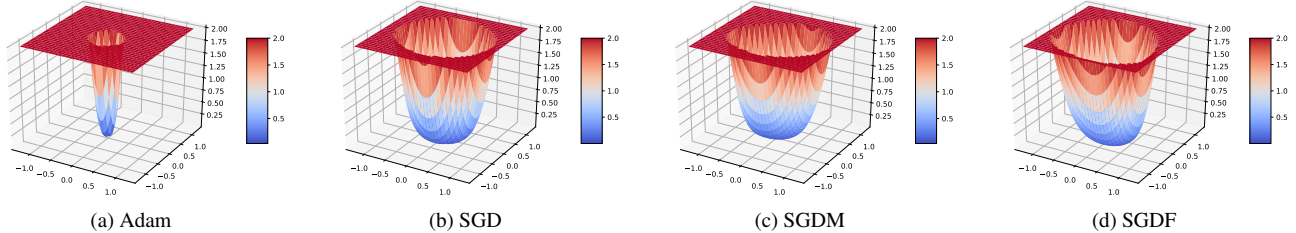


Figure 10. Visualization of loss landscape. Adam converges to sharp minima.

## E.9. Computational Cost Analysis

Tab. 16 reports the per-parameter arithmetic cost of several optimizers. We count elementwise multiplications, additions/subtractions, divisions, and square roots as unit-cost operations. Red numbers indicate the additional overhead of *coupled* weight decay, while green numbers indicate the smaller overhead of *decoupled* weight decay. Compared with plain stochastic gradient methods, adaptive optimizers (e.g., Adam and SGDF) incur extra operations for moment estimation and normalization. Their optimized variants (AdamW and optimized SGDF) reduce compute by removing redundant elementwise divisions and using decoupled weight decay.

Optimizer	Per-Parameter FLOPs	Operation Breakdown
SGD	$\approx 2$ ops/param (+2 ops) (+1 op)	{1 $\times$ , 1+}
SGDM	$\approx 4$ ops/param (+2 ops) (+1 op)	{2 $\times$ , 2+}
Adam	16 ops/param $\rightarrow$ 14 ops/param (+2 ops) (+1 op)	{7 $\times$ , 5+, 3 $\div$ , 1 $\sqrt{\phantom{x}}$ } $\rightarrow$ {7 $\times$ , 4+, 2 $\div$ , 1 $\sqrt{\phantom{x}}$ }
SGDF	22 ops/param $\rightarrow$ 20 ops/param (+2 ops) (+1 op)	{10 $\times$ , 6+, 2-, 2 $\div$ , 1 $\sqrt{\phantom{x}}$ } $\rightarrow$ {10 $\times$ , 6+, 1-, 1 $\div$ , 1 $\sqrt{\phantom{x}}$ }

Table 16. Arithmetic cost and operation breakdown of optimizers. **Red: Coupled Weight Decay, Green: Decoupled Weight Decay.**

Both **Adam** and **SGDF** reduce per-parameter cost through algebraic simplification and bias-correction restructuring. For **Adam**, the update follows  $m_t = \beta_1 m_{t-1} + (1 - \beta_1)g_t$ ,  $v_t = \beta_2 v_{t-1} + (1 - \beta_2)g_t^2$ , and  $\theta_{t+1} = \theta_t - \eta \frac{m_t / (1 - \beta_1^t)}{\sqrt{v_t / (1 - \beta_2^t)} + \epsilon}$ . In **AdamW**, redundant elementwise divisions are avoided by precomputing  $\text{step\_size} = \eta \frac{\sqrt{1 - \beta_1^t}}{1 - \beta_1^t}$  and using decoupled weight decay:  $\theta \leftarrow (1 - \eta\lambda)\theta - \text{step\_size} \frac{m_t}{\sqrt{v_t + \epsilon}}$ . This reduces roughly two operations per parameter (16  $\rightarrow$  14) while preserving the update.

Inspired by this design, **SGDF** refines adaptive updates via the residual-variance estimate. Let  $\hat{m}_t = m_t / (1 - \beta_1^t)$  and  $\hat{s}_t = s_t / c_{2,t}$ , where  $c_{2,t} = \frac{(1 + \beta_1)(1 - \beta_2^t)}{(1 - \beta_1)(1 - \beta_1^{2t})}$ . The Wiener gain is  $K_t = \frac{\hat{s}_t}{\hat{s}_t + (g_t - \hat{m}_t)^2 + \epsilon}$ , and the filtered gradient is  $g'_t = \hat{m}_t + K_t^\gamma (g_t - \hat{m}_t)$ , yielding  $\theta_{t+1} = \theta_t - \eta g'_t$ . A direct elementwise implementation explicitly forms  $\hat{s}_t = s_t / c_{2,t}$  (one elementwise division) and evaluates  $(g_t - \hat{m}_t)$  twice (once in  $K_t$ , once in  $g'_t$ ), resulting in about 22 operations per parameter.

Our optimized implementation avoids explicitly forming  $\hat{s}_t$  by substituting  $\hat{s}_t = s_t / c_{2,t}$  into  $K_t$  and multiplying numerator and denominator by  $c_{2,t}$ , obtaining the equivalent form  $K_t = \frac{s_t}{s_t + c_{2,t}((g_t - \hat{m}_t)^2 + \epsilon)}$ . This removes one elementwise division (replacing it with a scalar multiplication). In addition, we reuse the residual  $r_t = g_t - \hat{m}_t$  across the gain computation and the final filtered update, eliminating one redundant elementwise subtraction. With decoupled weight decay, the per-parameter cost is reduced from about 22  $\rightarrow$  20 operations.

Model	SGDM (h)	Adam (h)	SGDF (h)
<b>VGG13</b>	45.71	45.90	47.78 $\downarrow$ 0.63
<b>ResNet101</b>	35.11	35.32	39.77 $\downarrow$ 1.59
<b>DenseNet161</b>	57.68	58.03	64.81 $\downarrow$ 1.99

Table 17. Total training time (h) for 100 epochs with batch size 256 on FP16 AMP in  $224^2$  Pixel ImageNet.

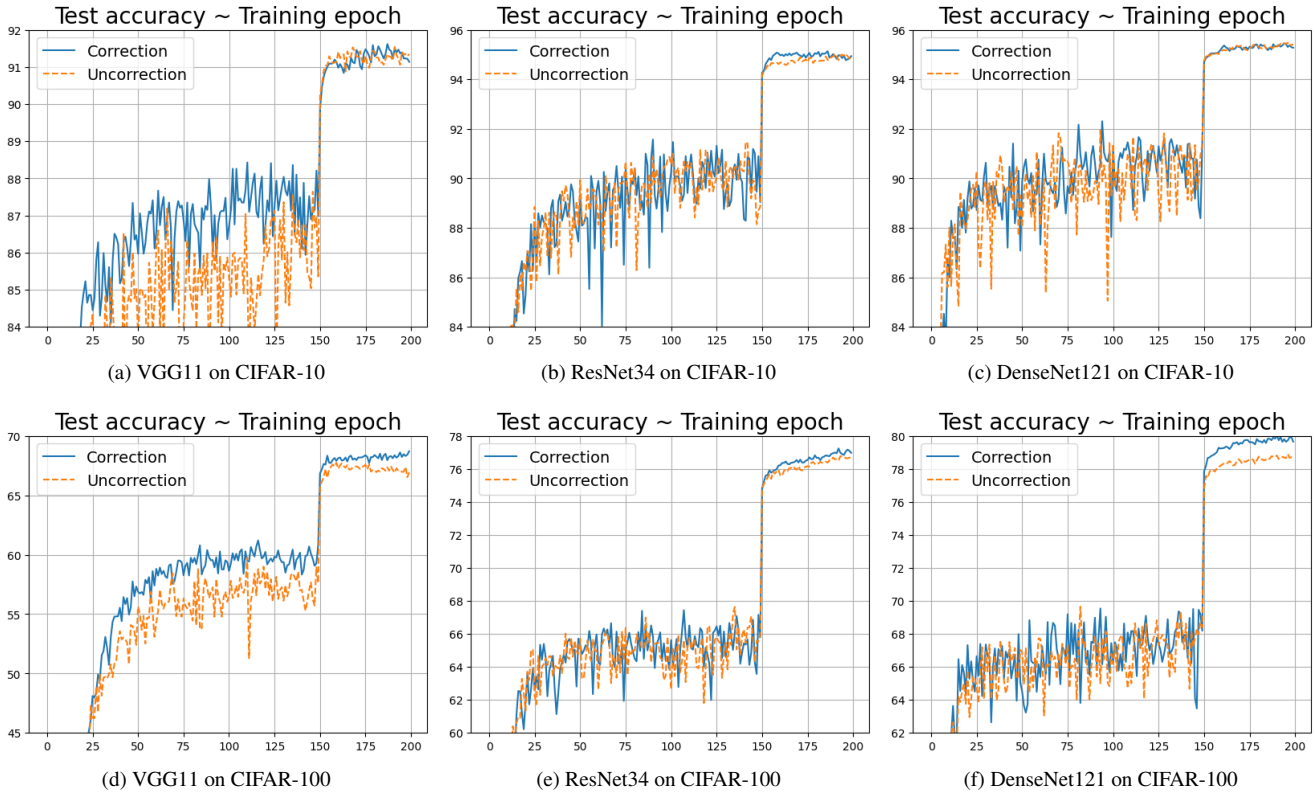


Figure 11. SGDF with or without the correction factor. The curve shows the accuracy of the test.

To complement the theoretical operation analysis, we further conducted an empirical runtime evaluation to quantify the real-world computational efficiency of different optimizers. Each optimizer was benchmarked on FP16 mixed-precision training for 100 epochs with a batch size of 256 across representative CNN backbones (VGG13, ResNet101, DenseNet161) on ImageNet. The measured wall-clock times are summarized in Tab. 17.

## E.10. Ablation Study

We derived a correction factor  $(1 - \beta_1)(1 - \beta_1^{2t}) / (1 + \beta_1)$  from the geometric progression to correct the variance of by the correction factor. So we test the SGDF with or without correction in VGG, ResNet, DenseNet on CIFAR. We report both test accuracy in Fig. 11. It can be seen that the SGDF with correction exceeds the uncorrected one. To better observe the effect of static momentum coefficients on the gradient estimation, while comparing our time-varying SGDF. We use VGG [69] because it is a very standard network with no modules that interfere with the gradient, allowing for a better representation of the optimizer’s update mechanism. We trained it with different SGD-based methods: Vanilla SGD, SGD with EMA, SGD with Filter, and SGD with CM. Then, we plot curve in Fig. 12 and use kernel density estimates of gradient values distribution over the first 100 iterations in Fig. 13.

From Fig. 12, applying SGD with EMA and Filter, convergence is faster than vanilla SGD. EMA has less fluctuation in test curves. WF demonstrates higher test accuracy with the same training set accuracy and reduced generalization gap. On the

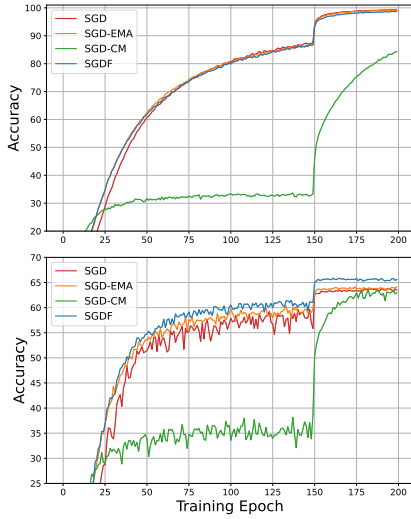


Figure 12. Train the VGG model on the CIFAR-100 dataset using the same initial learning rate of 0.1, and multiply it by a factor of 0.1 at the 150th epoch.

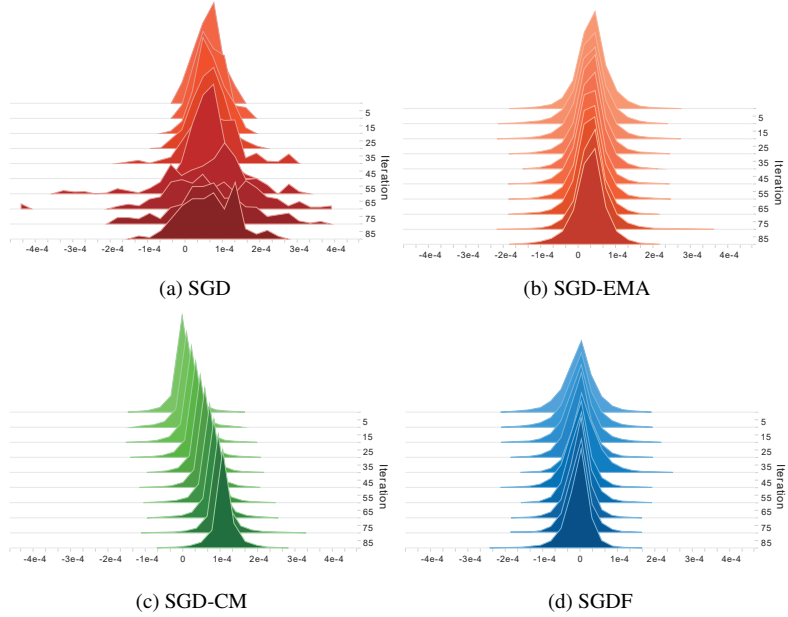


Figure 13. The gradient histogram of the VGG on the CIFAR-100 dataset. The x-axis is the gradient value and the height is the frequency. SGD trains the VGG without BN, the variance of the gradient fluctuates dramatically and the update is unstable.

other hand, CM is slow to converge and results fluctuate because of the larger bias and variance.

Fig. 13a shows high variance and uneven gradient values distribution in Vanilla SGD, resulting in training oscillations that hinder stable convergence. In contrast, Fig. 13b and Fig. 13d shows concentrated gradient distribution and not distorted. Especially, Fig. 13c shows that SGD-CM smooths values fluctuations but introduces *gradient shift*, causing bias and variance over time. Previous research highlights that momentum struggle to adapt to variations in the curvature of the objective function, potentially causing deviation in updates [17, 85].

### E.11. Extensibility of Filter-Estimated Gradients

The study involves evaluating the vanilla Adam optimization algorithm and its enhancement with an Optimal Linear Filter on the CIFAR-100 dataset. Fig. 14 contains detailed test accuracy curves for both methods across different models. The results indicate that the adaptive learning rate algorithms exhibit improved performance when supplemented with the proposed first-moment filter estimation. This suggests that integrating an Optimal Linear Filter with the Adam optimizer may improve performance.

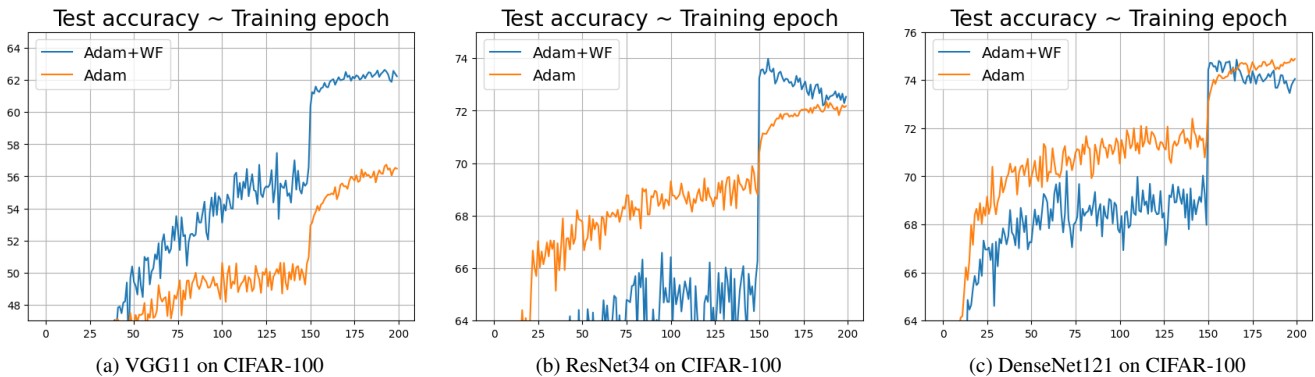


Figure 14. Test accuracy of CNNs on CIFAR-100 dataset. We train vanilla Adam and Adam combined with Optimal Linear Filter.

## E.12. Classical Momentum Discussion

In our framework, the EMA-Momentum is treated as a low-pass filter, in the nature of noise reduction. Cutkosky *et al.* [11] also proves the property that EMA-Momentum cancels out noise, further supporting our analysis. We further discuss classical momentum here.

Theoretically, we show that momentum converges faster than SGD in the setting of  $u$ -strong acceleration, but deep learning optimization does not always conform to this. Leclerc *et al.* [43] tested the classical momentum at different learning rates, taking the momentum factor  $\{0, 0.5, 0.9\}$ . It is empirically found that it is at small learning rates that the classical momentum speeds up the convergence of training losses. That is, SGD-CM can be either better or worse than SGD. In addition, Kunstner *et al.* [42] found that the classical momentum can only show an advantage over SGD when the batch size increases and approaches the full gradient, at which point the noise introduced by random sampling is almost non-existent. In our proof, we mentioned that SGD-CM introduces both bias and variance, but with a full gradient, SGD-CM does not introduce noise and only causes the gradient to produce bias.

We have not analyzed the nature of bias and variance for convergent solutions, but a certain amount of bias may lead to better results when the noise is reduced, and intuitively this may help the algorithm to discuss saddle points or local minima and converge to flatter regions, in a similar nature to the implicitly flat regularity introduced by noise [77]. Because the algorithm converges, the gradient at the position of convergence must be stable, and the classical momentum accumulation gradient, with its large values, must go to a smooth plateau in order to avoid oscillations. Also, it is implied that the gradient bias may not produce irretrievable results, since the bias decreases as the gradient converges, and the direction of the gradient may be more important. Sign SGD [3] takes sign for the gradient, which also converges, and only needs to be applied to the cosine learning rate decay.

Our overall opinion is that CM does not accelerate SGD, but brings better generalization. Early deep learning optimizations focused on reducing the noise introduced by SGD, resulting in several variance reduction algorithms, where reducing variance increases the speed of convergence [6]. The noise introduced by CM hinders convergence, but bias brings better generalization. Thus, the above empirical observation that the momentum method can only be accelerated at small learning rates is due to the reduced step size of SGD, which naturally slows down the convergence rate. Whereas the bias from CM offsets the effect of the reduced step size, and the step size reduces the variance of the gradient sequence. This also implies why deep learning uses warm-up to make the gradient more stable in the pre-training period[49].